

POLITECNICO DI TORINO

MASTER'S DEGREE IN CIVIL ENGINEERING



MASTER THESIS

**The Bridged Crack model with  $n$  fibres:  
Monotonic loading, local instabilities, and scale  
effects**

*Tutors*

Prof. Alberto CARPINTERI  
Ing. Federico ACCORNERO

*Candidate*

Ten. Riccardo MIOSI

Academic Year 2016-2017

*Alla mia dolce metà,  
per avermi stretto a sé  
dall'inizio alla fine.*

*Ai miei genitori,  
per esserci sempre stati.*

# *Ringraziamenti*

*Prima di tutto vorrei ringraziare il prof. Carpinteri e l'ing. Accornero per tutto il supporto fornitomi.*

*Antonio, Chiara, Giovanni e Marco con i quali ho diviso sudore e vita, ma soprattutto Sakher, che nonostante si allontani di "qualche" chilometro rimarrà sempre un fratello.*

*Alessandro, Daniele, Federico S. e Giorgio coi quali spero di rimanere sempre in contatto ovunque le nostre vite ci conducano.*

*Federico M. reduci di mille esperienze condivise, tu sì che puoi dire di avermi sopportato.*

*I miei ringraziamenti vanno ovviamente anche a Mamma Hdemia, alla scuola di applicazione e a tutti i comandanti che fin ora mi hanno mostrato la "Via".*

*E a Tutti coloro i quali mi sono stati vicini in questa doppia avventura Accademico-Universitaria.*

*Grazie a tutti,*

*Riccardo*

# Abstract

---

The main purpose of the present Master Thesis is to implement a software, which is capable of studying the damage propagation in fibre-reinforced structures subjected to bending moment.

At the beginning, different models taken from literature are analysed and compared. Actually, this review covers the scientific works produced in the last three decades.

After the Carpinteri's Bridged Crack model description for one fibre, the model is generalized to study an element reinforced by  $n$  fibres.

Then, it is shown how the analytical model has been implemented into a *MatLab* software.

Finally, some case studies are reported, showing how the structural response changes by varying the Carpinteri's brittleness number, and the number of fibres.

From the literature review, it emerges that different approaches have been used to study the constitutive response of composite materials; the most used ones coming from numerical or Finite Element Model analysis. Although these models are useful for studying some specific problems, the Bridged Crack model described in this work has a larger field of application.

Indeed, the constitutive flexural response of a beam made by a brittle matrix and reinforced with ductile reinforcement layers, can be analysed through the theoretical model summarized in this dissertation.

The Bridged Crack model is based on Fracture Mechanics concepts, and analyses the propagation phenomena of cracks in the critical cross section of an element in bending. The fibre action, which opposes to the crack opening and the crack propagation, is represented through two concentrated closing forces that are applied directly at the crack faces. These forces are evaluated applying compatibility conditions.

The flexural response of a fibre-reinforced element is controlled by a dimensionless parameter called brittleness number  $N_P$ , which depends on the reinforcement percentage, on the fibre yield strength, on the matrix fracture toughness, and on its characteristic size. In particular, by varying the brittleness number, a transition in the structural response arises. The response is *strain-hardening* for high  $N_P$  values, coming from high reinforcement percentage, large size, and/or low values of fracture toughness. Vice versa, for low  $N_P$  values, namely for beams with small reinforcement percentage, with small size, and/or with high values of fracture toughness, the structural response results *strain-softening*. The reinforcement induces some local

discontinuities in the moment-rotation diagram, caused by *snap-back* and *snap-through* instabilities.

Moreover, the application of the Bridged Crack model to beams reinforced with  $n$  fibres allows to remark how a diffuse reinforcement induces a structural response globally more ductile than the one related to a beam characterised by localized reinforcements.

One of the most useful applications remarked in this study is the possibility to define a minimum reinforcement criterion.

Varying the number of fibres, for each case study it is possible to define a specific brittleness number,  $N_P$ , which determines the transition from brittle to ductile behaviour (minimum reinforcement). It is worth noting that, in accordance to the slight increase in  $N_P$  related to the increase in the number of fibres, the minimum reinforcement condition varies from  $N_P = 0.5$  for an element reinforced with one single fibre, to  $N_P = 1.1$  for an element reinforced with ten fibres.

# Table of Contents

---

<b>Introduction</b> .....	1
<b>Part 1</b> .....	2
Chapter 1 Literature Review .....	2
<b>Part 2</b> .....	20
Chapter 2 The Single Fibre Discrete Model.....	20
2.1 General Considerations and Hypotheses .....	20
2.2 Localized Compliance of a Cracked Element.....	23
2.3 The Single Fibre Discrete Model - Formulation.....	26
2.4 Crack Opening at Reinforcement .....	27
2.5 Congruence Conditions .....	30
2.6 Crack Propagation Conditions .....	31
2.7 Localized Rotation .....	34
Chapter 3 The $n$ -Fibres Discrete Model.....	36
3.1 The $n$ -Fibres Discrete Model – Matrix Formulation.....	36
3.2 Crack Openings at Fibre level .....	37
3.3 Congruence Condition.....	38
3.4 Crack Propagation Condition .....	40
3.5 Localized Rotation .....	40
Chapter 4 Software Implementation .....	42
4.1 $\lambda_{ij}$ – Compliance <sub>ij</sub> .....	42
4.2 $[\lambda]$ – Compliance_Matrix.....	43
4.3 $\lambda_{iM}$ – Compliance <sub>iM</sub> .....	44
4.4 $\lambda_M$ – Compliance_vectorM .....	45
4.5 $\lambda_{MM}$ – Compliance_MM.....	45
4.6 $M_F, \Phi$ – Normalized_failure_M.....	46
4.7 Main.....	48
4.8 Graphic User Interface .....	49
Chapter 5 Case Studies.....	55
5.1 The Single Fibre Abacus.....	55
5.2 The Two-Fibres Abacus .....	56
5.3 The Three-Fibres Abacus.....	58
5.4 The Five-Fibres Abacus.....	59
5.5 The Ten-Fibres Abacus .....	61

**Conclusion** ..... 67

**References**..... 69

# Introduction

---

The main purpose of the present Master Thesis is to implement a software, which is capable of studying the damage propagation in fibre-reinforced structures subjected to bending moment.

In the first chapter, different models taken from literature are analysed and compared. Actually, this review covers the scientific works produced in the last three decades.

In the second chapter, Carpinteri's Bridged Crack model is described for one fibre.

In the third chapter, the model is generalized to study an element reinforced by  $n$  fibres.

In the fourth chapter, it is shown how the analytical model has been implemented into a *MatLab* software.

Finally, in the last chapter, some case studies are reported, showing how the structural response changes by varying the Carpinteri's brittleness number, and the number of fibres.

# Part 1

---

## Chapter 1 Literature Review

In (Carpinteri, Massabò, 1996), a nonlinear fracture mechanics model, which explains and reproduces the constitutive flexural behaviour of a brittle-matrix composite, is proposed. It embraces in a unified dimensionless formulation two peculiar models, i.e., the cohesive-crack and the bridged-crack, which are used to analyse the composite failure process. Dimensionless parameters, which depend on the mechanical and geometrical properties, characterize the structure in flexure. It is shown that, based on the assumptions of the bridged-crack model, which simulates the composite as a multiphase material, the flexural response is controlled by two dimensionless parameters, whereas, based on the assumptions of the cohesive-crack model, which simulates the composite as a homogeneous material, the parameters reduce to one. The influence of the dimensionless parameters on the behaviour is studied, along with the size-scale effects on the structural ductility. It is also shown how the matrix toughness affects the response. The two theoretical models are compared through the simulation of an experimental test on a fibre-reinforced beam, and it is shown that both the models can predict approximately the same overall behaviour.

In (Carpinteri, Massabò, 1997), a nonlinear fracture mechanics model is proposed for analysis of the flexural behaviour of brittle-matrix composites with uniformly distributed secondary phases. In accordance with the Barenblatt-Dugdale model the bridging or cohesive zone of the material is replaced by a fictitious crack along which a closing traction distribution is applied. The dimensionless formulation brings out the parameters synthetically controlling the structural behaviour and the size-scale effects. Different scaling transitions are predicted in the flexural behaviour of the composite depending on different modelling of the toughening mechanisms. When a homogenized toughening mechanism for the whole composite is considered along with closing tractions as a linearly decreasing function of the crack opening displacement, a ductile to brittle transition is found as the beam depth increases. On the other hand, when the matrix toughness and the toughening mechanism of the reinforcements are separately modelled, and the closing tractions have a constant value until a critical crack

opening displacement, a double brittle-ductile-brittle transition is found. Experimental tests on fiber-reinforced mortar beams in bending are successfully simulated.

In (Yang, Ravi-Chandar, 1998), antiplane shear crack growth is examined numerically in a precracked rectangular specimen subjected to quasi-static antisymmetric loading, by cohesive layer modelling. Material in the cohesive layer ahead of the crack tip is modelled to be linear elastic-softening with a damaging locus while bulk material of the specimen is assumed to be linear elastic. The evolution of physical and fictitious crack tips is obtained from solutions to the boundary value problem formulated. Critical values of the J-integral and crack opening displacement (COD) for onset of either stable or unstable crack growth are examined, and shown to be dependent upon initial crack length, loading distribution as well as material properties. It is also shown that a unique relationship between a critical value of J-integral and a critical COD cannot be obtained in general. The iterative method of Successive-Over-Relaxation (SOR) is applied in this work.

In (Fantilli, Ferretti, Iori, Vallini, 1999), to study the first cracked stage in R/C members in tension or bending two monodimensional models are proposed. The models analyse the transition from the pre-cracked stage to the post-cracked one by assuming a bond-slip relationship and one cohesive crack. The accuracy of these assumptions is checked by comparing the numerical results with some experimental data. The models are used to compute the minimum reinforcement ratio and to enlighten its size-effect.

In (Goldstein, Perlemuter, 1999), a mechanical and mathematical model is suggested for an interface crack with bonding in its end zones. Normal and shear bond tractions occurring under the action of the external loads are searched for by solving a system of two singular integrodifferential equations. The stress intensity factors at the crack tip are calculated taking the compensating action of the bonds into account. Energetic characteristics of the interface crack (the deformation energy release rate and the rate of the energy absorption by the bonds) are analysed. A sensitivity analysis is performed of the force and energetic characteristics of the interface crack to the end zone size, bond compliance and limit stretching.

In (Taliercio, Coruzzi, 1999), a numerical model is developed with the aim of describing the macroscopic mechanical response of unidirectional brittle-matrix fibre-reinforced composites subjected to stresses acting in any plane transverse to the fibres. Finite element analyses of a representative unit cell are performed, with suitable boundary conditions ensuring continuity of the displacement field across adjacent cells and periodicity of the strain field over the cell. A strain-softening constitutive law is adopted for the matrix in tension to allow, for instance, for brittleness induced by possible defects in a polymeric matrix. The perfectly plastic

case is also considered for sake of comparison. Results established for ductile composites are found to be inappropriate for brittle matrix composites: numerical analyses show that composites with softening matrix have transverse strength properties much poorer than perfectly plastic composites with matrix of equal strength, and even than the unreinforced matrix. An induced transverse anisotropy in the post-peak regime is also observed. A discussion on the proposed approach concludes the note.

(Ruiz, Elices, Planas, 1999) presented the essentials of a research program, both theoretical and experimental, designed to improve the understanding of the mechanical behaviour of lightly reinforced beams, particularly their transition from brittle to ductile behaviour. A simplified model — called the effective slip-length model— describes the concrete fracture as a cohesive crack and incorporates the effect of reinforcement bond-slip. A numerical algorithm is described which is computationally efficient, and so specially suited for parametric analyses of the problem. The experimental research is conducted on three-point bend, lightly reinforced microconcrete beams. Although the beams were of reduced size, the properties of the microconcrete were selected so that the behavior observed is representative of beams of ordinary size made of ordinary concrete. The experiments study the effect of steel ratio, beam depth and bond strength, and include the determination by independent tests of all the parameters of the model. The numerical predictions of the experimental results by the effective slip-length model are reasonably good. The model is able to capture minute experimental details, such as a secondary peak in the load for relatively large steel covers, and describes well the transitional behavior of lightly reinforced beams from brittleness to ductility. Based on numerical analyses, a closed-form expression is given for minimum reinforcement in bending which is compared to recommendations from building codes and formulas from other authors. The comparison shows that the recommendations in the codes could be improved to get safer or cheaper minimum reinforcement to avoid brittle behavior. It also shows that the influence of bond strength should be taken into account, and that generally speaking larger bond strength requires larger reinforcement, although the quantitative effect of the bond strength depends on the details of the beam, particularly on the reinforcement cover, and on the concrete and steel grades.

In (Ferro, 2002), a multilevel bridged crack model is proposed. It reproduces the constitutive flexural response of reinforced concrete members with fibres. Considered are two different reinforcements: the longitudinal bars (primary reinforcement) and the fibres (secondary reinforcement) distributed in the brittle cementitious matrix. The bridging actions exerted by the reinforcements onto the crack faces are assumed to be rigid-perfectly plastic as the primary

constituents. Cohesive softening applies to the fibres. From dimensional analysis, the constitutive flexural response is found to depend on three dimensionless parameters. The first  $\tilde{w}_c$ , controls the extension of the process zone. The remaining two parameters, referred to as brittleness numbers  $N_P^{(1)}$  and  $N_P^{(2)}$ , are related to the reinforcement phases. Specimen size scale is basic to the global structural behaviour. It can range from ductile to brittle as characterized by the two brittleness numbers. They depend on the reinforcement phase of matrix toughness, reinforcement yielding or slippage limit, reinforcement volume fraction and global structural size.

In (Carpinteri, Chiaia, 2002), the problem of scale-effects on the performances of concrete structures is discussed. Experimentally observed decrease of nominal tensile strength, accompanied by structural embrittlement, occurring in large structures is of crucial importance in modern concrete engineering. Most of the previous approaches to the problem are restricted to notched structures and they often fail to predict mechanical behaviour in real situations. The physical approach put forward by us takes into adequate account the effects of microstructural disorder and seems to be valid in the whole size range, at least for unnotched structures. Thereby, reliable predictions can be made of the material properties in large-sized concrete structures.

In (Marfia, Sacco, 2003), the paper aim is the development, assessment and use of suitable numerical procedures for the analysis of the crack evolution in cohesive materials. In particular, homogeneous as well as heterogeneous materials, obtained by embedding short stiff fibres in a cohesive matrix, are considered. Two-dimensional Mode I fracture problems are investigated. The cohesive constitutive law is adopted to model the process zone occurring at the crack tip. An elasto-plastic constitutive relationship, able to take into account the processes of fibre debonding and pull-out, is introduced to model the mechanical response of the short fibres. Two numerical procedures, based on the stress and on the energy approach, are developed to investigate the crack propagation in cohesive as well as fibre-reinforced materials, characterized by a periodic crack distribution. The results obtained using the stress and energy approaches are compared in order to evaluate the effectiveness of the procedures. Investigations on the size effect for microcracked periodic cohesive materials, and on the beneficial effects of the fibres in improving the composite material response, are developed.

In (Shehata, Shehata, Garcia, 2003), the minimum reinforcement issue is studied. Minimum reinforcement is provided in concrete beams in order to improve their behaviour towards cracking and ductility at failure. Generally, codes of practice equations for the minimum steel ratios, longitudinal and transversal, are mainly empirical and do not include all the influential

parameters in them. For this reason and due to the fact that they do lack of a theoretical background, different codes can give values for the minimum steel ratios that greatly differs from one another. Also the validity of these equations may be questioned particularly in the case of high strength concrete beams and prestressed concrete beams for which limited test data are available. In this work, a theoretical approach for the minimum steel ratios that are required for the ductile behaviour at failure in bending, shear and torsion, in concrete beams made of concrete with different strengths is presented. Comparisons are also made between the proposed expressions, the codes expressions and available test results.

In (Carpinteri, Ferro, Ventura, 2004), the bridged crack model is discussed. The bridged crack model has been demonstrated to be an efficient numerical tool for investigating the behaviour of structural elements in bending. In the model, Linear Elastic Fracture Mechanics concepts are used to determine the equilibrium and the compatibility equations of a beam segment subjected to bending in presence of a mode I crack. The model has been extended to include the presence of closing stresses as a function of the crack opening in addition to steel reinforcement closing traction. This allows the characterization of the mechanical behaviour of fibre reinforced structural elements. Some techniques, introduced for reducing significantly the computing time in presence of cohesive stresses, are presented in the paper and the model is extended by a criterion for detecting concrete crushing in compression. Some experimental results are commented in this light.

In (Carpinteri, Corrado, Paggi, Mancini, Ferro, 2007), the concept of Overlapping Crack Model, which is analogous to the cohesive one and permits to simulate material compenetration, is presented. The well-known Cohesive Crack Model describes strain localization with a softening stress variation in concrete members subjected to tension. An analogous behaviour is also observed in compression, when strain localization takes place in a damaged zone and the stress reaches the compressive strength with surface energy dissipation. The two aforementioned elementary models are merged into a more complex algorithm able to describe both cracking and crushing growths during loading processes in RC members. A numerical procedure based on elastic coefficients is developed, taking into account the proposed constitutive laws in tension and compression. With this algorithm, it is possible to effectively capture the flexural behaviour of RC beams by varying the reinforcement percentage and/or the beam depth.

In (Ferro, Carpinteri, Ventura, 2007), the minimum reinforcement issue is discussed. The problem of the assessment of minimum reinforcement in concrete members has been examined both theoretically and experimentally by the bridged crack model. The model has been

demonstrated to be an efficient numerical tool for investigating the behavior of structural elements in bending, and allowed to show the minimum reinforcement percentage depends on the structural element size, and decreases with increasing beam depths. In the model, Linear Elastic Fracture Mechanics concepts are used to determine the equilibrium and the compatibility equations of a beam segment subjected to bending in presence of a mode I crack. The model has been extended to include the presence of closing stresses as a function of the crack opening in addition to steel reinforcement closing traction. This allows to characterize the mechanical behaviour of fibre reinforced structural elements. A criterion for accounting for crushing in compression has been introduced as well, to bound from below (minimum reinforcement) and from above (maximum reinforcement) a region of stable and ductile mechanical behaviour as a function of the mechanical properties as well as of the size of the structural element. Some experimental results are commented in this light.

In (Chiaia, Fantilli, Vallini, 2007), the minimum reinforcement issue is discussed. In lightly reinforced concrete (RC) structures, the area of steel cannot be lower than a minimum value, so that the ultimate limit state can be reached under a yielding moment higher than the cracking moment. Also in the serviceability stage, a minimum amount of reinforcement should be provided in tensile zones, in order to reduce crack widths. In fibre-reinforced concrete (FRC) members, due to the presence of structural fibres in the cementitious matrix, the minimum amount of steel area can be significantly reduced. Fibre can guarantee tensile stresses in a cement-based matrix even in the presence of wide cracks. Therefore, for the same cross-section of steel, a reinforced FRC member in bending can show higher bending moments, and reduced crack widths, than those measured in classical RC beams. This is particularly true in case of massive members, like the structures of tunnel linings. For such elements, and starting from the constitutive relationships recommended by Rilem TC 162-TDF, a approach for the evaluation of minimum reinforcement area is proposed in this paper. By means of this nonlinear model, it is possible to calculate a reinforcement area lower than that calculated according to Eurocode 2 and Rilem TC 162-TDF prescriptions.

In (Fantilli, Mihashi, Vallini, 2007), the crack profile in RC, R/FRCC and R/HPFRCC members in tension is discussed. The theoretical approaches used for the evaluation of crack width in reinforced concrete (RC) structures, are generally based on the hypothesis of parallel crack surfaces. In this way, crack width measured on the concrete cover should be equal to that on the bar surface. The results of several experimental analyses, developed during the past years in many Research Institutes, do not justify this assumption. On the contrary, even in RC members under tensile actions, crack width appears wider on external surface than on rebar–

concrete interface. To better define the effective crack profile of RC structures, a model, able to analyse the whole structural response of RC ties, is here presented. In the proposed approach, all the physical phenomena involved in the cracking process are taken into account: the bond-slip behavior between steel rebar and tensile concrete, the nonlinear fracture mechanics of concrete in tension, and the mechanism of aggregate interlock. Crack profiles computed with this model seem to be in accordance with those experimentally measured in RC elements in tension. A good agreement between numerical results and experimental data is also found both in case of steel rebar and ordinary fibre reinforced cementitious composites (R/FRCC), and in case of steel rebar and high, performance fibre reinforced cementitious composites (R/HPFRCC).

In (Brasiliano, Souza, Doz, Brito, 2008), it is enlighten that during structures useful life they are submitted to deterioration processes that, depending on the intensity, may affect their performance and load capacity and, as a result, their safety. In this case, it is necessary to accomplish an inspection in order to evaluate the conditions of the structure and to locate and quantify the intensity of the damage. Another important point is to study the behaviour of brittle material beams with cracks, as an attempt of understanding the rupture mechanism and crack propagation phenomenon. In this paper, the Residual Error Method (Genovese, 2000) is applied to a concrete beam in order to identify and quantify damages in its structure. This method is based on the alteration produced by damage in the dynamic properties of structures. The results obtained by this method allowed to locate and to quantify damages in a beam. The phenomenon of crack propagation is studied by others methods too: the Fracture Mechanics approaches and the Discrete Element Method (DEM). Changes on the dynamic behaviour, crack trajectories, peak loads and energy variations were observed during the simulation.

In (Nazmul, Matsumoto, 2008), reinforced concrete beams with flexural cracks are simulated by the bridged crack model. The weight function method of determining stress intensity factors has been followed to derive a transformation between the crack bridging force (the rebar force) and the crack opening displacements (CODs). The matrix of the transformation is then approximated by its finite difference equivalent within finite dimensional vector spaces. Direct problem of the transformation solves for CODs, which require a known rebar force. Alternatively, the inverse problem works out the rebar force from known CODs. However, the inverse transformations of such convolution type integral equations become ill-posed if input CODs are perturbed. The Tikhonov regularization method is followed in its numerical form to regularize the linear ill-posed inverse problem. Restoration of mathematical stability and consistency are demonstrated by specific examples, where the results of the direct and the

corresponding inverse problem are cross checked. Results of the direct problem (i.e., the analytical CODs) are deliberately perturbed by adding machine generated random numbers of a certain width. The inverse problems are solved with these CODs to simulate practical situations, where measured CODs data will inevitably be noisy. Computations reveal that the inverse analysis of CODs satisfactorily determines the rebar force without cross-section information.

In (Sanborn, Prévost, 2008), it is enlighten how crack bridging by discontinuous fibres can make brittle materials tougher by transferring stresses from the crack tip to elsewhere in the matrix material. One important aspect of crack bridging is the nature of the interface between the fibres and the matrix material. In this paper, a two-dimensional numerical model of bridging a Mode I loaded crack by linear elastic discontinuous platelets is developed for two different types of interfaces. The first type is a perfectly bonded interface. The second type is an imperfect interface described as a stick–slip interface. A shear-lag model to predict platelet pullout is developed in detail to verify the numerical implementation of the stick–slip interface. An example of a crack tip bridged by a platelet is examined for both interfaces. The perfectly bonded interface will reduce the Stress Intensity Factor (SIF) of the crack greatly but introduces new stress concentrations at the platelet ends. The stick–slip interface can be tailored to also reduce the SIF while not introducing new stress concentrations.

In (Rizk, Marzouk, 2009), a formula to calculate minimum flexure reinforcement for thick high-strength concrete plates is presented. Most concrete codes have empirical equations to estimate the minimum steel reinforcement requirements for flexural members. High-strength thick concrete plates are used for offshore and containment structures for nuclear power generation. An accurate estimate of the minimum steel flexure reinforcement ratio can result in saving millions of dollars for a single project. The recommended concept utilizes the fracture mechanics principles to modify the sandwich panel model and account for thick slabs. A comparison between the proposed equations with experimental tests carried by Battista is conducted; also, a comparison of the proposed equation with different code formulas is illustrated. The results obtained by the proposed equations are confirmed by the Norwegian code (NS 3474E) and suggestions by Bosco and Carpinteri. In summary, the two new main contributions in this research are as follows: the first contribution considers the size effect through fracture mechanics, and the second contribution considers the torsional moment for thick plates in calculating the minimum reinforcement of thick plates.

In (Carpinteri, Corrado, 2009), an extended (fractal) Overlapping Crack Model to describe crushing size-scale effects in compression is presented. The inherent microstructural disorder

strongly influences the mechanical behaviour of heterogeneous materials such as concrete and rocks. Tensile and compression tests, in fact, evidenced a localization of strain and dissipated energy in the post-peak softening branch, with a consequent scale dependence of the stress–strain response. For this reason, the well-known Cohesive Crack Model and the proposed Overlapping Crack Model are useful tools for describing the size effects in tension and compression, respectively. In general, strain localization, damage and fracture, which are phenomena affecting the failure of concrete, are not rigorously interpretable in the framework of continuum mechanics. On the other hand, since the flaw and the aggregate distributions in quasibrittle materials are often self-similar (i.e. they look the same at different magnification levels), the microstructure may be correctly modelled by fractal sets. In this paper, the approach based on fractal geometry, that has profitably been applied for the tensile behaviour, is applied to obtain a fractal overlapping law from uniaxial compression tests. According to this approach, it is assumed that energy dissipation, stress and strain are not defined with respect to the canonical physical dimensions, though on fractal sets presenting noninteger physical dimensions. As a consequence, these classical parameters should be substituted by fractal quantities, which become the true material properties.

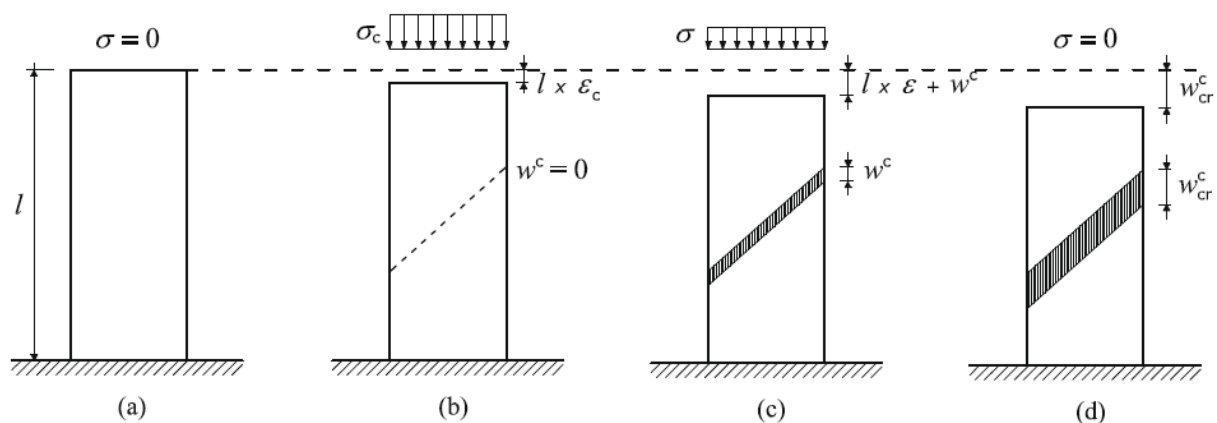


Fig 1. 1 – (Carpinteri, Corrado, 2009) Subsequential stages in the deformation history of a specimen in compression.

In (Carpinteri, Corrado, Mancini, Paggi, 2009), a numerical approach to modelling size effects on the flexural ductility of RC beams is presented. The problem of evaluating the rotation capacity of reinforced concrete (RC) beams in bending has been largely investigated from both the experimental and the analytical point of view during the last decades. Since the development of ductility is influenced by several design parameters, it is difficult to develop a predictive model that can fully describe the mechanical behaviour of RC beams. In particular,

the role of the size-scale effect, which has been evidenced by some experimental tests, is not yet completely understood. One of the main reasons is the inadequacy of the traditional models based on ad hoc stress–strain constitutive laws. In the present paper, a model based on the concept of strain localization is proposed, which is able to describe both cracking and crushing growths in RC beams during the loading process. In particular, the nonlinear behaviour of concrete in compression is modelled by the Overlapping Crack Model, which describes the strain localization due to crushing by means of a material interpenetration. With this algorithm in hand, it is possible to effectively capture the flexural behaviour of RC beams by varying the reinforcement percentage and/or the beam depth. An extensive comparison with experimental results demonstrates the effectiveness of the proposed approach.

In (Carpinteri, Corrado, Mancini, Paggi, 2009), an analytical/numerical model, referred to as the overlapping crack model, is proposed for the analysis of the mechanical behaviour of concrete in compression. Starting from the experimental evidence of strain localisation in uniaxial compression tests, the present model is based on a couple of constitutive laws for the description of the compression behaviour of concrete: a stress–strain law until the achievement of the compression strength and a stress–displacement relationship describing the post-peak softening behaviour. The displacement would correspond to a fictitious interpenetration and therefore the concept of overlapping crack in compression is analogous to the cohesive crack in tension. According to this approach, the slenderness and size-scale effects of concrete specimens tested under uniaxial compression are interpreted from an analytical point of view. Then, implementing the overlapping crack model into the finite element method, eccentric compression tests are numerically simulated and compared with experimental results. The influence of the size-scale, the specimen slenderness, as well as the degree of load eccentricity, is discussed in detail, quantifying the effect of each parameter on the ductility of concrete specimens.

In (Carpinteri, Corrado, Mancini, Paggi, 2009), a complete numerical algorithm that assumes a strain localization in concrete, both in tension and compression, is proposed for modelling cracking and crushing growths during the loading process of reinforced concrete beams in bending. With this algorithm based on nonlinear fracture mechanics models, it is possible to investigate the effects of the main mechanical and geometrical parameters on the rotational capacity with particular regard to the reinforcement percentage and the element size. A comparison with experimental results demonstrates the effectiveness of the proposed approach for a wide range of reinforcement percentages and beam depths. The obtained results show that the prescriptions concerning the admissible plastic rotations provided by the existing

design formulas are not conservative in the case of large structural sizes. To overcome such a drawback, a design diagram is proposed for practical purposes.

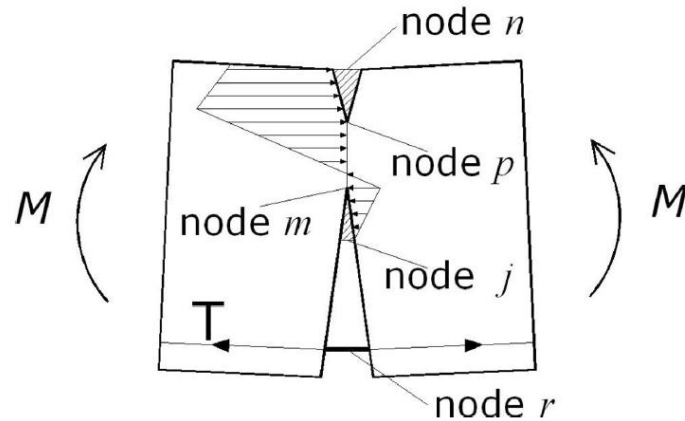


Fig 1. 2 – (Carpinteri, Corrado, Mancini, Paggi, 2009) Force distribution with cohesive crack in tension and crushing in compression.

In (Azevedo,Lemos, Almeida, 2010), a discrete particle model for reinforced concrete fracture analysis is proposed. The Discrete Element Method adopting particles for the domain discretization has been adopted in fracture studies of non-homogeneous continuous media such as concrete and rock. A model is proposed in which the reinforcement is modelled by 1D rigid-spring discrete elements. The rigid bars interact with the rigid circular particles that simulate the concrete through contact interfaces. The DEM enhanced model with reinforcement capabilities is evaluated using three point bending and four point bending tests on reinforced concrete beams without stirrups. Under three point bending, the model is shown to reproduce the expected final crack pattern, the crack propagation and the load displacement diagram. Under four point bending, the model is shown to match the experimental ultimate load, the size effect and the crack propagation and localization.

In (Georgiadi-Stefanidi, Mistakidis, Perdikaris, Papatheocharis, 2011), the numerical simulation of the bending behaviour of fibre reinforced cementitious matrix (FRCM) beams is studied. For the production of the FRCM specimens, a high-strength cementitious matrix with hooked-end steel fibres is used. Two types of FRCM beams are considered. The first type has no conventional steel reinforcement, while the second one includes longitudinal and transverse reinforcement steel bars. For comparison reasons, conventional reinforced concrete (RC) beams are also studied. The beams are tested under static and cyclic loading. The response of the tested beams is simulated by means of effective two-dimensional finite element models, in which the

contribution of the FRCM is taken into account by means of two different layers of finite elements. The first one represents the cementitious matrix while the second one accounts for the contribution of the steel fibres in a homogenized manner. The presented models are able to follow the nonlinearities that appear in the corresponding physical models. The validity of the proposed methodology is established by comparing the numerical results with the corresponding experimental results.

In (Carpinteri, Carmona, Ventura, 2011), the failure mode transitions in reinforced concrete beams is discussed. The bridged crack model is an efficient theoretical and numerical tool for investigating the behaviour of structural reinforced concrete (RC) elements in bending. The model is based on linear elastic fracture mechanics concepts and equilibrium and compatibility equations are applied to a Mode I cracked beam segment. The model is extended to include both compression crushing and shear cracking, assuming a shape for the hypothetical crack trajectory and determining the shear crack initiation point and the load versus crack depth propagation curve. In this paper, the three collapse mechanisms—flexure, shear, and crushing—are considered jointly, so that failure modes can be immediately compared to detect which one dominates and the related failure load. Consequently, the model predicts all the mutual transitions between the different mechanisms, and these transitions are shown by varying the governing nondimensional parameters. A global transition scheme is introduced for illustrating the relevant size/scale effects.

In (Wu, Rong, Zheng, Dong, 2013), a crack-propagation criterion is proposed for mixed-mode I–II fracture in concrete. In this criterion, crack propagation is initiated when the difference between the stress-intensity factor at the crack tip caused by the external force and that by the cohesive stress satisfies the crack-initiation equation. On the basis of this criterion, a numerical method is developed to simulate mixed-mode I–II crack propagation in concrete. To verify the criterion, three sets of experimental data are selected: one is obtained from the self-conducted test and the other two are collected from the literature. The numerical results show that the calculated load versus crack-mouth opening and sliding displacement curves and crack trajectories are in good agreement with experimental results. Therefore, once the mode I initial cracking toughness, elastic modulus, fracture energy, poisson's ratio, and tensile strength of concrete are available, the whole mixed-mode I–II fracture process in concrete can be predicted with reasonable accuracy.

In (Carpinteri, El-Khatieb, Cadamuro, 2013), the failure mode transitions in RC beams is studied. The analysis of reinforced concrete beams in flexure taking into account the nonlinear behaviour of concrete is addressed by a numerical approach based on the Cohesive-Overlapping

Crack Model. An extensive experimental research has been proposed by Bosco and Carpinteri (Scale effects and transitional phenomena of reinforced concrete beams in flexure. ESIS Technical Committée 9 Round Robin proposal, 1993), Bosco et al. (Scale effects and transitional failure phenomena of reinforced concrete beams in flexure. Report to ESIS Technical Committée 9, 1996) and El-Khatieb (Transizione di scala duttile-fragile per le travi in calcestruzzo armato. PhD Thesis, 1997) in order to obtain a rational explanation for failure transitional phenomena of RC beams by varying steel percentage and/or beam slenderness and/or beam size-scale. In the present paper, collapse mechanisms due to concrete tensile cracking, concrete compressive crushing and steel yielding and/or slippage are analysed and a numerical vs. experimental comparison is presented in order to validate the proposed model.

In (Zesers, Tamužs, 2014), a crack bridged by discrete fibres in an infinite medium is modelled. A crack model is developed to consider nonlinearities in the fibre stress–displacement relation independently of the actual physical processes governing this relation. The effects of fibre size and placement on the intensity of crack tip stress are considered. As an example, a crack in a short-steel-fibre-reinforced concrete matrix composite is considered. Variations in the intensity of crack tip stress due to fibre debonding, pullout, and associated stress discontinuities are considered.

In (Wu Z.-M., Wu Y.-F., Dong, Wu X., Zheng, 2014), owing to its importance in evaluating the fracture behaviour of concrete, crack extension resistance has been studied based mainly on experimental results. In this paper, an analytical method is developed for determining the crack extension resistance curve of concrete. It is assumed that, when the difference in stress intensity factor caused by external forces and by the cohesive stress within the fracture process zone is equal to the initial cracking toughness, crack propagation is initiated. According to this assumption, the crack extension resistance curve of concrete is expressed analytically as either the stress intensity factor caused by external forces, or the sum of the initial cracking toughness and the stress intensity factor by the cohesive stress within the fracture process zone. One advantage of this method is that, unlike other methods, the experimentally measured load–crack mouth opening displacement curve is not required in calculating the crack extension resistance curve. Based on numerical results, it is found that the crack extension resistance curve is independent of initial crack length. Also, for a given fracture energy, the shape of the cohesive stress–crack opening displacement curve exhibits no significant effect on the crack extension resistance curve.

In (Perelmuter, 2014), a nonlocal fracture criterion with accounting of the work during bonds deformation at the fracture process zone has been implemented analytically for analysis

of bridged cracks growth. This criterion consists of two conditions: (1) the necessary energy condition of the crack tip limit equilibrium, which takes into account the energy release rate to the crack tip and the rate of deformation energy consumed by bonds in the crack bridged zone; (2) the sufficient condition is the equality of the crack opening at the bridged zone trailing edge to the bond limit stretching. Subcritical and quasi-static regimes of bridged cracks growth have been formulated on these fracture conditions. Regimes of bridged cracks growth are analysed in detail for the case of an internal straight bridged crack in homogeneous material with bonds traction, which is constant and independent of the external loading. Analytical expressions are obtained for the deformation energy release rate and for the rate of deformation energy consumed by bonds. The main fracture parameters, the critical external load and the crack bridged zone size in the limit equilibrium state are determined and analyzed. The limit cases of a crack which is filled with bonds and a crack with a small-scale bridged zone are considered. A comparative study with the well-known force fracture criterion for bridged crack growth is performed.

In (Cox, Bale, Begley, Blacklock, Do, Fast, Naderi, Novak, Rajan, Rinaldi, Ritchie, Rossol, Shaw, Sudre, Yang, Zok, Marshall, 2014), it is review the development of virtual tests for high-temperature ceramic matrix composites with textile reinforcement. Success hinges on understanding the relationship between the microstructure of continuous-fibre composites, including its stochastic variability, and the evolution of damage events leading to failure. The virtual tests combine advanced experiments and theories to address physical, mathematical, and engineering aspects of material definition and failure prediction. Key experiments include surface image correlation methods and synchrotron-based, micrometre-resolution 3D imaging, both executed at temperatures exceeding 1,500°C. Computational methods include probabilistic algorithms for generating stochastic virtual specimens, as well as a augmented finite element method that deals efficiently with arbitrary systems of crack initiation, bifurcation, and coalescence in heterogeneous materials. Conceptual advances include the use of topology to characterize stochastic microstructures. The challenge of predicting the probability of an extreme failure event in a computationally tractable manner is discussed while retaining the necessary physical detail.

In (Mobasher, Yao, Soranakom, 2015), analytical solutions for flexural design of hybrid steel fibre reinforced concrete beams are discussed. Hybrid reinforced concrete (HRC) is referred to as a structural member that combines continuous reinforcement with randomly distributed chopped fibres in the matrix. Equations to determine the moment–curvature relationship, ultimate moment capacity, and minimum flexural reinforcement ratio are

explicitly derived. Parametric studies of the effect of residual tensile strength and reinforcement ratio are conducted and results confirm that the use of discrete fibres increases residual tensile strength and enhances moment capacity marginally. However improvements in post-crack stiffness and deformation under load is substantial in comparison to conventional steel reinforcement. Quantitative measures of the effect of fibre reinforcement on the stiffness retention and reduction of curvature at a given applied moment are obtained. The approach can also be presented in a form of a design chart, representing normalized moment capacity as a function of residual tensile strength and reinforcement ratio. Numerical simulations are conducted on the steel fiber reinforced concrete (SFRC) and HRC beam tests from published literature and the analytical solutions predict the experimental flexural responses quite favorably.

In (Fayyad, Lees, 2015), the minimum flexural reinforcement ratio is discussed. Minimum reinforcement ratios are specified for reinforced concrete structures to provide enough ductility. The aims are to control cracking in the serviceability limit state and to prevent sudden failure by ensuring sufficient ductility after the loss of tensile stress in concrete due to cracking. This can provide a warning before collapse and time to take preventive or remedial measures. A review of past research reveals that there are large variations, and sometimes contradictions, in proposed minimum reinforcement requirements for flexural members. In this paper, a fracture mechanics-based model is used to study different local phenomena such as tensile and compressive concrete softening to more precisely describe the behaviour of reinforced concrete beams. The findings show a decrease in the minimum reinforcement ratio with increasing beam size. This contradicts the provisions of prevailing codes and standards which suggest no change in the minimum reinforcement ratio with size.

In (Chen, Ho, 2015), it is remarked that the authors have previously conducted an experimental study that showed that strain gradient would improve the maximum concrete stress and strength of reinforced concrete (RC) members under flexure. As a continued study, the authors extend the investigation of strain gradient effect on flexural strength and ductility of RC beams to higher strength concrete up to 100 MPa by theoretical analysis. In this study, the flexural strength of RC beams is evaluated using nonlinear strain-gradient-dependent stress–strain curves of concrete applicable to both normal-strength and high-strength concrete. On the basis of this, a parametric study is conducted to investigate the combined effects of strain gradient and concrete strength on the flexural strength and ductility of RC beams. It was evident from the results that both the flexural strength and ductility of RC beams would be improved with strain gradient considered. From the results, two formulas are proposed for the strain-

gradient-dependent concrete stress block parameters  $\alpha$  and  $\beta$ . A constant value of 0.0032 is proposed for the ultimate concrete strain in flexural strength design with strain gradient effect considered. Lastly, for practical engineering design purpose, design formulas and charts have been presented for flexural strength and ductility of RC beams incorporating strain gradient effect.

In (Osmiani, Mohamed, Treiber, Allegri, Partridge, 2016), a constitutive model for tufts bridging a mode I delamination is presented. The tuft is modelled as a rod, laterally supported by an elastic medium and clamped at both ends. A fracture mechanics approach is introduced to describe the progressive debonding of the tuft from the embedding laminate. The debonding model requires the identification of stiffness, strength and toughness properties, which depend both on the laminate/tuft architecture and the constituent materials. Such identification is carried out via experimental data obtained from tensile tests on single tufts inserted in a pre-delaminated non-crimp fabric composite. The experimental results are complemented by micro-scale finite element analysis. The mode I bridging law obtained from the constitutive model is implemented into a meso-scale cohesive zone formulation. This formulation is applied to predict the response to delamination of tufted Double Cantilever Beam (DCB) coupons. The cohesive zone approach is validated by means of experimental data from DCB tests. It is shown that the proposed micro- to meso-scale modelling approach yields results in good agreement with the experiments.

(Fantilli, Chiaia, Gorino, 2016) remarks that nonlinear models, capable of taking into account all the phenomena involved in the cracking and in the failure of lightly reinforced concrete beams, are nowadays available for a rigorous calculation of the minimum reinforcement. To simplify the current approaches, a procedure is proposed in this paper. Specifically, the ductility index, which is lower than zero for under-reinforced concrete beams in bending, is introduced. The results of a general model, as well as the data measured in several tests, reveal the existence of two linear relationships between ductility index, crack width, and the amount of steel reinforcement. The above relationships can be applied to a wide range of lightly reinforced concrete beams, regardless of the geometrical dimensions and of the mechanical properties of materials. Accordingly, if only a few tests are combined with this linear relationships, a design-by-testing procedure can be used to calculate the minimum reinforcement, which guarantees both the control of cracking in service and the ductility at failure

In (Fantilli, Chiaia, Gorino, 2016), a unified approach is introduced for the evaluation of the minimum reinforcement due to the fact that the structural behaviour of lightly reinforced

concrete (LRC) and fibre-reinforced concrete (FRC) beams in bending is similar and depends on the amount of reinforcing bars and fibres, respectively. Such approach is based on the definition of the ductility index (DI), which is a function of the difference between the ultimate bending moment and the effective cracking moment. DI is higher than zero when LRC and FRC beams show a ductile response, whereas it is negative in the case of a brittle behaviour. In accordance with several experimental data, the linear dependence of DI on the amount of reinforcement can be demonstrated. Thus, a design-by-testing procedure can be established to determine the minimum reinforcement (that is, reinforcing bars or fibres) of a concrete beam, which corresponds to DI equal to zero.

In (Mi, Li, Hu, Xu, Shi, 2016), an analytical solution is proposed for investigating the mechanical behaviour of a crack in steel-reinforced concrete. In this solution, an elastic–plastic constitutive law was assumed to satisfactorily describe the behaviour of the steel bar, and the bridging traction was deduced from the deformation of steels. The curves of the load versus crack mouth opening displacement predicted by the proposed method could be fitted to experimental results. It was analytically demonstrated that the ultimate load-carrying capacity calculated by the developed method is not sensitive to the shape of the softening curve for a large beam with high reinforcement ratio.

In (Wang, Xia, 2017), a combined modelling and experimental effort is made to examine the cohesive fracture mechanisms of heterogeneous elastic solids. A two-phase laminated composite, which mimics the key microstructural features of many tough engineering and biological materials, is selected as a model material system. Theoretical and finite element analyses with cohesive zone modelling are performed to study the effective fracture resistance of the heterogeneous material associated with unstable crack propagation and arrest. A crack-tip-position controlled algorithm is implemented in the finite element analysis to overcome the inherent instability issues resulting from crack pinning and depinning at local heterogeneities. Systematic parametric studies are carried out to investigate the effects of various material and geometrical parameters, including the modulus mismatch ratio, phase volume fraction, cohesive zone size, and cohesive law shape. Concurrently, a novel stereolithography-based three-dimensional (3D) printing system is developed and used for fabricating heterogeneous test specimens with well-controlled structural and material properties. Fracture testing of the specimens is performed using the tapered double-cantilever beam (TDCB) test method. With optimal material and geometrical parameters, heterogeneous TDCB specimens are shown to exhibit enhanced effective fracture energy and effective fracture toughness than their homogeneous counterparts, which is in good agreement with the modelling predictions. The

integrative computational and experimental study presented here provides a fundamental mechanistic understanding of the fracture mechanisms in brittle heterogeneous materials and sheds light on the rational design of tough materials through patterned heterogeneities.

## Part 2

---

### Chapter 2

## The Single Fibre Discrete Model

In the following chapter, the single fibre discrete model is discussed to analyse the bending response of fragile materials reinforced with only one layer of ductile and continuous fibres. The model is based on the linear elastic fracture mechanic.

In section 2.1 the fundamental characteristics and hypotheses of the model are explained, the validity of which is discussed for reinforced concrete only.

In section 2.2 an energetic method for the evaluation of the compliances of a cracked specimen is studied. Then the compliances calculated are used in the theoretical model.

At the end, in sections 2.3 and the following, the detailed mechanical model is shown.

### 2.1 General Considerations and Hypotheses

The first single fibre discrete model was proposed by Carpinteri to analyse the bending response of reinforced concrete beams.

Reinforced concrete beams collapse due to different non-linear phenomena, which interest each material and their interaction. These phenomena are located especially in the process zone near the crack.

The proposed model is based on the schemes in figure 2.1, referred to the cracked section, which represents the critical zone of the reinforced concrete beam. Some simple potential collapsing mechanisms are studied:

- a) Fragile propagation of cracks in concrete;
- b) The yield of the reinforcing fibres;
- c) The relative slippage between fibres and concrete.

Therefore, the global mechanical response of the reinforced concrete section very much depends on the combination of these potential collapses, which are influenced by the geometric and mechanic characteristics of the cross section. The constitutive response of the bending

section is characterized by the moment-rotation relation, which is obtained by varying the crack depth. Indeed, by controlling the depth of the crack, it is possible to remark catastrophic and fragile collapses, which instead would not be visible if the process were controlled by the load or a global deformation parameter.

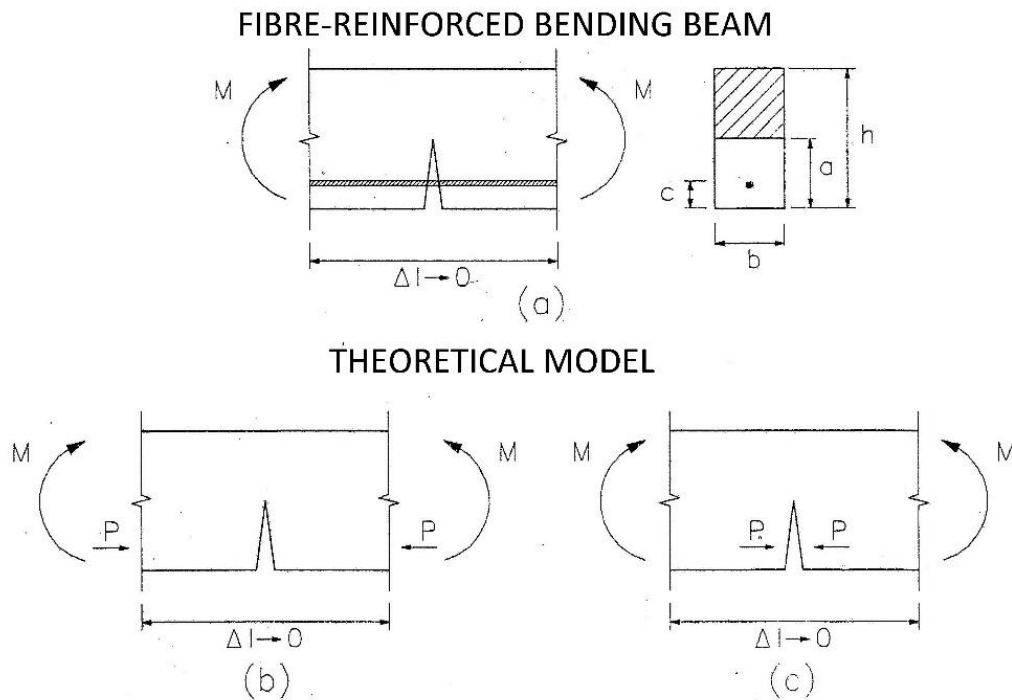


Fig 2. 1 – Fibre-reinforced element and theoretical schemes.

Notice that the structural response is represented by a moment-rotation curve instead of a moment-curvature one as in the classical approach. In fact, curvature could not be considered a characteristic parameter in the post-crack phase. Curvature is usually evaluated as the mean value of the measured rotation in a specific length of an element. Defining the curvature this way implies that the rotation is continuous in that specific length of the element. In fact, the rotation is localized in the cracked zones and becomes dependent on the distance between crack faces. Therefore, the length of the base, where measures are taken from, can affect the curvature, especially at the beginning of the post-crack phase, where we can easily find a softening behaviour in the element response.

We will see how a non-dimensional parameter, the so-called brittleness number, controls the local response of the element; the brittleness number depends on the reinforcement percentage, on the yield strength, on the concrete toughness and on a beam characteristic

dimension. The brittleness number is extremely useful to predict the beam response, when it decreases, we have a transition from a *strain-hardening* to a *strain-softening* behaviour. The *snap-back* and *snap-through* instabilities are perfectly shown by the model; indeed these kinds of instabilities are typical for the discontinuous response of composite materials.

In the theoretical model some hypotheses are assumed, which refers to the behaviour and schematization of the cross section materials:

1) The concrete is considered linear elastic and perfectly fragile in traction. A singularity in the stress field is hypothesised at the tip of the crack and the propagation of the crack is defined through the tensional method, which can be used only for materials with a reduced plastic zone. Actually, concrete has an excellent toughness and is characterized by an extended process zone, therefore the linear elastic fracture mechanics should not be applied for this material.

However, experimental results for reinforced concrete beams have shown that their collapse is governed by the toughness provided by the iron rebars, confirming the theoretical model. Therefore, the hypothesis of a fragile material permits the formulation of an extremely useful and simple model, through which it is possible to understand the fundamental non-linear characteristics of the section response.

2) Concrete is assumed linear elastic in compression. This hypothesis can be considered correct for low-reinforced beams, in which compressed concrete does not reach such a high strain to make concrete have a non-linear response because the collapse is governed by the fragile propagation of the crack.

3) Iron rebars are only considered for their bridging action, which control the opening and propagation of the crack. The fibres are taken into consideration by reducing the stress intensity factor at the tip of the crack thanks to the force applied as shown in the fig 2.2. The Carpinteri's first model hypothesizes the force  $P$  acting as shown in fig 2.2 (b), instead the most recent version of the model considers the force  $P$  acting directly on the faces of the crack (c).

4) The stress-strain curve of the iron is assumed elastic-plastic.

5) The model admits the case in which slippage between fibres and matrix can occur, by defining a rigid perfectly plastic bond-slip relation.

Notice that the above described theoretical model does not need the classical hypotheses of plane sections and perfect adherence between iron and concrete. Indeed as largely demonstrated by experimental tests, these hypotheses are not realistic in the post-crack and collapse phases.

For a given bending moment, the fig 2.1 structure are not statically defined due to the unknown force  $P$ , which can be evaluated only with an opportune congruence condition.

In the first Carpinteri's model, the congruence equation was defined for the localized rotation between the two faces of the crack.

In the final version of the model, the congruence equation was defined for the crack opening at the fibre level. Which is null until the iron rebars reach the yielding stress (hypothesis 4) or the pull-out force (hypothesis 5). Thus, the force becomes defined as the minimum of the two limit forces and the crack opening at the fibre level becomes different from zero. These models can predict the ductile-fragile transition, which occurs varying the geometrical and mechanical characteristics.

Although the mechanical model has been formulated to analyse reinforced concrete beams, it can be applied to study every fragile material as ceramics, metals or concrete, reinforced with rebars, fibres, and ductile particles or rivets, which respects the previous hypotheses.

## 2.2 Localized Compliance of a Cracked Element

The stiffness of an element is highly influenced by the presence of a crack. To evaluate the stresses acting on a hyperstatic structure in which a cracked element is present, it is necessary to know the element compliance characteristics that permit us to verify the congruence.

Also in a fragile isolated element with reinforcements controlling the crack opening and propagation, some hyperstatic reactions occur in the reinforcement, e.g. rivets in metal sheets, iron rebars in concrete, and discontinuous fibres in ceramics. In this kind of composite materials, internal hyperstatic reactions occur directly on the crack faces, therefore to evaluate them you have to solve congruence equations. To be able to solve the equations, the compliance of a cracked element is required.

Let us consider the beam of fig. 2.2 (a), clamped at the base and a concentrated force  $P$  on the other end. The beam, made of a linear elastic fragile material, has a crack the length of which is  $a$ . The element compliance  $\lambda_{TOT}$ , is defined as:

$$\lambda_{TOT} = \lambda_0 + \lambda = \frac{\delta_0 + \delta}{P} \quad (2.1)$$

Where  $\lambda_0$  and  $\delta_0$  are the respectively the compliance and the displacement of the un-cracked element, while  $\lambda$  and  $\delta$  are the increments which occur due to the presence of the crack. In this section, our focus will only be on the local compliance and displacement,  $\lambda$  and  $\delta$ .

Let us assume that for a certain value of the force  $P$  the crack length increases of a value  $da$ . The new configuration of the beam is characterized by a force equal to  $P + dP$  and a  $\delta + d\delta$ , as

shown in the fig 2.2 (b), the local compliance increases to  $\lambda + d\lambda$ . If load controls the process, the AC segment describes the element response; instead, if the process is controlled by displacement, the AD segment becomes representative.

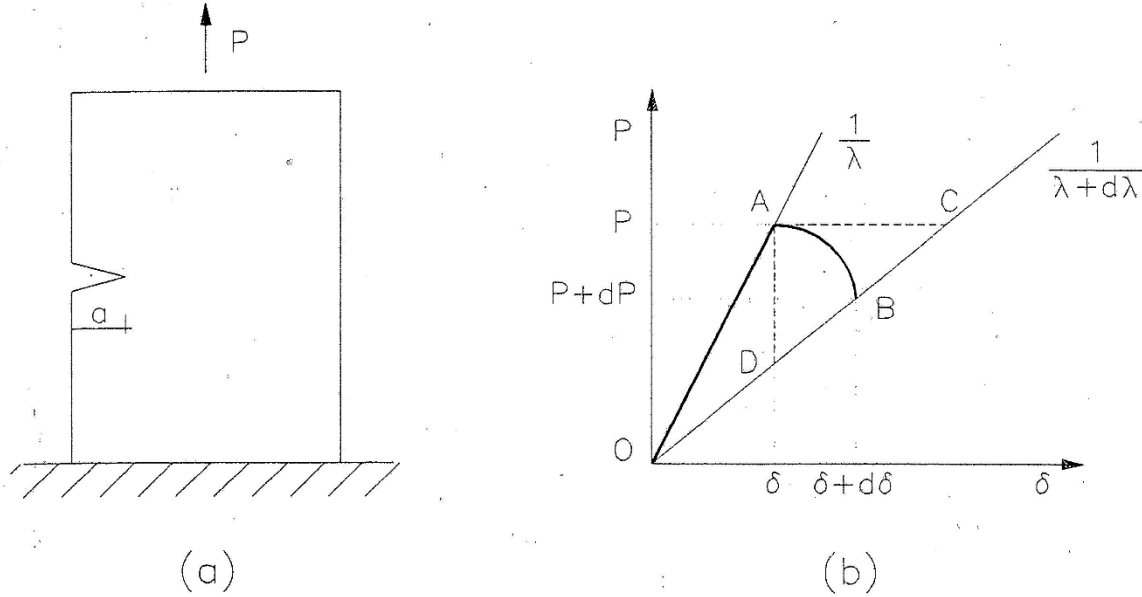


Fig 2. 2-Schemes used to define compliance.

After the crack propagation, the variation of the total potential energy,  $dW$ , of the system is equal to:

$$dW = dU - dL \quad (2.2)$$

Where  $U$  is the potential elastic deformation energy and  $L$  is the potential energy of the external load. Applying the Clapeyron's theorem, we obtain:

$$dW = \frac{1}{2}Pd\delta + \frac{1}{2}\delta dP - Pd\delta \quad (2.3)$$

Where the first two terms are the variation of the potential energy, calculated as the difference between OBF and OAE areas, and the third term is the work made by the external force. Taking in consideration that  $d\delta = \lambda dP + Pd\lambda$  we obtain:

$$dW = -\frac{1}{2}P^2d\lambda \quad (2.4)$$

Notice that  $dW$  is independent from the slope of the softening AB segment, which means that the total potential energy, released when the crack propagates, is independent from load conditions. Due to the relation:

$$Gbda = -dW \quad (2.5)$$

You can easily write:

$$G = \frac{1}{2b} P^2 \frac{d\lambda}{da} \quad (2.6)$$

Where  $b$  is the base of the beam.

This analysis is the base of the experimental method, called *Compliance Method*, used to evaluate the critical stress intensity factor,  $K_{IC}$ , by measuring the compliance at different depths of crack.

Integrating the (2.6) relation, we obtain the localized compliance of an element, the crack depth of which is  $a$ :

$$\lambda = \int_0^a \frac{2G}{P^2} b da = \frac{2}{E} \int_0^a \frac{K_I^2}{P^2} b da \quad (2.7)$$

Where  $K_I$  is the stress intensity factor caused by the force  $P$  and can be easily found in manuals.

When there are more than one generalized acting force,  $P_i$ , the dual displacement can be defined by applying the superposition principle:

$$\delta_i = \sum_{j=1}^n \lambda_{ij} P_j \quad (2.8)$$

Where  $\lambda_{ij}$  is the displacement of the point, in which  $P_i$  is applied, due to a unitary  $P_j$  force. Applying the Clapeyron's theorem, we can find the total potential energy variation caused by the crack propagation as:

$$dW = - \sum_{i=1}^n \sum_{j=1}^n \frac{1}{2} P_i P_j d\lambda_{ij} \quad (2.9)$$

Taking into account the (2.5) relation:

$$dW = -Gbda = - \frac{(K_{I1} + \dots + K_{Im})^2}{E} b da = - \sum_{i=1}^n \sum_{j=1}^n \frac{(K_{Ii} K_{Ij})}{E} b da \quad (2.10)$$

Integrating (2.9) and (2.10) relations we obtain two different expressions of the total potential energy variation  $W$ , caused by the presence of a crack whose depth is  $a$ :

$$W = - \int_0^a Gb da = - \sum_{i=1}^n \sum_{j=1}^n \int_0^a \frac{(K_{Ii} K_{Ij})}{E} b da \quad (2.11)$$

$$W = - \sum_{i=1}^n \sum_{j=1}^n \frac{1}{2} P_i P_j \lambda_{ij} \quad (2.12)$$

Comparing (2.11) with (2.12) we can find an expression for the compliance of a cracked element:

$$\lambda_{ij} = \frac{2}{E} \int_0^a \frac{K_{Ii} K_{Ij}}{P_i P_j} b da \quad (2.13)$$

Applying Betti's Theorem,  $\lambda_{ij}$  is equal to  $\lambda_{ji}$ , and for  $i=j$  we reobtain equation (2.7):

$$\lambda_{ii} = \frac{2}{E} \int_0^a \frac{K_{ii}^2}{P_i^2} b da \quad (2.14)$$

### 2.3 The Single Fibre Discrete Model - Formulation

Consider a cross section of a beam in which a moment  $M$  is applied, fig 2.2. The beam is made of an elastic-fragile material, reinforced by a continuous ductile fibre and with  $h$ ,  $b$ ,  $c$  respectively as height, base and fibre position. The aim is to analyse the bending behaviour of the section shown in fig. 2.3 (a); a crack is present in the element, the length of which is  $a$  and in which the unknown concentrated forces  $P$ , takes into account the reinforce reactions. Moreover, the normalized crack length and the normalized position of the fibre are defined respectively as  $\xi = \frac{a}{h}$  and  $\zeta = \frac{c}{h}$ . The hypotheses are discussed in the 2.1 section, however they are briefly reassumed here.

The matrix is assumed linear elastic and the fracture propagation criterion is in accordance with the linear elastic fracture mechanic. The stress-strain curve of the fibre is assumed elastic-plastic. The bond-slip relation between the fibre reaction and the relative fibre-matrix slippage is assume rigid-plastic.

Notice that the last two statements make the reaction force of the fibre,  $P$ , dependant on the crack opening at the fibre level,  $w$ , with a rigid-plastic relation, fig 2.3 (b). Indeed the  $w$  opening can be caused by either the plastic flow of the infinitesimal portion of fibre between the two crack faces, when the fibre reaches its yield strength, or by the relative fibre-matrix slippage, when the adherence resistance is exceeded. Therefore, the maximum bridging reaction,  $P_p$ , will be or the fibre plastic reaction force or the pull-out force, defined as:

$$P_p = A_f \sigma_y \quad (2.15)$$

Where  $A_f$  is the reinforce element area and  $\sigma_y$  is, in the former case, the yield strength and, in the latter case, the fibre tension when the pull-out force is reached.

Notice that the fibre could represent a layer of reinforcements all located in the same coordinate  $c$ ; in this case, the area  $A_f$  is the summation of the fibres areas, which composes the layer. The proposed scheme is equal to a system in which the two crack faces are bonded by a non-linear spring at the coordinate  $c$ , the stiffness of which remains infinite until the force in the fibre reaches  $P_p$ , when reached the stiffness becomes null.

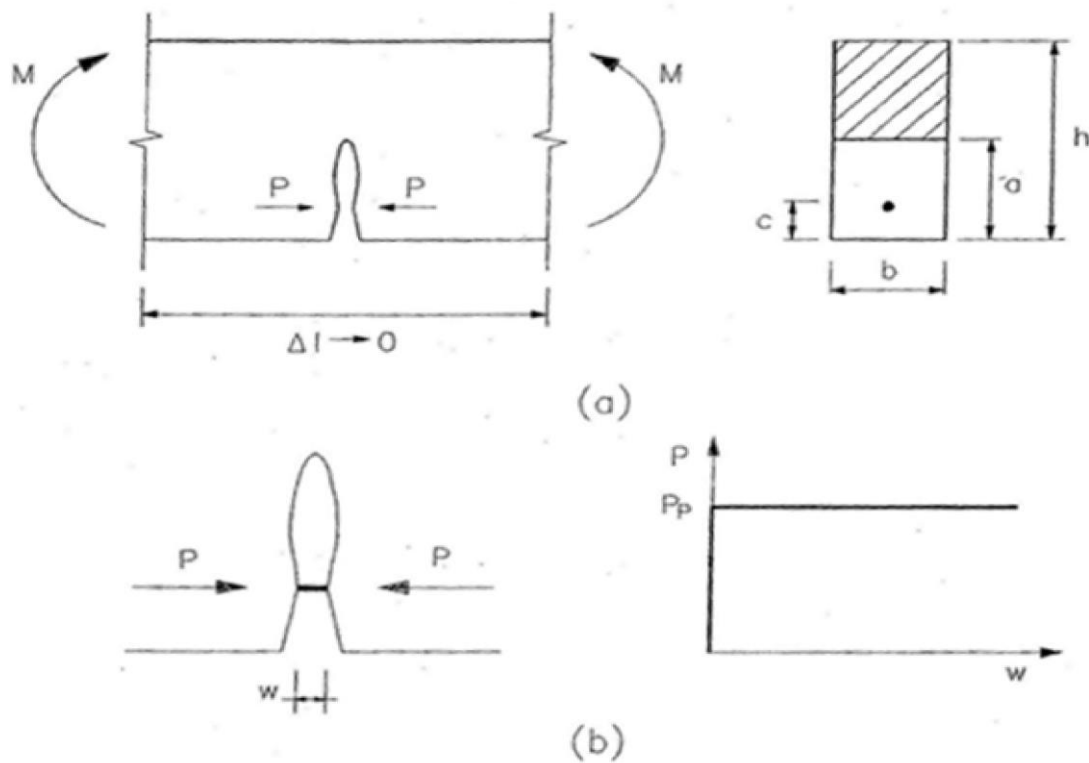


Fig 2. 3- Theoretical scheme of the single fibre discrete model.

The section collapse response is evaluated according to the fig 2.3 schemes; simulating the crack propagation process, by varying the crack depth from  $a_0$  to a prefixed height. The equilibrated and congruent configurations are studied, by varying the crack depth, which are in an incipient propagation state (moving equilibrium). The problem, which is statically indeterminate, is resolved using a proper congruence equation involving the crack opening,  $w$ , which permits to evaluate the force,  $P$ . In the following sections, the subsequent parts of model are duly shown.

## 2.4 Crack Opening at Reinforcement

The crack opening at reinforcement,  $w$ , can be defined applying the superposition principle:

$$w = w_M + w_P = \lambda_{PM}M - \lambda_{PP}P \quad (2.16)$$

Where  $w_M$  and  $w_P$  are, respectively, the openings due to bending moment,  $M$ , and closure force,  $P$ .  $\lambda_{PM}$  and  $\lambda_{PP}$  are the localized compliances, which are the openings due to, respectively, a unitary moment and a unitary concentrated force. The negative sign comes from the scheme in which  $P$  is a closure force.

The procedure used to evaluate the localized compliances, based on an energetic balance, is presented in the 2.2 section. From the (2.13), according to the fig 2.3 (a) scheme -where the only acting forces are the bending moment,  $M$ , and the fibre reaction,  $P$ - using the normalized coordinates, we obtain the expression of the mixed local compliance:

$$\lambda_{PM} = \frac{2hb}{E} \int_{\zeta}^{\xi} \frac{K_{IM}K_{IP}}{PM} d\xi \quad (2.17)$$

Where  $K_{IP}$  and  $K_{IM}$ , are the intensity factor for the tension at the tip of the crack, caused respectively by the applied moment,  $M$ , and by the re-closure force applied in  $c$ ;  $E$  is the Young's Modulus. Notice that the lower extreme of the integration, which in the general equation (2.13) was equal to zero, here it is equal to  $\zeta$ . Indeed,  $\zeta$  is the crack height at which the reinforcement start to express bridging action and subsequently the intensity factor  $K_{IP}$  becomes different from zero.

In the same way we can obtain the compliance,  $\lambda_{PP}$ , through the (2.14) relation:

$$\lambda_{PP} = \frac{2hb}{E} \int_{\zeta}^{\xi} \frac{K_{IP}^2}{P^2} d\xi \quad (2.18)$$

The intensity factors can be defined as:

$$K_{IM} = \frac{M}{bh^2} Y_M(\xi) \quad (2.19)$$

$$K_{IP} = \frac{P}{bh^2} Y_P(\xi, \zeta) \quad (2.20)$$

By substituting the expressions of the intensity factors into the (2.17) and (2.18) relations, we obtain:

$$\lambda_{PM} = \frac{2}{Ehb} \int_{\zeta}^{\xi} Y_P(\xi, \zeta) Y_M(\xi) d\xi \quad (2.21)$$

$$\lambda_{PP} = \frac{2}{Eb} \int_{\zeta}^{\xi} Y_P^2(\xi, \zeta) d\xi \quad (2.22)$$

Where  $Y_M(\xi)$  and  $Y_P(\xi, \zeta)$  are the polynomial functions which are present in the intensity factor formulas and can be easily found in manuals for fracture mechanics.

The integrals shown in the (2.21) and (2.22) have a singularity at the lower integration extreme, when  $\xi = \zeta$ . However, while the (2.21) singularity is removable, the (2.22) one is not, and the improper integral does not converge. Therefore, the  $\lambda_{PP}$  compliance can be defined with the following procedure. The third model hypothesis, which represent the closure action that the fibre applies on the crack faces in  $c$ , does not take into account the fibre dimensions, which

are known and different from zero. Suppose that the fibre had a diameter,  $d$ , and the normalized coordinate is defined as:  $\bar{d} = \frac{d}{h}$ . The action coming from the fibre can be better expressed by spreading it in a distributed pressure,  $p$ , acting on the crack segment included between  $c - \frac{d}{2}$  and  $c + \frac{d}{2}$ , and equal to  $p = \frac{P}{bd}$ . The  $\lambda_{pp}$  compliance, which defines the opening of the crack in  $c$  due to the unitary pressure  $p$ , results:

$$\lambda_{pp} = \frac{2}{Eb} \frac{1}{\bar{d}} \int_{\zeta}^{\xi} \int_{\zeta - \frac{\bar{d}}{2}}^{\zeta + \frac{\bar{d}}{2}} Y_P(\xi, x) dx Y_P(\xi, \zeta) d\xi \quad (2.23)$$

In which the improper integral converges.

To assure the simplicity of the Carpinteri's original model, the hypothesis of concentrated force, to describe the fibre, is maintained by defining a proper truncation point in the numerical evaluation of the improper integral. Therefore, the local compliance,  $\lambda_{pp}$ , can be numerically evaluated as:

$$\lambda_{pp} = \frac{2}{Eb} \int_{\zeta + \delta}^{\xi} Y_P^2(\xi, \zeta) d\xi \quad (2.24)$$

In which  $\delta$  is evaluated by imposing that the results coming from the (2.23) are equal to (2.24) ones.

The first expression for the cut-off,  $\delta$ , was proposed by Carpinteri and Massabò; solving numerically the integrals, they found out a good value for the cut-off is  $\delta = 10^{-5}$ .

Carpinteri and Ventura proposed a second more accurate expression. They re-analysed this numerical issue and observed that, if the area of the spreading zone is assumed to be equal to the area of the reinforcing element, then the height of the spreading zone divided by the total height,  $h$ , of the cress section must be equal to the reinforcement percentage,  $\rho_i$ , which is defined as the ratio of the  $i$ -th reinforcement cross section to the total beam cross section:  $\rho_i = A_i/bh$ . Thus, one should not consider the diameter  $d$  of the reinforcing element, because the model is only bi-dimensional, in that it does not account explicitly for the beam thickness  $b$ . They found that the cut-off is basically independent from the crack depth,  $\zeta$ , and the reinforcement position,  $\zeta_i$ . Consequently, considering a single reinforcement and the values  $\zeta = 0.5$  and  $\zeta_i = 0.1$ , they obtained that the cut-off values can be conveniently expressed through the following linear law:

$$\delta = 9 \times 10^{-6} + 0.044771\tilde{d} \quad (2.25)$$

Where  $\tilde{d}$  is no longer equal to the normalized fibre diameter, as previously remarked, but coincides with the reinforcement percentage,  $\rho_i$ .

In fig. 2.4 the compliances are graphed by varying the crack depth for three different fibre positions,  $\zeta = 0.05, 0.10, 0.15$ . It can be easily noticed how both diagrams define coherently a local compliance, which is null when the crack tip is on the fibre level and becomes infinite when the cross section is completely cracked.

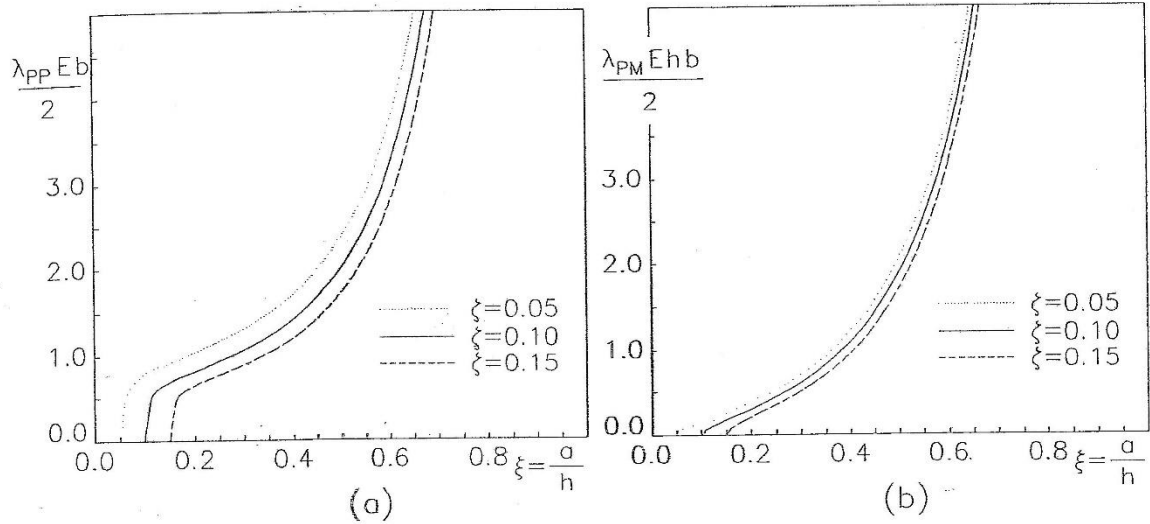


Fig 2. 4-Localized compliances.

## 2.5 Congruence Conditions

The hyper-static reaction,  $P$ , is evaluated by imposing the congruence condition: the crack opening,  $w$ , at the fibre level is null until  $P$  reaches  $P_P$ . Notice that this condition comes from the assumption of a rigid-plastic curve between  $P$  and  $w$ . Therefore, we obtain:

$$w = \lambda_{PM}M - \lambda_{PP}P = 0 \quad (2.26)$$

The bridging force,  $P$ , can be obtained by substituting the expressions of the localized compliances, (2.21) and (2.22), in this relation; normalizing  $P$ , we obtain:

$$\frac{Ph}{M} = \frac{\lambda_{PM}h}{\lambda_{PP}} = \frac{1}{r^{II}(\xi, \zeta)} \quad (2.27)$$

Where  $r^{II}(\xi, \zeta)$  is defined as follow:

$$r^{II}(\xi, \zeta) = \frac{\int_{\zeta}^{\xi} Y_P^2(\xi, \zeta) d\xi}{\int_{\zeta}^{\xi} Y_P(\xi, \zeta) Y_M(\xi) d\xi} \quad (2.28)$$

In fig. 2.5 (a), the normalized bridging force trend is shown by varying the crack depth for three different fibre positions,  $\zeta = 0.05, 0.10, 0.15$ . Notice that the bridging reaction is always

creasent when the crack depth increases and if the distance between the fibre and the intrados is increased.

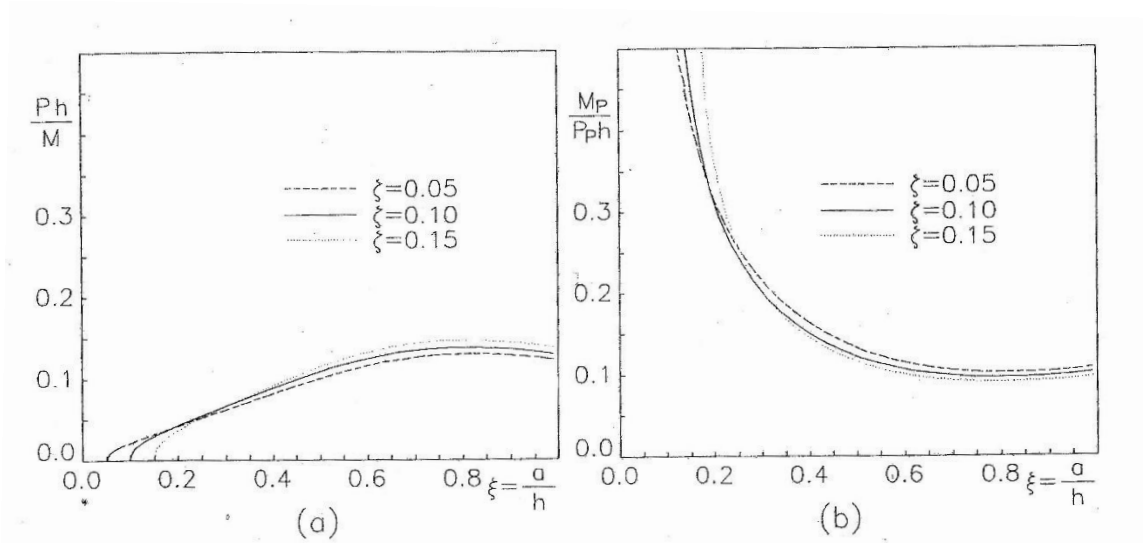


Fig 2. 5- (a) Hyper-static reaction; (b) Plastic-flow bending moment.

The plastic moment occurs when either the fibre-matrix slippage occurs or the fibre turn from elastic to plastic state and can be obtained by imposing  $P = P_P$ :

$$\frac{M_P}{P_P h} = r^{II}(\xi, \zeta) \quad (2.29)$$

The correspondent diagram is shown in fig. 2.5 (b). Notice that the plastic-flow bending moment decreases when the crack depth increases; thus, when the crack depth is higher, less load increments are needed to make  $P$  equal to  $P_P$ .

When the limit condition is reached, the crack opens at the fibre height and  $w$  becomes unknown. However, the problem in this phase is statically determined because the closure force is known and equal to  $P_P$ .  $w$  becomes:

$$w = \lambda_{PM}M - \lambda_{PP}P_P \quad (2.30)$$

## 2.6 Crack Propagation Conditions

According to the linear elastic fracture mechanic, a singular tensional field is defined at the crack tip, measured by the stress intensity factor,  $K_I$ , which depends on the element geometry, crack length and loads. Particularly, the superposition principle allows us express the  $K_I$  of the problem as:

$$K_I = K_{IM} - K_{IP} = \frac{M}{h^{1.5}b} Y_M(\xi) - \frac{P}{h^{0.5}b} Y_P(\xi, \zeta) \quad \text{If } P < P_P \quad (2.31)$$

$$K_I = K_{IM} - K_{IP} = \frac{M}{h^{1.5}b} Y_M(\xi) - \frac{P_P}{h^{0.5}b} Y_P(\xi, \zeta) \quad \text{If } P = P_P \quad (2.32)$$

Where the negative sign comes from the fact that  $P$  is a closure force. By substituting the expression (2.27) in (2.31) we obtain:

$$K_I = \frac{M}{h^{1.5}b} Y_M(\xi) - \frac{1}{r^{II}(\xi, \zeta)} \frac{M}{h^{1.5}b} Y_P(\xi, \zeta) \quad \text{If } P < P_P \quad (2.33)$$

The crack propagation condition is defined by the tensional criterion:

$$K_I = K_{IC} \quad (2.34)$$

Where  $K_{IC}$  is the critical stress intensity factor, which represents the matrix toughness and can be found through experimental tests. By substituting (2.31) and (2.33) in (2.34), it is possible to calculate the bending moment which makes the crack propagate. The crack-propagation moment,  $M_F$ , is defined as:

$$M_F = \frac{K_{IC} h^{1.5} b}{Y_M(\xi) - \frac{Y_P(\xi, \zeta)}{r^{II}(\xi, \zeta)}} \quad \text{If } P < P_P \quad (2.35)$$

$$M_F = \frac{K_{IC} h^{1.5} b}{Y_M(\xi)} + \frac{P_P h}{Y_M(\xi)} Y_P(\xi, \zeta) \quad \text{If } P = P_P \quad (2.36)$$

Normalizing the (2.35) and (2.36) relations:

$$\frac{M_F}{K_{IC} h^{1.5} b} = \frac{r^{II}(\xi, \zeta)}{r^{II}(\xi, \zeta) Y_M(\xi) - Y_P(\xi, \zeta)} \quad \text{If } P < P_P \quad (2.37)$$

$$\frac{M_F}{K_{IC} h^{1.5} b} = \frac{1}{Y_M(\xi)} [1 + N_P Y_P(\xi, \zeta)] \quad \text{If } P = P_P \quad (2.38)$$

Where the dimensionless number,  $N_P$ , also known brittleness number, has the following expression:

$$N_P = \frac{P_P}{K_{IC} h^{0.5} b} = \frac{\sigma_y \rho h^{0.5}}{K_{IC}} \quad (2.39)$$

Notice that the brittleness number increases when the reinforcement percentage,  $\rho$ , and the cross section height increases and decreases when the matrix toughness increases.

The dimensionless brittleness number introduction and the particular normalization of the crack-propagation moment comes from an application of Buckingham's theorem to the study of the bending beam collapse. Indeed, the cross section has two different collapse mechanisms, the crack propagation and the fibre plastic flow between the two crack faces, both controlled

by two parameters, the stress,  $\sigma_y [F][L]^{-2}$ , and the critical intensity factor,  $K_{IC} [F][L]^{-2.5}$ . The dimensional analysis allows us to define a characteristic parameter, which represent synthetically the section collapse response. This parameter is the brittleness number, which is obtained by normalizing  $P_P$  through the dimensions chosen as fundamental,  $K_{IC}$  and  $h$ . In addition, also the crack-propagation moment, which characterizes the cross section resistance at the crack depth variation, has been normalized through the same fundamental dimensions.

It is possible to unify the two previous (2.37) and (2.38) expressions by introducing a parameter,  $\alpha(\xi, \zeta) = \frac{P}{P_P}$ . Thanks to (2.27) and (2.29) expressions,  $\alpha$  can be also defined as the ratio between the applied bending moment,  $M$ , and the plastic moment,  $M_P$ ,  $\alpha(\xi, \zeta) = \frac{M}{M_P}$ . Particularly, this relation is valid when the crack reaches its propagation limit.

Substituting  $P = \alpha P_P$  in (2.31), which defines the stress intensity factor at the crack tip, we obtain:

$$K_I = K_{IM} - K_{IP} = \frac{M}{h^{1.5}b} Y_M(\xi) - \frac{\alpha(\xi, \zeta) P_P}{h^{0.5}b} Y_P(\xi, \zeta) \quad (2.40)$$

Thus, it is possible to obtain an expression of the normalized crack-propagation moment by substituting (2.34) in (2.40):

$$\frac{M_F}{K_{IC} h^{1.5} b} = \frac{1}{Y_M(\xi)} [1 + \alpha(\xi, \zeta) N_P Y_P(\xi, \zeta)]$$

$$\alpha(\xi, \zeta) = \begin{cases} 1 & \text{If } P = P_P \\ \frac{P}{P_P} = \frac{M_F}{M_P} = \frac{1}{N_P} \frac{1}{r^{II}(\xi, \zeta) Y_M(\xi) - Y_P(\xi, \zeta)} & \text{If } P < P_P \end{cases} \quad (2.41)$$

Where  $\alpha$  has been found through the ratio between  $M_F$ , (2.37), and  $M_P$ , (2.29). Notice that  $\alpha$  is smaller than one and consequently the fibre reaction force is elastic, if  $N_P$  is higher than  $(r^{II}(\xi, \zeta) Y_M(\xi) - Y_P(\xi, \zeta))^{-1}$ , it becomes dependant on the crack depth; vice versa  $\alpha$  is equal to one and the fibre reaction force is plastic.

It is useful to define the dimensionless plastic moment, normalizing it through the fundamental dimensions. Referring to the (2.29) equation, we obtain:

$$\frac{M_P}{K_{IC} h^{1.5} b} = \frac{r^{II}(\xi, \zeta) P_P h}{K_{IC} h^{1.5} b} = r^{II}(\xi, \zeta) N_P \quad (2.42)$$

Fixing the geometrical and mechanical characteristics of the section in exam and knowing the crack depth and  $N_P$  values, the (2.42) relation has two different solutions, one for the fibre plasticized and one for the fibre in elastic phase. The only acceptable solution is the one with

the lowest crack-propagation moment, which gives the section resistance for the collapsing mechanisms taken into account in the theoretical model.

## 2.7 Localized Rotation

The section localized rotation,  $\Phi$ , which is the rotation increment caused by the crack, can be calculated in function of the applied bending moment, thanks to the superposition principle, as already done for  $w$ . We obtain:

$$\phi = \phi_M + \phi_P = \lambda_{MM}M - \lambda_{MP}P \quad (2.43)$$

Where  $\Phi_M$  and  $\Phi_P$  represent the localized rotation respectively caused by the applied bending moment,  $M$ , and the bridging force,  $P$ , instead  $\lambda_{MM}$  and  $\lambda_{MP}$  are the local compliances.

More specifically,  $\lambda_{MM}$  represents the local rotation caused by a unitary bending moment and can be evaluated through the (2.14) relation:

$$\lambda_{MM} = \frac{2}{Eh^2b} \int_0^\xi Y_M^2(\xi) d\xi \quad (2.44)$$

The mixed compliance,  $\lambda_{MP}$ , which defines the local rotation caused by a unitary force applied in  $\zeta$ , is equal to the crack opening at the fibre level caused by a unitary bending moment,  $\lambda_{PM}$  (2.21), thanks to Betti's theorem.

The localized rotation correspondent to the crack opening,  $M_F$ , results:

$$\phi_F = \lambda_{MM} \left( M_F - \frac{\lambda_{MP}}{\lambda_{MM}} \alpha P_P \right) \quad (2.45)$$

This expression can also be written as:

$$\phi_F = \lambda_{MM} (M_F - r^I(\xi, \zeta) h \alpha P_P) \quad (2.46)$$

Where:

$$r^I(\xi, \zeta) = \frac{\lambda_{MP}}{\lambda_{MM}h} = \frac{\int_\zeta^\xi Y_P(\xi, \zeta) Y_M(\xi) d\xi}{\int_0^\xi Y_M^2(\xi) d\xi} \quad (2.47)$$

Substituting the expression (2.41) of the crack-propagation moment and the definition of the brittleness number,  $N_P$ , we obtain:

$$\phi_F = \frac{2}{Eh^2b} \int_0^\xi Y_M^2(\xi) d\xi K_{IC} b h^{1.5} \left\{ \frac{1}{Y_M(\xi)} [1 + \alpha(\xi, \zeta) Y_P(\xi, \zeta) N_P] - r^I(\xi, \zeta) \alpha(\xi, \zeta) N_P \right\} \quad (2.48)$$

From (2.48), it is possible to express the localized rotation in a normalized form:

$$\frac{\phi_F}{\frac{2K_{IC}}{Eh^{0.5}}} = \frac{\int_0^\xi Y_M^2(\xi) d\xi}{Y_M(\xi)} \{1 + [Y_P(\xi, \zeta) - r^I(\xi, \zeta)Y_M(\xi)]\alpha(\xi, \zeta)N_P\} \quad (2.49)$$

It is interesting to evaluate the localized rotation,  $\Phi_p$ , at the plastic flow limit,  $M = M_P$ , in the hypothesis of the plastic flow preceding the crack propagation:

$$\phi_P = \lambda_{MM}M - \lambda_{MP}P_P = M_P\lambda_{MM} \left[1 - \frac{r^I(\xi, \zeta)}{r^{II}(\xi, \zeta)}\right] \quad \text{If } M_P < M_F \quad (2.50)$$

Substituting the localized compliance expression,  $\lambda_{MM}$ , into the (2.50) relation, and taking into account the (2.36), we obtain:

$$\frac{\phi_P}{\frac{2K_{IC}}{Eh^{0.5}}} = N_P \int_0^\xi Y_M^2(\xi) d\xi [r^{II}(\xi, \zeta) - r^I(\xi, \zeta)] \quad \text{If } M_P < M_F \quad (2.51)$$

## Chapter 3

# The $n$ -Fibres Discrete Model

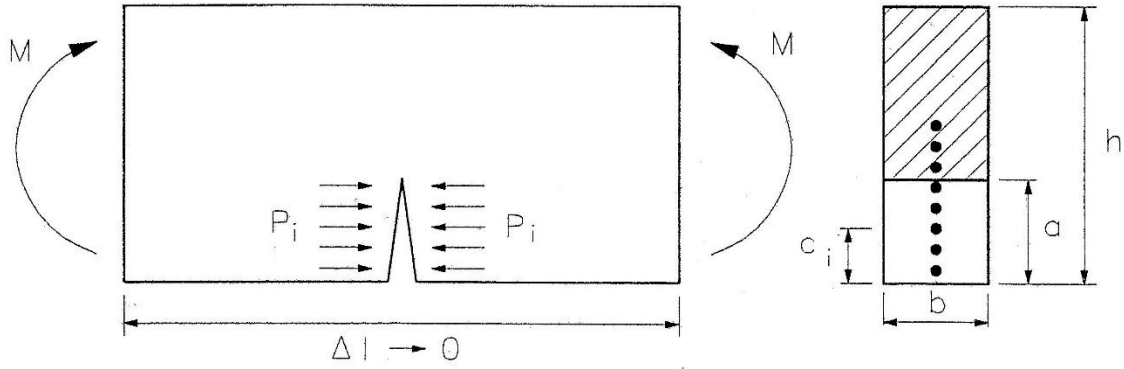
In the following Chapter the  $n$ -fibres discrete model is discussed, which is an extension of the model proposed in chapter 2, to study the bending behaviour of elements reinforced with more than only one localized reinforcement, e.g. fibres, rebars, and rivets. This model studies the crack growth on a bended element by taking into account the bridging forces through concentrated forces acting directly on crack faces.

There are several applications for this model, for example it can easily studies the structural bending response of cementitious materials, reinforced both with rebars and with fibres. The model is also capable of analysing the micro-scale behaviour of multi-phase composites, reinforced by secondary phases uniformly distributed on fragile matrix. In fact, at a micro-structural level the crack growth process is always discontinuous, characterized by local instability, which are caused by the bridging action of each reinforcement element.

### 3.1 The $n$ -Fibres Discrete Model – Matrix Formulation

Let us consider a cross-section of a cracked beam, the height of which is  $b$  and the width of which is  $h$ . Moreover a bending moment,  $M$ , acts in the cracked beam as shown in fig 3.1. The beam is constituted by an elastic-fragile matrix and reinforced by a discrete number of continuous and ductile fibres,  $n$ . Only  $m$  fibres are included by the crack, the depth of which is  $a$ , and  $c_i$  represents the coordinate of the  $i$ -th reinforcement. Actually, the  $i$ -th fibre can be representative of a reinforcement layer located in  $c_i$ ; in this case, the equivalent fibre area will be defined as the summation of all the fibre areas of the layer. The normalized crack depth and the normalized coordinate of the  $i$ -th fibre are respectively  $\xi = \frac{a}{h}$  and  $\zeta_i = \frac{c_i}{h}$ .

The matrix stress-strain curve is assumed to be linear-elastic and a crack-propagation criterion is defined through the linear elastic fracture mechanic principles.

Fig 3. 1- Theoretical scheme of the  $n$ -fibres discrete model.

The bridging force, which the  $m$  fibres apply on crack faces, is represented by closure concentrated forces, which are indeterminate, fig 3.1. The bridging force relation between the reaction force,  $P_i$ , and the relative crack opening,  $w_i$ , is assumed to be rigid-plastic with the aim of describing both a fibre plasticization mechanism and a relative slippage between fibres and matrix.

The bending constitutive response of the cross section is evaluated through an approach analogue to the single fibre model. Therefore, when near the incipient collapse, congruence and equilibrium are defined, at different crack depths. The statically undetermined problem is resolved by applying a series of congruence equations, which refers to a crack opening at the various fibres layers; these permit us to evaluate the  $m$  hyper-static unknown,  $P_1, \dots, P_m$ .

### 3.2 Crack Openings at Fibre level

The relative crack opening,  $w_i$ , at the  $i$ -th fibre level is defined by the superposition principle as:

$$w_i = w_{iM} + \sum_{j=1}^m w_{ij} = \lambda_{iM}M - \sum_{j=1}^m \lambda_{ij}P_j = 0 \quad (3.1)$$

Where  $w_{iM}$  and  $w_{ij}$  are the crack opening at the  $i$ -th fibre level caused respectively by the extern bending moment,  $M$ , and the  $j$ -th fibre reaction force,  $P_j$ ;  $\lambda_{iM}$  and  $\lambda_{ij}$  are the respectively localized compliances, which are caused by the crack presence. In the 2.2 section, the energetic balance, which permits to evaluate the generic localized compliances of a cracked element, has been discussed. In particular, when a bending moment,  $M$ , and  $m$  concentrated forces,  $P_1, \dots, P_m$ , act on crack faces, the (2.13) equation of the generic localized compliance, leads to:

$$\lambda_{iM} = \frac{2}{E} \int_{c_i}^a \frac{K_{iM}K_{ii}}{MP_i} b da \quad (3.2)$$

$$\lambda_{ij} = \frac{2}{E} \int_{c_i}^a \frac{K_{Ii} K_{Ij}}{P_i P_j} b da \quad \text{if } c_i \leq c_j \quad (3.3)$$

Substituting the expressions of the intensity factors, (2.19) and (2.20), into the (3.2) and (3.3) relations, we obtain:

$$\lambda_{iM} = \frac{2}{Ehb} \int_{\zeta_i}^{\xi} Y_{P_i}(\xi, \zeta_i) Y_M(\xi) d\xi \quad (3.4)$$

$$\lambda_{ij} = \lambda_{ji} = \frac{2}{Eb} \int_{\zeta_i}^{\xi} Y_{P_i}(\xi, \zeta_i) Y_{P_j}(\xi, \zeta_j) d\xi \quad \text{If } \zeta_i \leq \zeta_j \quad (3.5)$$

The scheme, assumed to represent the cross-section, permits us to analyse the hyper-static problem in matrix form. Let us define the openings vector  $\{w\} = \{w_1, \dots, w_m\}^T$ , the components of which are the crack openings at the bridging fibres, and the  $m$  fibres unknown reactions  $\{P\} = \{P_1, \dots, P_m\}^T$ . Moreover, let us define the vector of the localized compliances that come from bending moment  $\{\lambda_M\} = \{\lambda_{1M}, \dots, \lambda_{mM}\}^T$  and the matrix of the localized compliances that come from bridging reactions  $[\lambda]$ , the  $ij$ -generic element of which is  $\lambda_{ij}$ . Notice that the  $[\lambda]$  is symmetric because  $\lambda_{ij} = \lambda_{ji}$  for Betti's theorem.

Therefore, from the (3.1) expression it is possible to define the openings vector  $\{w\}$  as:

$$w = \{\lambda_M\}M - [\lambda]\{P\} \quad (3.6)$$

### 3.3 Congruence Condition

During the load process, before reaching a generic fibre plasticization, the bridging action keeps the crack locally closed. Thus, the congruence condition is expressed by the following linear system, in which  $[\lambda]$  is positive defined and symmetric:

$$w = \{\lambda_M\}M - [\lambda]\{P\} = 0 \quad (3.7)$$

The system solution leads to the definition of the unknown reaction-forces vector  $\{P\}$ , which depends on the applied bending moment,  $M$ ; it results:

$$\frac{\{P\}h}{M} = [\lambda]^{-1} \{\lambda_M\}h = \left\{ \frac{1}{r_{II}} \right\} \quad (3.8)$$

Where, analogously to the single fibre model, the dimensionless reaction-forces vector is defined as  $\left\{ \frac{1}{r_{II}} \right\}$ , see eq. (2.29).

In the thicker curves, present in fig. 3.2, the fibres dimensionless reaction forces are shown at each crack depth for a section reinforced by two fibres layers,  $\zeta_1=0.1$  and  $\zeta_2=0.2$ .

Notice that the reaction forces grows with the crack depth, while the section stiffness decreases. The dotted line defines the first fibre reaction force if the second fibre was not present. It is evident how adding a second layer of fibres increases the plastic moment at which the external fibres layer reaches its plastic limit.

The plastic moment,  $M_{pi}$ , can be evaluated by inverting the (3.8) expression and substituting the  $i$ -th  $\{P\}$  vector component with the maximal bridging force,  $P_{pi}$ . In fig 3.2 (b) it is shown how the moment, needed for reaching the fibres plasticisation, is lower when the crack depth is higher, moreover when the crack depth is high, the moment which causes the second fibre plasticization is almost the same as the first one.

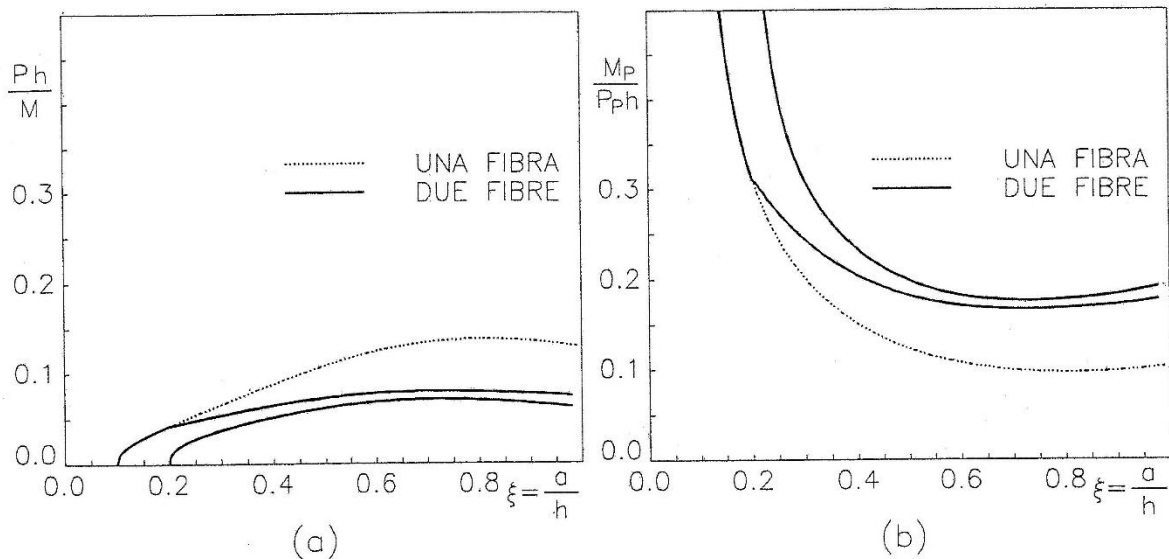


Fig 3. 2- (a) The two fibres hyper-static reactions; (b) Plastic moments.

When the  $i$ -th plastic moment is exceeded, the crack opening  $w_i$ , at the fibre level, becomes other than zero and unknown. In this phase, the problem is solved by imposing a null opening in correspondence of the  $m-1$  fibres not yet plasticized, through the (3.1) equation. Therefore, a linear system of  $m-1$  equation in  $m-1$  unknown is obtained, because the reaction force in the  $i$ -th fibre is known and equal to its maximal value,  $P_{pi}$ .

An analogue procedure is followed to solve the hyper-static problem when the following section fibres plasticize. Notice that the number of equations is always equal to the number of unknowns.

### 3.4 Crack Propagation Condition

The stress intensity factor  $K_I$ , which measures the singular stress field present at the crack tip, is evaluated by the superposition principle. And it is equal to:

$$K_I = K_{IM} - \sum_{i=1}^m K_{Ii} = \frac{M}{h^{1.5}b} Y_M(\xi) - \sum_{i=1}^m \frac{\alpha_i(\xi, \zeta_i) P_{Pi}}{h^{0.5}b} Y_i(\xi, \zeta_i) \quad (3.9)$$

Where  $\alpha_i(\xi, \zeta_i)$  is equal to  $\frac{P_i}{P_{Pi}}$ . When the crack depth increases,  $\alpha_i$ , which depends on the applied bending moment and the  $m$  fibres reaction forces, can be evaluated through the (3.8) expression or analogue relations when one or more fibres are plasticized.

The crack-propagation condition is defined by the tensional criterion:

$$K_I = K_{IC} \quad (3.10)$$

Where  $K_I$  is the stress intensity factor defined by the (3.9) relation and  $K_{IC}$  is the respective critical value, characteristic of the material composing the matrix.

By imposing the crack-propagation condition to the (3.9) relation, an expression for the crack-propagation moment,  $M_F$ , can be evaluated. In a dimensionless form, we obtain:

$$\frac{M_F}{K_{IC} h^{1.5} b} = \frac{1}{Y_M(\xi)} \left[ 1 + \sum_{i=1}^m \frac{\alpha_i(\xi, \zeta_i) P_{Pi}}{K_{IC} h^{0.5} b} Y_{Pi}(\xi, \zeta_i) \right] \quad (3.11)$$

If all the fibres are realized with the same material, the limit plastic-flow stresses coincide  $\sigma_{yi} = \sigma_y, (i = 1, 2, \dots, n)$  and the (8.11) equation can be expressed as follows:

$$\frac{M_F}{K_{IC} h^{1.5} b} = \frac{1}{Y_M(\xi)} \left[ 1 + \frac{N_P}{\rho} \sum_{i=1}^m \rho_i \alpha_i(\xi, \zeta_i) Y_{Pi}(\xi, \zeta_i) \right] \quad (3.12)$$

Where  $\rho_i$  is the percentage relative to the  $i$ -th reinforcement and  $N_P$  is the brittleness number that is defined as:

$$N_P = \frac{P_P}{K_{IC} h^{0.5} b} = \frac{\sigma_y \rho h^{0.5}}{K_{IC}} \quad (3.13)$$

In which  $\rho$  is the section total reinforcement percentage,  $A$  is the section total fibres area,  $A = \sum_{i=1}^n A_i$  and  $P_P = \rho \sigma_y$ . The brittleness number,  $N_P$ , depends on the section height, total reinforcement percentage and matrix toughness.

### 3.5 Localized Rotation

The localized rotation, namely the one caused only by the crack presence, can be defined by applying the superposition principle analogously to what has been done with the evaluation

of the crack openings vector  $\{w\}$ . It results dependant on the applied moment and the  $m$  reaction forces, through the following expression:

$$\phi = \phi_M + \sum_{i=1}^m \phi_i = \lambda_{MM}M - \sum_{i=1}^m \lambda_{Mi}P_i = \lambda_{MM}M - \{\lambda_M\}^T\{P\} \quad (3.14)$$

Where  $\Phi_M$  and  $\Phi_i$  are the localized rotations caused respectively by the bending moment,  $M$ , and the concentrated forces,  $P_i$ .  $\lambda_{Mi}$  is the localized rotation caused by two unitary reaction forces applied in  $c_i$  and, according to the Betti's theorem, coincides to  $\lambda_{iM}$  that has been defined in the (3.4) relation. The local compliance  $\lambda_{MM}$  represents the rotation caused by a unitary bending moment and it is defined as:

$$\lambda_{MM} = \frac{2}{Eh^2b} \int_0^\xi Y_M^2(\xi) d\xi \quad (3.15)$$

The rotation,  $\Phi$ , can be calculated for each equilibrated and congruent configuration at each crack depth. After having evaluated, for each crack depth, the crack propagation moment,  $M_F$  (3.12) eq., and the respective localized rotation, (3.15) eq., the bending constitutive curve of the composite material can be obtained. It is in function of the geometrical and mechanical element properties through the brittleness number,  $N_P$ , which is the dimensionless parameter that synthetically governs the section structural response.

## Chapter 4

# Software Implementation

The algorithm described in chapter 3 – the discontinuous bridged crack model for fibres-reinforced materials in flexure – has been implemented in a software, which is capable of studying the crack propagation in bending beams. In this chapter, the software *functions* are reported and described.

### 4.1 $\lambda_{ij}$ – Compliance<sub>ij</sub>

The Compliance<sub>ij</sub> function calculates the generic element,  $\lambda_{ij}$ , of the compliance matrix,  $[\lambda]$ .

The shape function,  $Y_P(\xi, \zeta)$ , used is the one proposed in (Tada, Paris, Irwin, 1985) and it is equal to:

$$g_1(\xi) = 0.46 + 3.06 \xi + 0.84(1 - \xi)^5 + 0.66\xi^2(1 - \xi)^2$$

$$g_2(\xi) = -3.53\xi^2$$

$$g_3(\xi) = 6.17 - 28.22\xi + 34.54\xi^2 - 14.39\xi^3 - (1 - \xi)^{1.5} - 5.88(1 - \xi)^5 - 2.64\xi^2(1 - \xi)^2$$

$$g_4(\xi) = -6.63 + 25.16\xi - 31.04\xi^2 + 14.41\xi^3 + 2(1 - \xi)^{1.5} + 5.04(1 - \xi)^5 + 1.98\xi^2(1 - \xi)^2$$

$$G(\xi, \zeta) = g_1(\xi) + g_2(\xi) \frac{\zeta}{\xi} + g_3(\xi) \left(\frac{\zeta}{\xi}\right)^2 + g_4(\xi) \left(\frac{\zeta}{\xi}\right)^3$$

$$Y_P(\xi, \zeta) = \frac{2}{\sqrt{\pi\xi}} \frac{1}{(1-\xi)^{1.5} \sqrt{1-\left(\frac{\zeta}{\xi}\right)^2}} G(\xi, \zeta) \quad (4.1)$$

The Compliance<sub>ij</sub> function script is below reported:

```

1. function [l_ij] = Compliance_ij(zi,zj,epsi,b,E)
2.
3. %Compliance_ij Calculate the compliance at node i due to reclosure force at
4. %node j
5. %
6. %Synopsis: [l_ij] = Compliance_ij(zi,zj,epsi,h,b,E)
7. %
8. %Input:  zi   = normalized position of fiber i
9. %        zj   = normalized position of fiber j
10. %       epsi  = normalized position fo crack tip
11. %        b    = width of element
12. %        E    = Young Modulus
13. %Output: l_ij = compliance at node i due to reclosure force at node j
14.
15. g1 = @(e) 0.46+3.06*e+0.84*(1-e).^5+0.66*e.^2.*(1-e).^2;
16. g2 = @(e) -3.52.*e.^2;
17. g3 = @(e) 6.17-28.22*e+34.54*e.^2-14.39*e.^3-(1-e).^1.5-5.88*(1-e).^5-
    2.64*e.^2.*(1-e).^2;
18. g4 = @(e) -6.63+25.16*e-31.04*e.^2+14.41*e.^3+2*(1-e).^1.5+5.04*(1-
    e).^5+1.98*e.^2.*(1-e).^2;
19. Gi = @(e) g1(e)+g2(e).*(zi./e)+g3(e).*(zi.^2./e.^2)+g4(e).*(zi.^3./e.^3);
20. Y_Pi = @(e) (2./(pi.*e).^0.5).*(1./((1-e).^1.5.*(1-(zi./e).^2).^0.5)).*Gi(e);
21. Gj = @(e) g1(e)+g2(e).*(zj./e)+g3(e).*(zj.^2./e.^2)+g4(e).*(zj.^3./e.^3);
22. Y_Pj = @(e) (2./(pi.*e).^0.5).*(1./((1-e).^1.5.*(1-(zj./e).^2).^0.5)).*Gj(e);
23. Y = @(e) Y_Pi(e).*Y_Pj(e);
24. zj = max(zj,zi) + 10^-5;
25. l_ij = real((2/(b*E))*integral(Y,zj,epsi));
26. if isnan(l_ij)
27.     l_ij = 0;
28. end
29. end

```

## 4.2 $[\lambda]$ – Compliance\_Matrix

The Compliance\_Matrix function collects all  $\lambda_{ij}$  the element in the compliance matrix,  $[\lambda]$ .

The function script is below reported:

```

1. function [l] = Compliance_Matrix(nf,z0,zf,epsi,b,E)
2.
3. %Compliance_Matrix Calculate the local compliance matrix
4. %
5. %Synopsis: [l] = Compliance_Matrix(nf,z0,zf,epsi,h,b,E)
6. %
7. %Input:  nf   = number of fibers
8. %        z0   = normalized position of first fiber
9. %        zf   = normalized position of last fiber
10. %       epsi  = normalized position fo crack tip
11. %        b    = width of element
12. %        E    = Young Modulus
13. %Output: l    = local compliance matrix
14.
15. zi = z0;
16. zj = z0;
17. i = 1;
18. j = 1;
19. passo = (zf-z0)/(nf-1);
20. flag = true;
21. while flag
22.     while zi < epsi && zi <= zf
23.         l(i,j) = Compliance_ij(zi,zj,epsi,b,E);

```

```

24.     zi = zi + passo;
25.     i = i + 1;
26.     end
27.     [m,n] = size(l);
28.     flag = j < m;
29.     j = j + 1;
30.     i = 1;
31.     zi = z0;
32.     zj = zj + passo;
33. end
34. end

```

### 4.3 $\lambda_{iM}$ – Compliance\_iM

The Compliance\_iM function calculates the compliance,  $\lambda_{iM}$ , at the i-th fiber position caused by the bending moment,  $M$ .

The shape function,  $Y_M(\xi)$ , used is the one proposed in (Tada, Paris, Irwin, 1985) and it is equal to:

$$Y_M(\xi) = 6(1.99\xi^{0.5} - 2.47\xi^{1.5} + 12.97\xi^{2.5} - 23.17\xi^{3.5} + 24.8\xi^{4.5}) \quad \text{If } \xi \leq 0.6$$

$$Y_M(\xi) = \frac{3.99}{(1-\xi)^{1.5}}, \quad \xi \geq 0.6 \quad (4.2)$$

The Compliance\_iM function script is below reported:

```

1. function [l_iM] = Compliance_iM(zi,epsi,h,b,E)
2.
3. %Compliance_iM Calculate the compliance at node i due to M
4. %
5. %Synopsis: [l_iM] = Compliance_iM(zi,epsi,h,b,E)
6. %
7. %Input:  zi   = normalized position of fiber i
8. %        epsi = normalized position fo crack tip
9. %        h    = height of element
10. %        b    = width of element
11. %        E    = Young Modulus
12. %Output: l_iM = compliance at node i due to M
13.
14. if epsi<=0.6
15.     Y_M = @(e) 6*(1.99*e.^0.5-2.47*e.^1.5+12.97*e.^2.5-23.17*e.^3.5+24.8*e.^4.5);
16. else
17.     Y_M = @(e) 3.99./((1-e).^1.5);
18. end
19. g1 = @(e) 0.46+3.06*e+0.84*(1-e).^5+0.66*e.^2.*(1-e).^2;
20. g2 = @(e) -3.52.*e.^2;
21. g3 = @(e) 6.17-28.22*e+34.54*e.^2-14.39*e.^3-(1-e).^1.5-5.88*(1-e).^5-
    2.64*e.^2.*(1-e).^2;

```

```

22. g4 = @(e) -6.63+25.16*e-31.04*e.^2+14.41*e.^3+2*(1-e).^1.5+5.04*(1-
    e).^5+1.98*e.^2.*(1-e).^2;
23. Gi = @(e) g1(e)+g2(e).*(zi./e)+g3(e).*(zi.^2./e.^2)+g4(e).*(zi.^3./e.^3);
24. Y_Pi = @(e) (2./(pi.*e).^0.5).*(1./((1-e).^1.5.*(1-(zi./e).^2).^0.5)).*Gi(e);
25. Y = @(e) Y_M(e).*Y_Pi(e);
26. l_iM = (2/(h*b*E))*integral(Y,zi,epsi);
27. if isnan(l_iM)
28.     l_iM = 0;
29. end
30. end

```

#### 4.4 $\lambda_M$ – Compliance\_vectorM

The Compliance\_vectorM function collects all  $\lambda_{iM}$  the element in the compliance vector,  $\lambda_{iM}$ . The function script is below reported:

```

1. function [l_M] = Compliance_vectorM(nf,z0,zf,epsi,h,b,E)
2.
3. %Compliance_vectorM Calculate the compliance vector due to M
4. %
5. %Synopsis: [l_M] = Compliance_vectorM(nf,z0,zf,epsi,h,b,E)
6. %
7. %Input:  nf   = number of fibers
8. %        z0   = normalized position of first fiber
9. %        zf   = normalized position of last fiber
10. %        epsi = normalized position fo crack tip
11. %        h    = height of element
12. %        b    = width of element
13. %        E    = Young Modulus
14. %Output: l_M = compliance vector due to M
15.
16. z = z0;
17. i = 1;
18. passo = (zf-z0)/(nf-1);
19. while epsi>z && zf>=z
20.     l_M(i) = Compliance_iM(z,epsi,h,b,E);
21.     z = z + passo;
22.     i = i + 1;
23. end
24. end

```

#### 4.5 $\lambda_{MM}$ – Compliance\_MM

The Compliance\_MM function calculates the compliance,  $\lambda_{MM}$ , in bending caused by the bending moment,  $M$ . The function script is below reported:

```

1. function [l_MM] = Compliance_MM(eps_i,h,b,E)
2.
3. %Compliance_MM Calculate the compliance due to M
4. %
5. %Synopsis: [l_MM] = Compliance_MM(eps_i,h,b,E)
6. %
7. %Input:  eps_i = normalized position fo crack tip

```

```

8. %      h   = height of element
9. %      b   = width of element
10. %     E   = Young Modulus
11. %Output: l_iM = compliance due to M
12.
13. if epsi<=0.6
14.     Y_M = @(e) 6*(1.99*e.^0.5-2.47*e.^1.5+12.97*e.^2.5-23.17*e.^3.5+24.8*e.^4.5);
15. else
16.     Y_M = @(e) 3.99./((1-e).^1.5);
17. end
18. Y     = @(e) Y_M(e).*Y_M(e);
19. l_MM = (2/((h^2)*b*E))*integral(Y,0,epsi);
20. end

```

## 4.6 $M_F, \Phi$ – Normalized\_failure\_M

The Normalized\_failure\_M function calculates the crack propagation moment for first,  $M_F$ , and then its respective rotation,  $\Phi$ .

Calculations are made iterative by increasing the acting bending moment,  $M$ . First of all, for each  $M$  the fibres tensional state is evaluated, after that there are two possible ways to exit the loop and find the correct value of the crack propagation moment, the former occurs when all the fibres are plasticized and the respective  $M_F$  is the correct one, the latter occurs when the acting bending moment,  $M$ , exceeds  $M_F$ .

The function script is below reported:

```

1. function [M_f,PHI] = Normalized_failure_M(nf,z0,zf,epsi,h,b,E,sigma_y,r,K_IC)
2.
3. %Normalized_failure_M Calculate the normalized crack-propagation moment
4. %and its respective local rotation
5. %
6. %Synopsis: [M_f,PHI] = Normalized_failure_M(nf,z0,zf,epsi,h,b,E,sigma_y,r,K_IC)
7. %
8. %Input:  nf      = number of fibers
9. %        z0      = normalized position of first fiber
10. %        zf      = normalized position of last fiber
11. %        epsi    = normalized position of crack tip
12. %        h       = height of element
13. %        b       = width of element
14. %        E       = Young Modulus
15. %        sigma_y = yield strength fibers
16. %        r       = fiber radius
17. %        K_IC    = critical stress intensity factor
18. %Output: M_f    = crack-propagation moment
19. %        PHI     = local rotation
20.
21. l = Compliance_Matrix(nf,z0,zf,epsi,b,E);
22. l_M = Compliance_vectorM(nf,z0,zf,epsi,h,b,E);
23. l_MM = Compliance_MM(eps_i,h,b,E);
24. if epsi<=0.6
25.     Y_M = 6*(1.99*epsi^0.5-2.47*epsi^1.5+12.97*epsi^2.5-
26.     23.17*epsi^3.5+24.8*epsi^4.5);
27. else
28.     Y_M = 3.99./((1-epsi)^1.5);
29. end

```

```

29. g1 = 0.46+3.06*epsi+0.84*(1-epsi)^5+0.66*epsi^2*(1-epsi)^2;
30. g2 = -3.52*epsi^2;
31. g3 = 6.17-28.22*epsi+34.54*epsi^2-14.39*epsi^3-(1-epsi)^1.5-5.88*(1-epsi)^5-
    2.64*epsi^2*(1-epsi)^2;
32. g4 = -6.63+25.16*epsi-31.04*epsi^2+14.41*epsi^3+2*(1-epsi)^1.5+5.04*(1-
    epsi)^5+1.98*epsi^2*(1-epsi)^2;
33. Gi = @(zi) g1+g2*(zi/epsi)+g3*(zi.^2/epsi.^2)+g4*(zi.^3/epsi.^3);
34. Y_Pi = @(zi) (2/(pi*epsi)^0.5)*(1/((1-epsi)^1.5*(1-(zi/epsi).^2).^0.5))*Gi(zi);
35. roi = (pi*r^2)/(h*b);
36. N_P = (sigma_y * roi* nf * h^0.5)/K_IC;
37. M = 10000;
38. flag = 1;
39. while flag
40.     P = inv(1) * l_M' * M;
41.     [m,n] = size(P);
42.     m = max(m,n);
43.     lt = 1;
44.     l_Mt = l_M;
45.     lp = [];
46.     i = 1;
47.     P(i)> sigma_y*roi*h*b;
48.     while P(i)> sigma_y*roi*h*b
49.         lp(:,i) = lt(:,1);
50.         lt(1,:) = [];
51.         lp(1,:) = [];
52.         lt(:,1) = [];
53.         l_Mt(1) = [];
54.         l0 = lp(:,1) * sigma_y*roi*h*b;
55.         for t=2:i
56.             l0 = l0 + lp(:,t) * sigma_y*roi*h*b;
57.         end
58.         P = inv(lt) * (l_Mt' * M - l0);
59.         if isempty(P)
60.             passo = (zf-z0)/(nf-1);
61.             i=1;
62.             for g=z0:passo:min(epsi,zf)
63.                 P(i)= sigma_y*roi*h*b;
64.                 i=i+1;
65.             end
66.             break
67.         end
68.         i = i +1;
69.         [o,n] = size(P);
70.         o = max(o,n);
71.         p = m - o;
72.         for t = 1:p
73.             while o > 0
74.                 P(o+1) = P(o);
75.                 o = o -1;
76.             end
77.             P(1) = sigma_y*roi*h*b;
78.             [o,n] = size(P);
79.             o = max(o,n);
80.         end
81.         if i-1==m
82.             break
83.         end
84.     end
85.     if P(m)==sigma_y*roi*h*b
86.         flag = 0;
87.     end
88.     passo = (zf-z0)/(nf-1);
89.     Z(1) = z0;
90.     for i=2:nf
91.         Z(i) = Z(i -1) + passo;
92.     end

```

```

93.     [m,n] = size(P);
94.     m = max(m,n);
95.     for i=1:m
96.         Y_P(i)=Y_Pi(Z(i));
97.     end
98.     alpha = P/(sigma_y*roi*h*b);
99.     S = 0;
100.    for i=1:m
101.        S = S + roi*alpha(i)*Y_P(i);
102.    end
103.    M_f = K_IC*h^1.5*b*(1/Y_M)*(1+N_P*S/(roi*nf));
104.    if M>M_f
105.        flag=0;
106.    else
107.        M = M + 100;
108.    end
109.    M_f =M_f/(K_IC*h^1.5*b);
110. end
111. M_f1 =M_f*(K_IC*h^1.5*b);
112. [m,n] = size(P);
113. m = max(m,n);
114. S = 0;
115. for i=1:m
116.     S = S + alpha(i)*roi*l_M(i);
117. end
118. PHI= (M_f1*l_MM - N_P*S/(roi*nf));
119. end

```

## 4.7 Main

For each crack depth, the Main function makes The Normalized\_failure\_M function run; collects the results and then plots the element response curve. The function script is below reported:

```

1. function [] = Main(nf,z0,zf,epsi,h,b,E,sigma_y,r,K_IC)
2.
3. %Main Collect and plot the Results
4. %
5. %Synopsis: [] = Main(nf,z0,zf,epsi,h,b,E,sigma_y,r,K_IC)
6. %
7. %Input:  nf      = number of fibers
8. %        z0      = normalized position of first fiber
9. %        zf      = normalized position of last fiber
10. %        epsi    = normalized position fo crack tip
11. %        h       = height of element
12. %        b       = width of element
13. %        E       = Young Modulus
14. %        sigma_y = tensile strenght of fibers
15. %        r       = radius of fibers
16. %        K_IC    = critical stress intensity factor
17. %
18. %Output: Plot of M_f and PHI
19.
20. i=1;
21. passo = (zf-z0)/(nf-1);
22. Z(1) = z0;
23. for t=2:nf
24.     Z(t) = Z(t -1) + passo;
25. end

```

```

26. t=1;
27. while epsi < Z(t)
28.     t = t+1;
29. end
30. [M_f(i),PHI(i)]= Normalized_failure_M(nf,z0,zf,epsi,h,b,E,sigma_y,r,K_IC);
31. i = i+1;
32. flag = 1;
33. while epsi<0.7
34.     if flag
35.         if epsi < Z(t)
36.             epsi = Z(t) + 0.001;
37.             t = t+1;
38.             if t > nf
39.                 flag = 0;
40.             end
41.         else
42.             epsi = epsi + 0.005;
43.         end
44.     else
45.         epsi = epsi + 0.005;
46.     end
47.     [M_f(i),PHI(i)]= Normalized_failure_M(nf,z0,zf,epsi,h,b,E,sigma_y,r,K_IC);
48.     i = i+1;
49. end
50. f = plot([0,PHI],[0,M_f]);
51. f.LineWidth = 2.00;
52. t = xlabel('\Phi[rad]','interpret','latex','fontsize',18);
53. t.FontWeight = 'bold';
54. t.Color = 'blu';
55. p = ylabel('\frac{M}{K_{IC}}bh^{\frac{3}{2}}','interpret','latex','fontsize',20);
56. p.FontWeight = 'bold';
57. p.Color = 'blu';
58. end

```

## 4.8 Graphic User Interface

The GUI is simply composed by only one window, which is divided into two section; the first one collects all the input data, a button makes the program calculate and the result –the element response curve– is plotted in the second below section. In fig. 4.1 the graphic interface is shown; although there are some suggested units, written near each input line, the program is capable of working with every congruent units system, because the results are dimensionless.

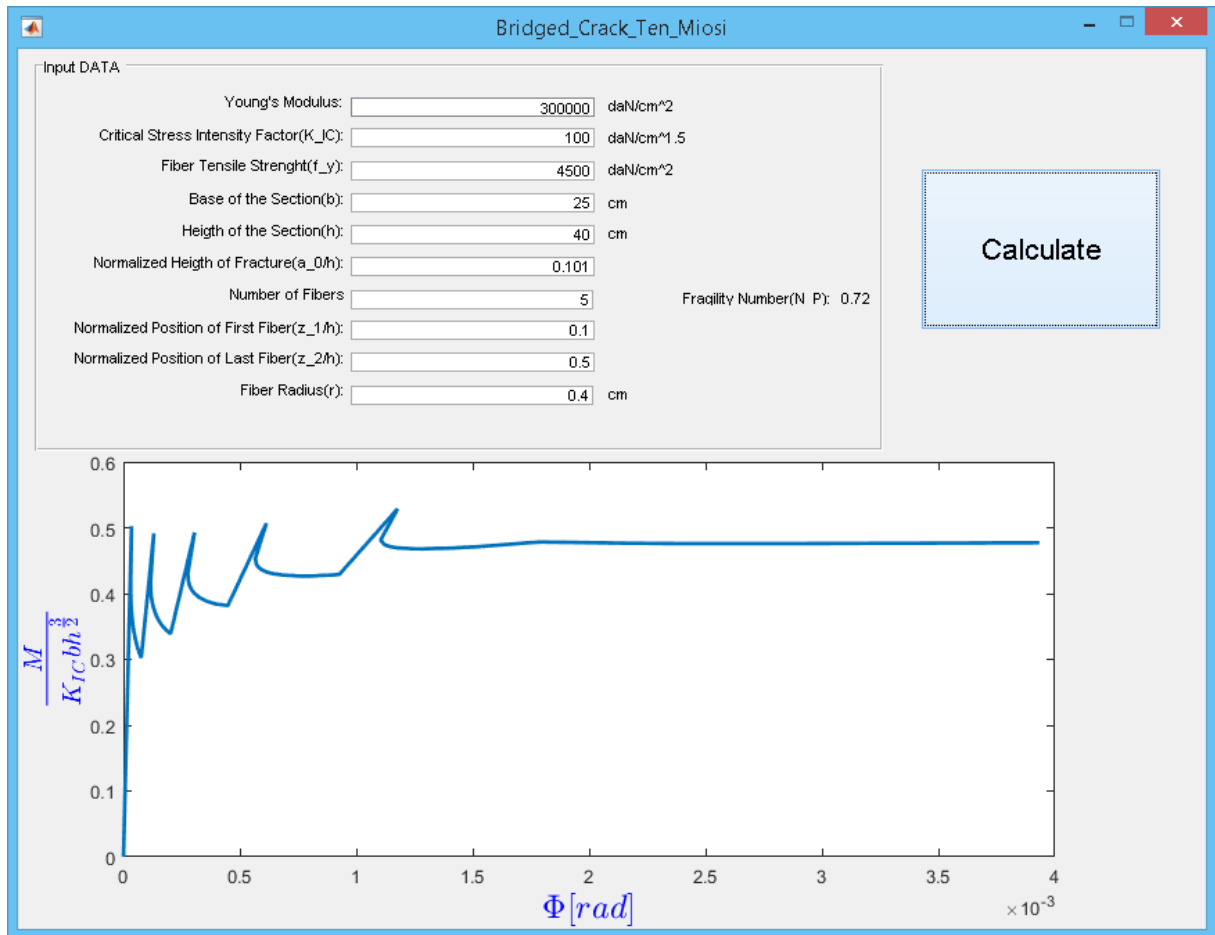


Fig 4. 1- Program GUI.

The function script is below reported:

```

1. function varargout = Bridged_Crack_Ten_Miosi(varargin)
2.
3. % BRIDGED_CRACK_TEN_MIOSI MATLAB code for Bridged_Crack_Ten_Miosi.fig
4. % BRIDGED_CRACK_TEN_MIOSI, by itself, creates a new BRIDGED_CRACK_TEN_MIOSI or
5. % raises the existing
6. % singleton*.
7. % H = BRIDGED_CRACK_TEN_MIOSI returns the handle to a new BRIDGED_CRACK_TEN_MIO
8. % SI or the handle to
9. % the existing singleton*.
10. % BRIDGED_CRACK_TEN_MIOSI('CALLBACK',hObject,eventData,handles,...) calls the l
11. % ocal
12. % function named CALLBACK in BRIDGED_CRACK_TEN_MIOSI.M with the given input arg
13. % uments.
14. % BRIDGED_CRACK_TEN_MIOSI('Property','Value',...) creates a new BRIDGED_CRACK_T
15. % EN_MIOSI or raises the
16. % existing singleton*. Starting from the left, property value pairs are
17. % applied to the GUI before Bridged_Crack_Ten_Miosi_OpeningFcn gets called. An
18. % unrecognized property name or invalid value makes property application
19. % stop. All inputs are passed to Bridged_Crack_Ten_Miosi_OpeningFcn via varargin.

```

```

19. % Begin initialization code - DO NOT EDIT
20.
21. gui_Singleton = 1;
22. gui_State = struct('gui_Name',       mfilename, ...
23.                  'gui_Singleton',   gui_Singleton, ...
24.                  'gui_OpeningFcn', @Bridged_Crack_Ten_Miosi_OpeningFcn, ...
25.                  'gui_OutputFcn',  @Bridged_Crack_Ten_Miosi_OutputFcn, ...
26.                  'gui_LayoutFcn',  [], ...
27.                  'gui_Callback',    []);
28. if nargin && ischar(varargin{1})
29.     gui_State.gui_Callback = str2func(varargin{1});
30. end
31.
32. if nargin
33.     [varargout{1:nargout}] = gui_mainfcn(gui_State, varargin{:});
34. else
35.     gui_mainfcn(gui_State, varargin{:});
36. end
37. % End initialization code - DO NOT EDIT
38.
39.
40. % --- Executes just before Bridged_Crack_Ten_Miosi is made visible.
41. function Bridged_Crack_Ten_Miosi_OpeningFcn(hObject, eventdata, handles, varargin)
42. % hObject    handle to figure
43. % Choose default command line output for Bridged_Crack_Ten_Miosi
44. handles.output = hObject;
45.
46. % Update handles structure
47. guidata(hObject, handles);
48.
49.
50. function varargout = Bridged_Crack_Ten_Miosi_OutputFcn(hObject, eventdata, handles)
51. % varargout  cell array for returning output args (see VARARGOUT);
52. % hObject    handle to figure
53. % handles    structure with handles and user data (see GUIDATA)
54. % Get default command line output from handles structure
55. varargout{1} = handles.output;
56.
57.
58. % hObject    handle to E (see GCBO)
59. function E_CreateFcn(hObject, eventdata, handles)
60. if ispc && isequal(get(hObject,'BackgroundColor'), get(0,'defaultUicontrolBackground
    Color'))
61.     set(hObject,'BackgroundColor','white');
62. end
63.
64. % Save the new E value
65. handles.metricdata.E = E*10^5;
66. guidata(hObject,handles)
67.
68. function E_Callback(hObject, eventdata, handles)
69. E = str2double(get(hObject, 'String'));
70. if isnan(E)
71.     set(hObject, 'String', 0);
72.     errordlg('Input must be a number','Error');
73. end
74.
75.
76. % hObject    handle to K_IC (see GCBO)
77. function K_IC_Callback(hObject, eventdata, handles)
78. K_IC = str2double(get(hObject, 'String'));
79. if isnan(K_IC)
80.     set(hObject, 'String', 0);
81.     errordlg('Input must be a number','Error');
82. end

```

```

83.
84. % Save the new K_IC value
85. handles.metricdata.K_IC = K_IC*(100^(3/2)*10);
86. guidata(hObject,handles)
87.
88. function K_IC_CreateFcn(hObject, eventdata, handles)
89. if ispc && isequal(get(hObject,'BackgroundColor'), get(0,'defaultUicontrolBackground
    Color'))
90.     set(hObject,'BackgroundColor','white');
91. end
92.
93.
94. % hObject    handle to f_y (see GCBO)
95. function f_y_Callback(hObject, eventdata, handles)
96. f_y = str2double(get(hObject, 'String'));
97. if isnan(f_y)
98.     set(hObject, 'String', 0);
99.     errordlg('Input must be a number','Error');
100. end
101.
102. % Save the new f_y value
103. handles.metricdata.f_y = f_y*10^5;
104. guidata(hObject,handles)
105.
106. function f_y_CreateFcn(hObject, eventdata, handles)
107. if ispc && isequal(get(hObject,'BackgroundColor'), get(0,'defaultUicontrolBackgr
    oundColor'))
108.     set(hObject,'BackgroundColor','white');
109. end
110.
111.
112. % hObject    handle to b (see GCBO)
113. function b_Callback(hObject, eventdata, handles)
114. b = str2double(get(hObject, 'String'));
115. if isnan(b)
116.     set(hObject, 'String', 0);
117.     errordlg('Input must be a number','Error');
118. end
119.
120. % Save the new b value
121. handles.metricdata.b = b/100;
122. guidata(hObject,handles)
123.
124. function b_CreateFcn(hObject, eventdata, handles)
125. if ispc && isequal(get(hObject,'BackgroundColor'), get(0,'defaultUicontrolBackgr
    oundColor'))
126.     set(hObject,'BackgroundColor','white');
127. end
128.
129.
130. % hObject    handle to h (see GCBO)
131. function h_Callback(hObject, eventdata, handles)
132. h = str2double(get(hObject, 'String'));
133. if isnan(h)
134.     set(hObject, 'String', 0);
135.     errordlg('Input must be a number','Error');
136. end
137.
138. % Save the new h value
139. handles.metricdata.h = h/100;
140. guidata(hObject,handles)
141.
142. function h_CreateFcn(hObject, eventdata, handles)
143. if ispc && isequal(get(hObject,'BackgroundColor'), get(0,'defaultUicontrolBackgr
    oundColor'))
144.     set(hObject,'BackgroundColor','white');

```

```

145.     end
146.
147.
148.     % hObject    handle to epsi (see GCBO)
149.     function epsi_Callback(hObject, eventdata, handles)
150.         epsi = str2double(get(hObject, 'String'));
151.         if isnan(eps)
152.             set(hObject, 'String', 0);
153.             errordlg('Input must be a number','Error');
154.         end
155.
156.         % Save the new epsi value
157.         handles.metricdata.epsi = epsi;
158.         guidata(hObject,handles)
159.
160.     function epsi_CreateFcn(hObject, eventdata, handles)
161.         if ispc && isequal(get(hObject,'BackgroundColor'), get(0,'defaultUicontrolBackgr
oundColor'))
162.             set(hObject,'BackgroundColor','white');
163.         end
164.
165.
166.     % hObject    handle to nf (see GCBO)
167.     function nf_Callback(hObject, eventdata, handles)
168.         nf = str2double(get(hObject, 'String'));
169.         if isnan(nf)
170.             set(hObject, 'String', 0);
171.             errordlg('Input must be a number','Error');
172.         end
173.
174.         % Save the new nf value
175.         handles.metricdata.nf = nf;
176.         guidata(hObject,handles)
177.
178.     function nf_CreateFcn(hObject, eventdata, handles)
179.         if ispc && isequal(get(hObject,'BackgroundColor'), get(0,'defaultUicontrolBackgr
oundColor'))
180.             set(hObject,'BackgroundColor','white');
181.         end
182.
183.
184.     % hObject    handle to z1 (see GCBO)
185.     function z1_Callback(hObject, eventdata, handles)
186.         z1 = str2double(get(hObject, 'String'));
187.         if isnan(z1)
188.             set(hObject, 'String', 0);
189.             errordlg('Input must be a number','Error');
190.         end
191.
192.         % Save the new z1 value
193.         handles.metricdata.z1 = z1;
194.         guidata(hObject,handles)
195.
196.     function z1_CreateFcn(hObject, eventdata, handles)
197.         if ispc && isequal(get(hObject,'BackgroundColor'), get(0,'defaultUicontrolBackgr
oundColor'))
198.             set(hObject,'BackgroundColor','white');
199.         end
200.
201.
202.     % hObject    handle to z2 (see GCBO)
203.     function z2_Callback(hObject, eventdata, handles)
204.         z2 = str2double(get(hObject, 'String'));
205.         if isnan(z2)
206.             set(hObject, 'String', 0);
207.             errordlg('Input must be a number','Error');

```

```

208.     end
209.
210.     % Save the new z2 value
211.     handles.metricdata.z2 = z2;
212.     guidata(hObject,handles)
213.
214.     function z2_CreateFcn(hObject, eventdata, handles)
215.     if ispc && isequal(get(hObject,'BackgroundColor'), get(0,'defaultUicontrolBackgr
oundColor'))
216.         set(hObject,'BackgroundColor','white');
217.     end
218.
219.
220.     % hObject    handle to r (see GCBO)
221.     function r_Callback(hObject, eventdata, handles)
222.     r = str2double(get(hObject, 'String'));
223.     if isnan(r)
224.         set(hObject, 'String', 0);
225.         errordlg('Input must be a number','Error');
226.     end
227.
228.     % Save the new r value
229.     handles.metricdata.r = r/100;
230.     guidata(hObject,handles)
231.
232.     function r_CreateFcn(hObject, eventdata, handles)
233.     if ispc && isequal(get(hObject,'BackgroundColor'), get(0,'defaultUicontrolBackgr
oundColor'))
234.         set(hObject,'BackgroundColor','white');
235.     end
236.
237.
238.     % --- Executes on button press in calculate.
239.     function calculate_Callback(hObject, eventdata, handles)
240.     N_P = (handles.metricdata.f_y * ((pi*handles.metricdata.r^2)/(handles.metricdat
a.h*handles.metricdata.b)) * handles.metricdata.nf * handles.metricdata.h^0.5)/handl
es.metricdata.K_IC;
241.     N_P = num2str(round(N_P,2));
242.     Main(handles.metricdata.nf,handles.metricdata.z1,handles.metricdata.z2,handles.m
etricdata.epsi,handles.metricdata.h,handles.metricdata.b,handles.metricdata.E,handl
es.metricdata.f_y,handles.metricdata.r,handles.metricdata.K_IC)
243.     set(handles.N_P, 'String', N_P);

```

## Chapter 5

### Case Studies

In this chapter, some case studies are shown for different number of reinforcement fibres and brittleness number,  $N_p$ . Indeed, the results are reported in an abacus form, which better displays the fragile-ductile transition occurring for a specific brittleness number value,  $N_{pt}$ .

#### 5.1 The Single Fibre Abacus

The beam constitutive response can be evaluated by studying the evolution of crack propagation and defining for each crack depth the crack-propagation moment,  $M_F$ , and its relative localized rotation,  $\Phi_p$ , respectively defined through (3.12) and (3.14) relations. The dimensionless crack-propagation moment results dependant on the crack depth, the fibres state, through  $\alpha$ , and the mechanic and geometric characteristics of the cross-section, through the brittleness number,  $N_p$ .

In fig 5.1 normalized moment-rotation curves are shown, obtained by varying the brittleness number,  $N_p$ , for a beam, with one layer of reinforcement positioned in  $c = 0.1h$  and with an initial crack equal to the reinforcement height. The cases analysed are the ones obtained by varying  $N_p$  from 0.1 to 1.0, at intervals of 0.1.

Notice how different structural responses are predicted by the model by varying  $N_p$ , which is the syntactical parameter that guides the collapse response. Thus, different cross-sections, characterized by the same brittleness number have the same response qualitatively. This means that, if the matrix characteristic are constants, the same structural response will be obtained while studying different elements, as long as the product between the reinforcement ratio and the square root of the height is constant. By analysing the various fig 2.6 diagrams, a structural response transition can be noticed, which, from fragile or *strain-softening* for low  $N_p$  values, becomes ductile or *strain-hardening* for high  $N_p$  values. For the studied section, the brittleness number transition value,  $N_{pt}$ , is near to 0.5. Instable responses are expected for elements with a high matrix toughness, low reinforcement ratio and low height. Vice versa, ductile responses are expected for elements with a low matrix toughness, high reinforcement ratio and high height. Notice that, according to the model, in case of constant ratio reinforcement and matrix toughness, if the height increases, the element response will be more fragile.

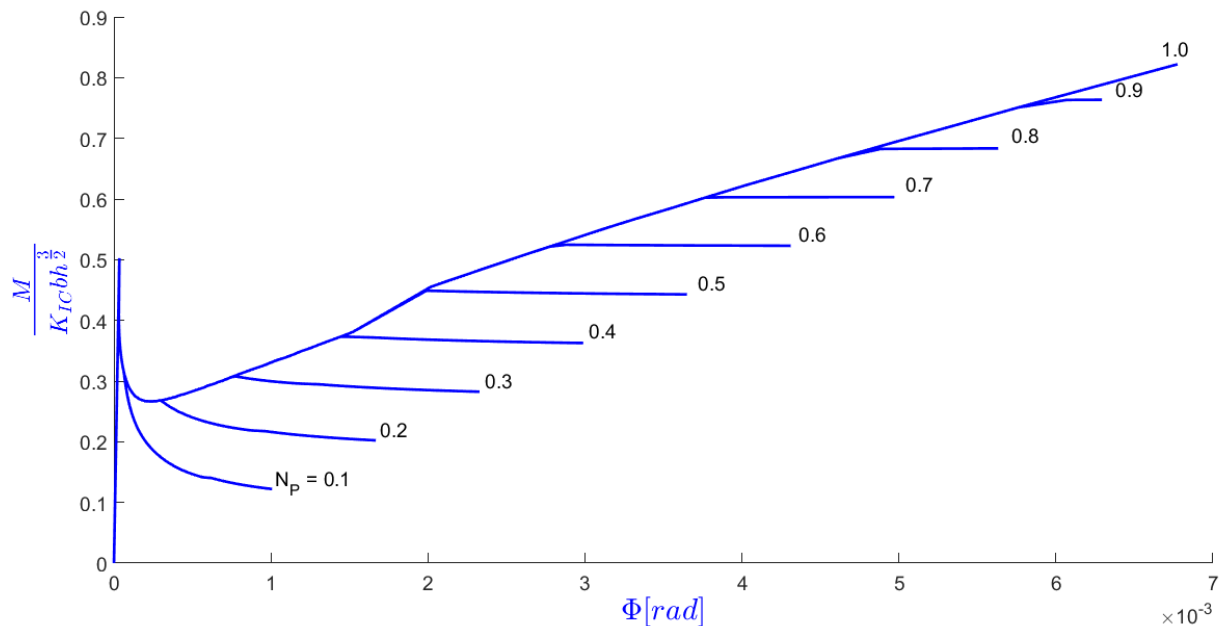


Fig 5. 1- The single fibre abacus.

The curves obtained for  $N_p < N_{pt}$  are characterized by softening branches, which can be experimentally observed only if the load process is controlled by a global strain parameter, because only a continuous bending moment diminution can prevent the crack from propagating uncontrolled.

The curves obtained for  $N_p > N_{pt}$  presents an initial instable crack propagation, characterized by a snap-through discontinuity, followed by a hardening branch. In a classical load-controlled experimental test, the response curve will be characterized by an immediate rotation increment at a constant load. The transition brittleness number,  $N_{pt}$ , allows us to define the minimum reinforcement that a section, with a known height, needs to have to be ductile.

## 5.2 The Two-Fibres Abacus

In fig 5.2 and 5.3 normalized moment-rotation curves are shown, obtained by varying the brittleness number,  $N_p$ , for a beam, with two layers of reinforcement positioned in  $c = 0.1$ ;  $0.2$   $h$  and with an initial crack equal to the first reinforcement height. The cases analysed are the ones obtained by varying  $N_p$  from 0.1 to 1.0, at intervals of 0.1.

Notice that the curves obtained for different  $N_p$  values are no longer superposed until a specific  $N_p$  value is reached, this phenomenon depends on the fibre stress state, in fact when a

fibre reaches its plastic limits, it is no longer able to increase its reaction force and therefore the respective crack-propagation moment results lower.

The considerations made for the previous case can be also made identically for this one, the only thing that has varied is the brittleness number transition value,  $N_{pt}$ , which in this case is near to 0.7.

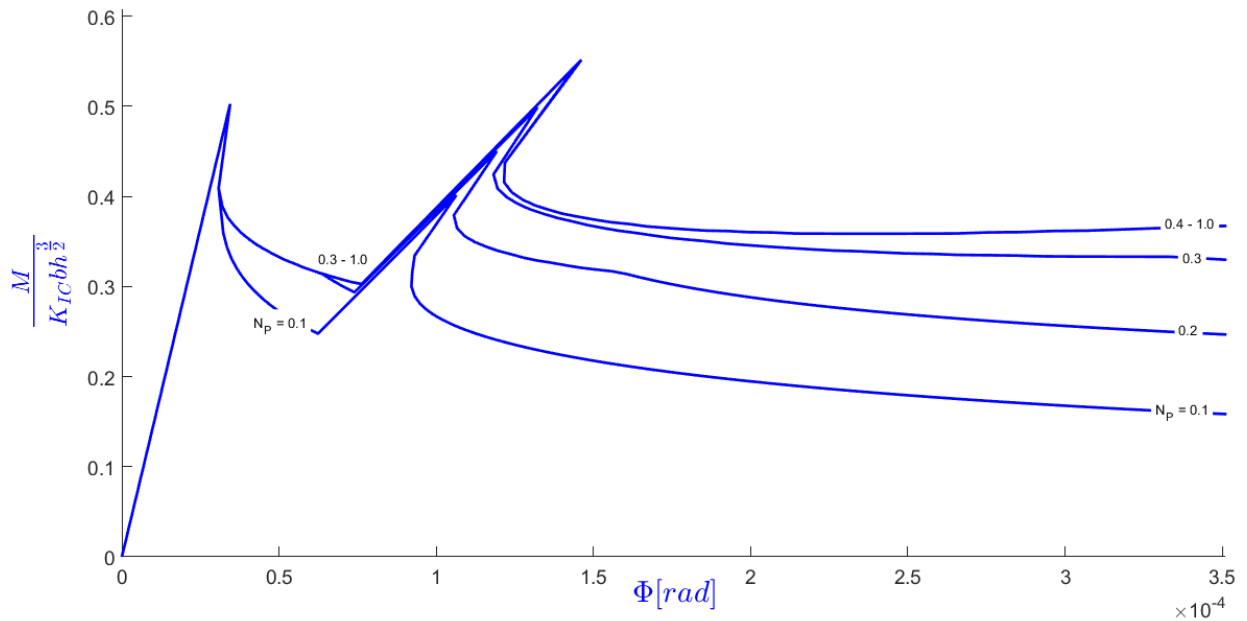


Fig 5. 2- The two-fibres abacus (zoom 1).

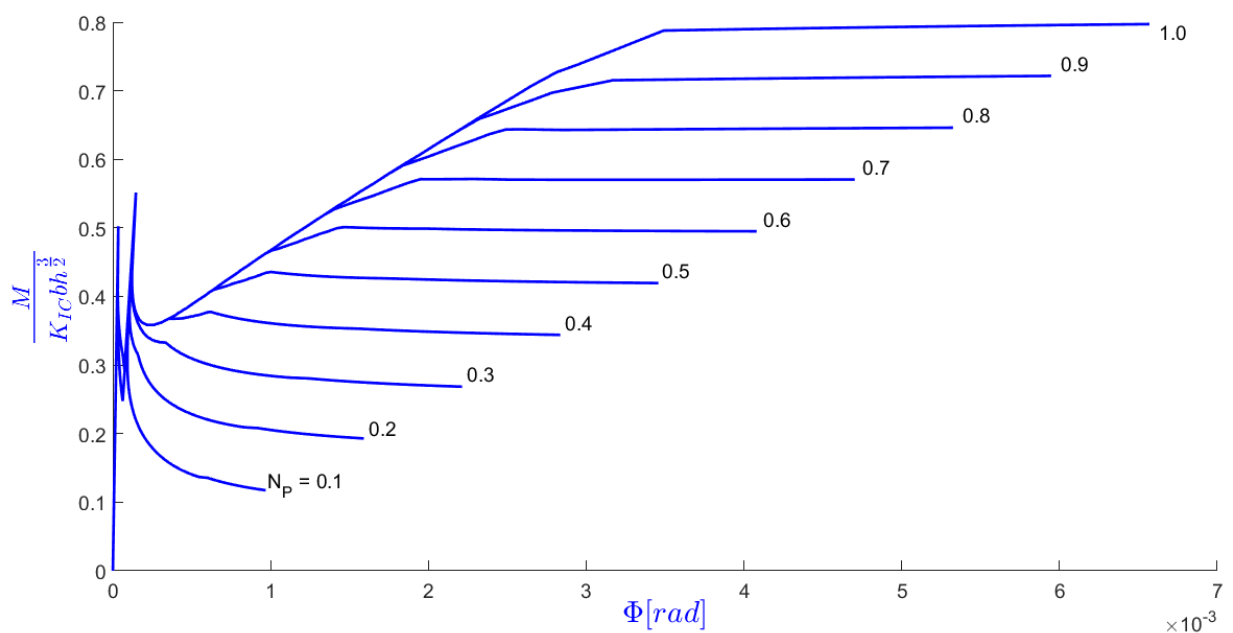


Fig 5. 3- The two-fibres abacus.

### 5.3 The Three-Fibres Abacus

In fig 5.4 and 5.5 normalized moment-rotation curves are shown, obtained by varying the brittleness number,  $N_p$ , for a beam, with three layers of reinforcement positioned in  $c = 0.1; 0.2; 0.3 h$  and with an initial crack equal to the first reinforcement height. The cases analysed are the ones obtained by varying  $N_p$  from 0.1 to 1.0, at intervals of 0.1.

The considerations made for the previous case can be also made identically for this one, the only thing that has varied is the brittleness number transition value,  $N_{pt}$ , which in this case is near to 0.9.

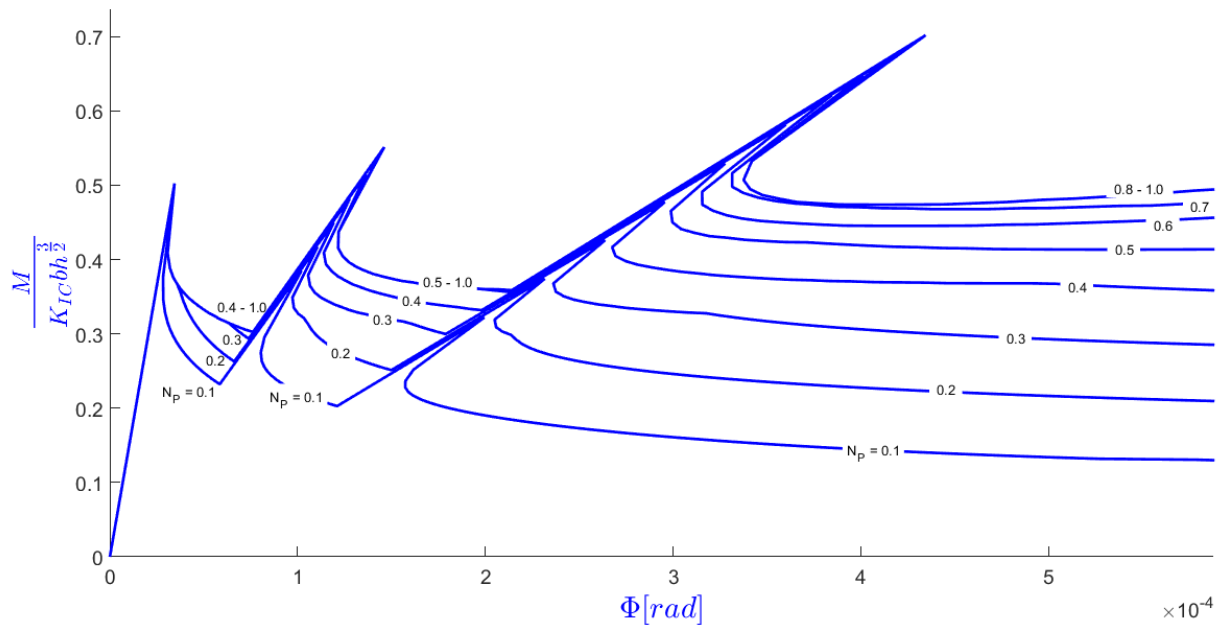


Fig 5. 4- The three-fibres abacus (zoom 1).

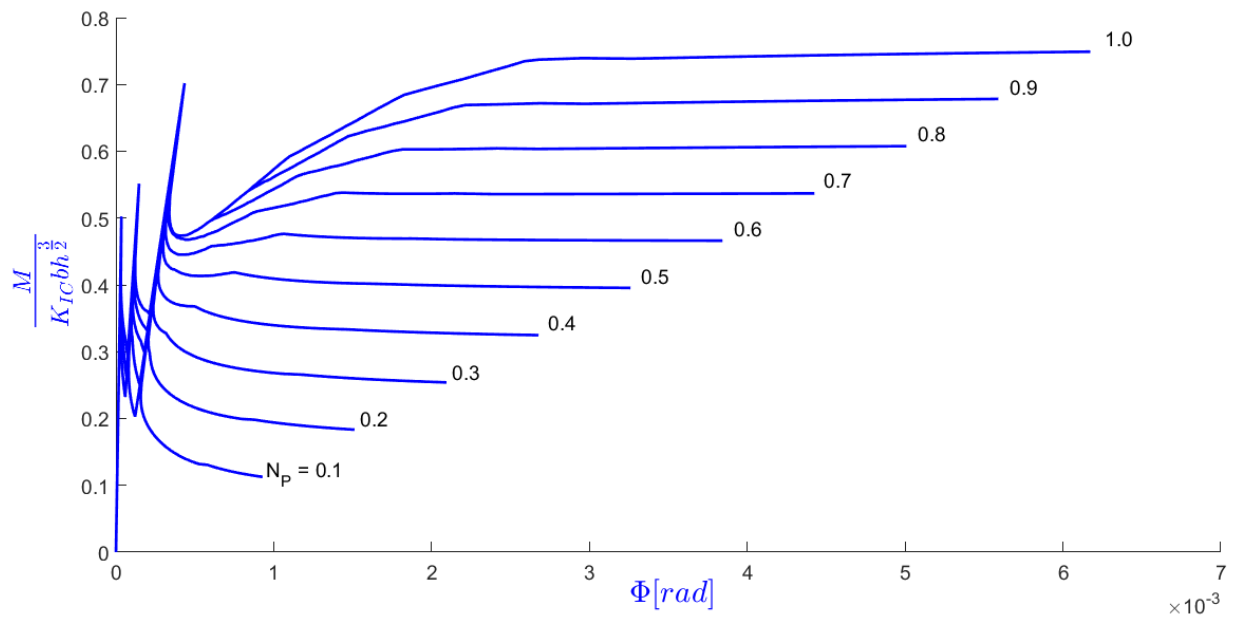


Fig 5. 5- The three-fibres abacus.

## 5.4 The Five-Fibres Abacus

In fig 5.6, 5.7 and 5.8 normalized moment-rotation curves are shown, obtained by varying the brittleness number,  $N_p$ , for a beam, with five layers of reinforcement positioned in  $c = 0.1$ ;  $0.2$ ;  $0.3$ ;  $0.4$ ;  $0.5 h$  and with an initial crack equal to the first reinforcement height. The cases analysed are the ones obtained by varying  $N_p$  from 0.1 to 1.0, at intervals of 0.1.

The considerations made for the previous case can be also made identically for this one, the only thing that has varied is the brittleness number transition value,  $N_{pt}$ , which in this case is near to 1.0.

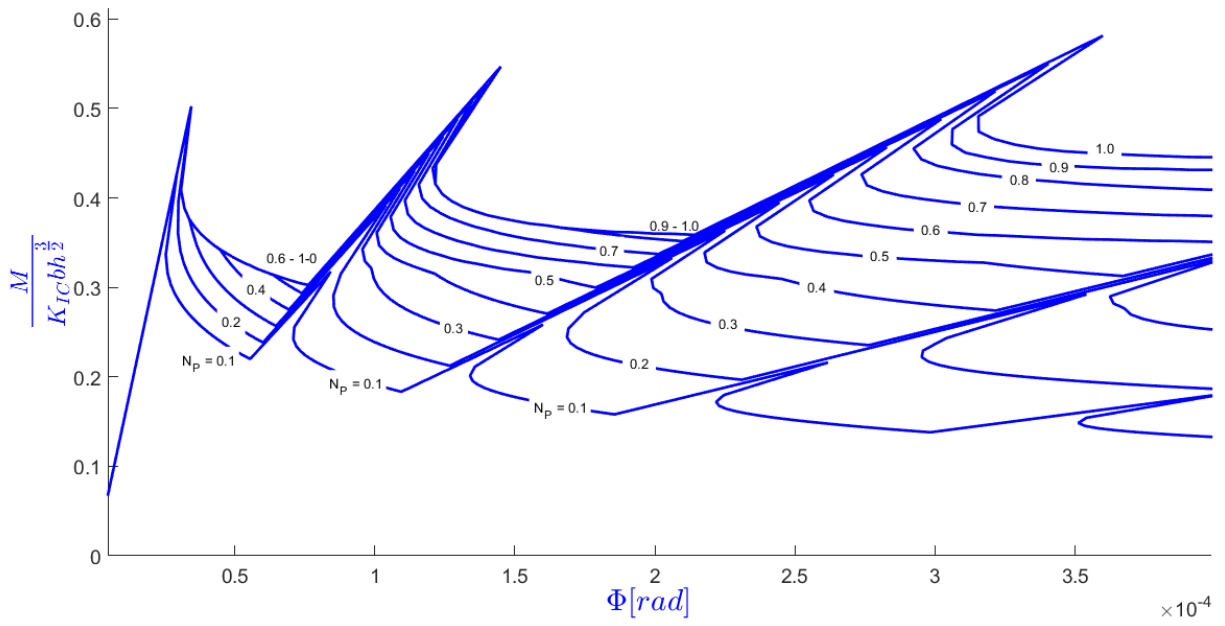


Fig 5. 6- The five-fibres abacus (zoom 1).

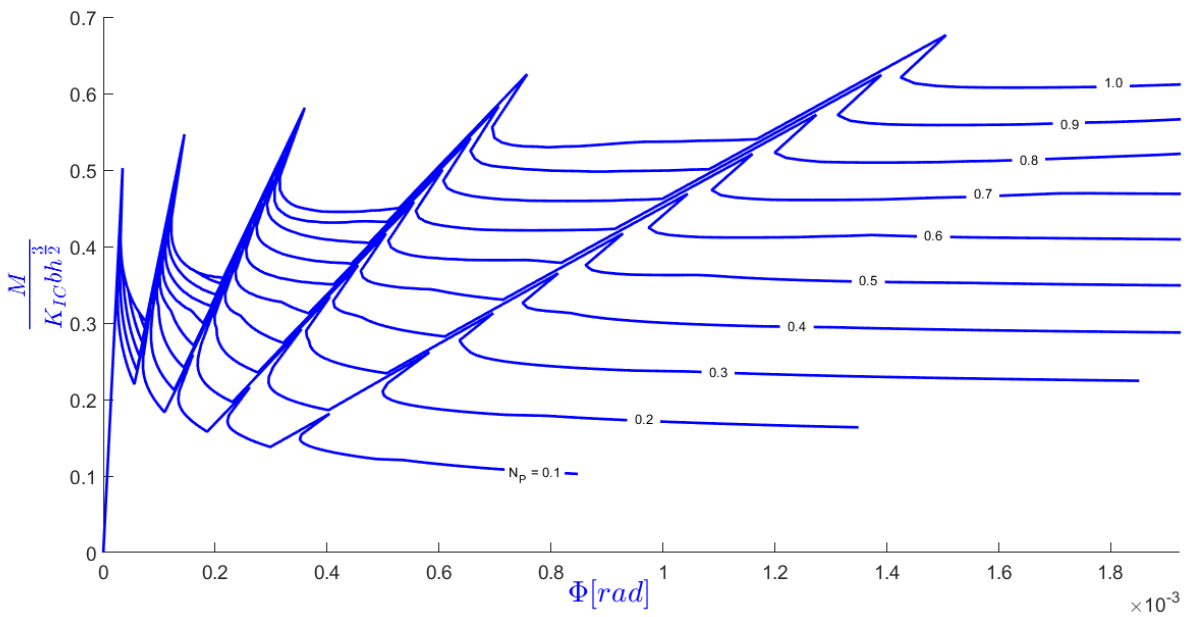


Fig 5. 7- The five-fibres abacus (zoom 2).

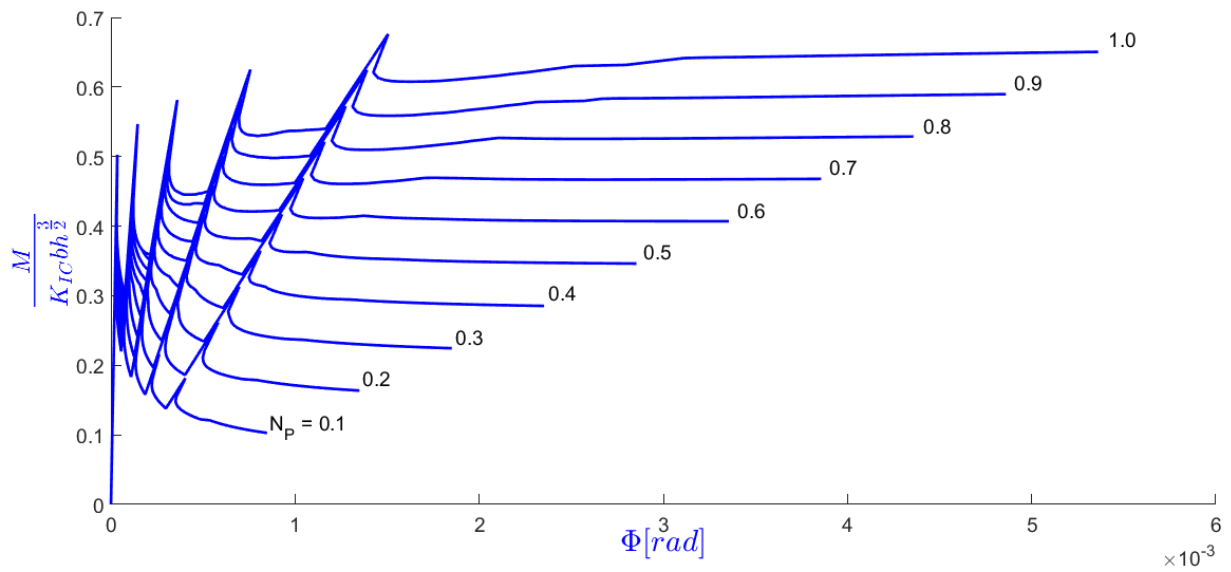


Fig 5. 8- The five-fibres abacus.

## 5.5 The Ten-Fibres Abacus

In fig 5.9, 5.10, 5.11 and 5.12 normalized moment-rotation curves are shown, obtained by varying the brittleness number,  $N_p$ , for a beam, with ten layers of reinforcement positioned in  $c = 0.05; 0.1; 0.15; 0.2; 0.25; 0.3; 0.35; 0.4; 0.45; 0.5 h$  and with an initial crack equal to the first reinforcement height. The cases analysed are the ones obtained by varying  $N_p$  from 0.1 to 1.0, at intervals of 0.1.

The considerations made for the previous case can be also made identically for this one; however, the brittleness number transition value,  $N_{pt}$ , has varied and in this case is near to 1.1.

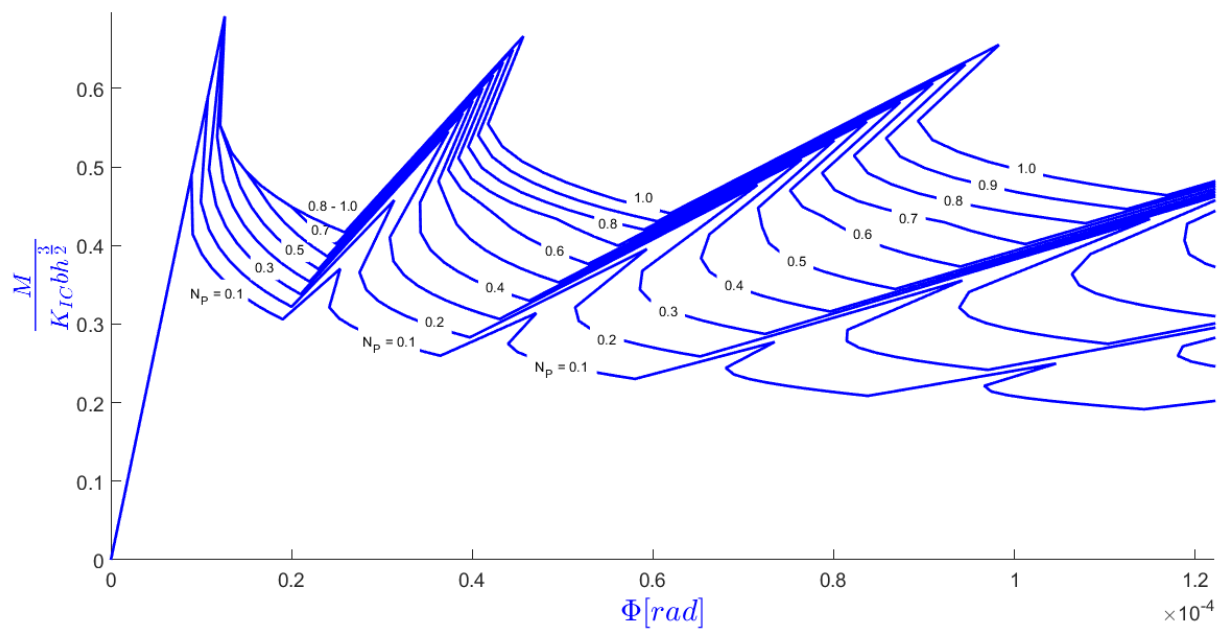


Fig 5. 9- The ten-fibres abacus (zoom 1).

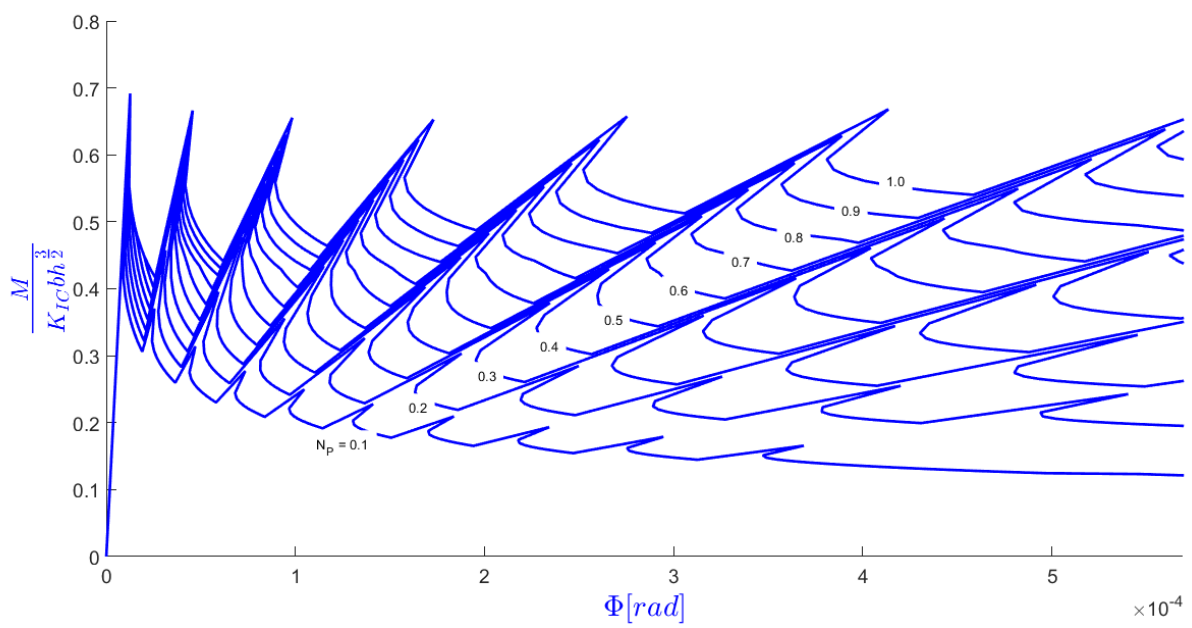


Fig 5. 10- The ten-fibres abacus (zoom 2).

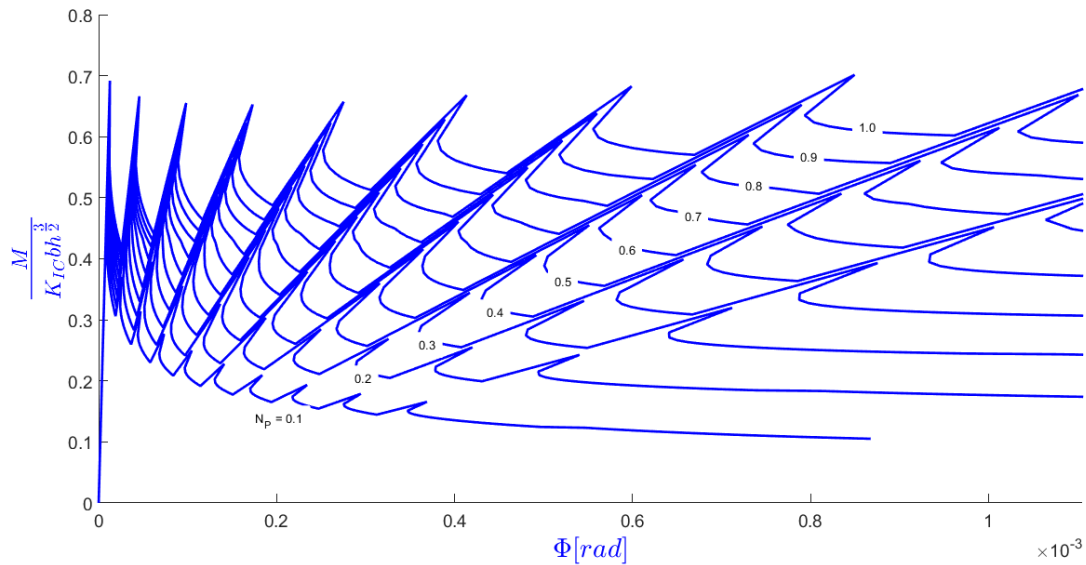


Fig 5. 11- The ten-fibres abacus (zoom 3).

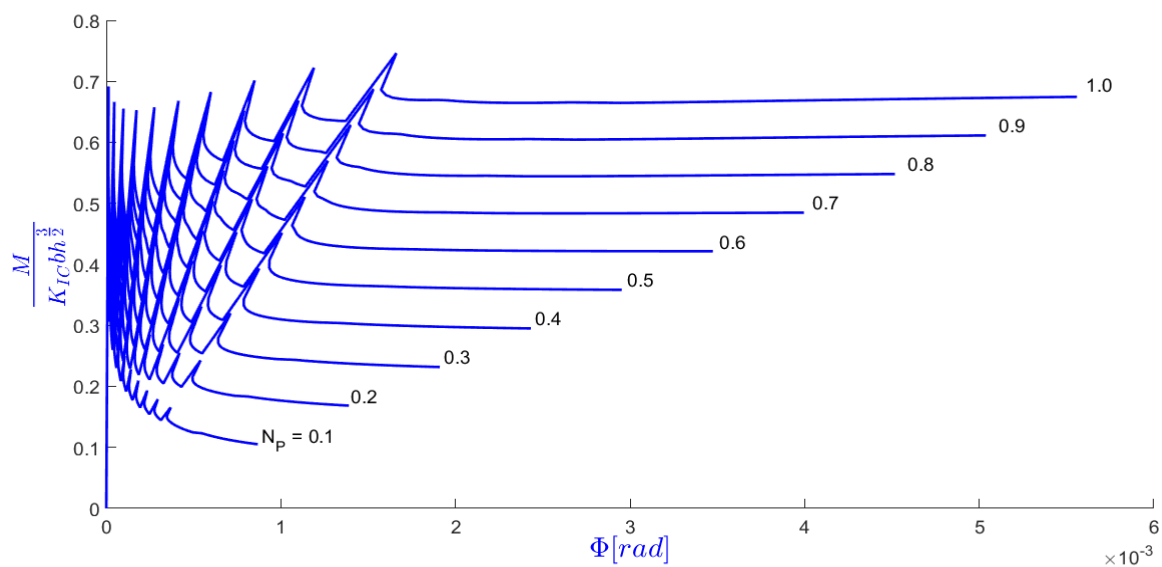


Fig 5. 12- The ten-fibres abacus.

Moreover, this case is perfect to depict the advantage coming from a higher fibres number, which can be enlighten by a direct comparison between the ten-fibres abacus and the five-fibres one; thank to the fact that for both cases the lever arm of the fibres reaction forces and the reinforcement percentage are exactly the same.

For the same geometrical and mechanical characteristics in, particular for the same lever arm and reinforcement percentage, the classical resistance theory predicts for the two section the same structural response. Vice versa, the response curves, fig 5.13, shows how the presence

of a higher fibres number induces a better response in the post-crack phases. Indeed, the ten-fibre element presents a higher crack-propagation moment than the five-fibre one.

When all the fibres are plasticized for both the ten-fibre element and the five-fibre one the curves become coincident. Therefore, both elements present the same ultimate bearing load but the fibres distribution influences the first crack-propagation phase.

What have been just said is true for a low value of brittleness number and for a high number of reinforcement fibres, fig. 5.13. Instead, in fig. 5.14, it is shown how the gap between the two curves ultimate bearing loads increases when the brittleness number is higher and the number of reinforcement fibres lower.

The congruence equation (3.14) explains the phenomenon. In presence of a higher fibres number, the crack is maintained closed in more points along the beam height,  $w_i = 0$ , due to the fibres bridging forces, in the load phase that precedes the fibres plasticization. This phenomenon makes the gap between the two crack faces smaller. This consideration is qualitatively shown in the fig 5.15. The phenomenon observed can assume a notable importance if the bending beam crack has to be maintained under control and in general it could influence the structure durability. Therefore, the structural response gives better results in presence of a diffuse reinforcement, obviously by fixing the brittleness number and the lever arm to a constant value.

In addition, another positive aspect of a diffuse reinforcement is the fact that there is a decrease in the number of the *crack-jumps*, namely the rapid and immediate crack propagation that occurs in a load-controlled process when a local reinforcement is overpassed.

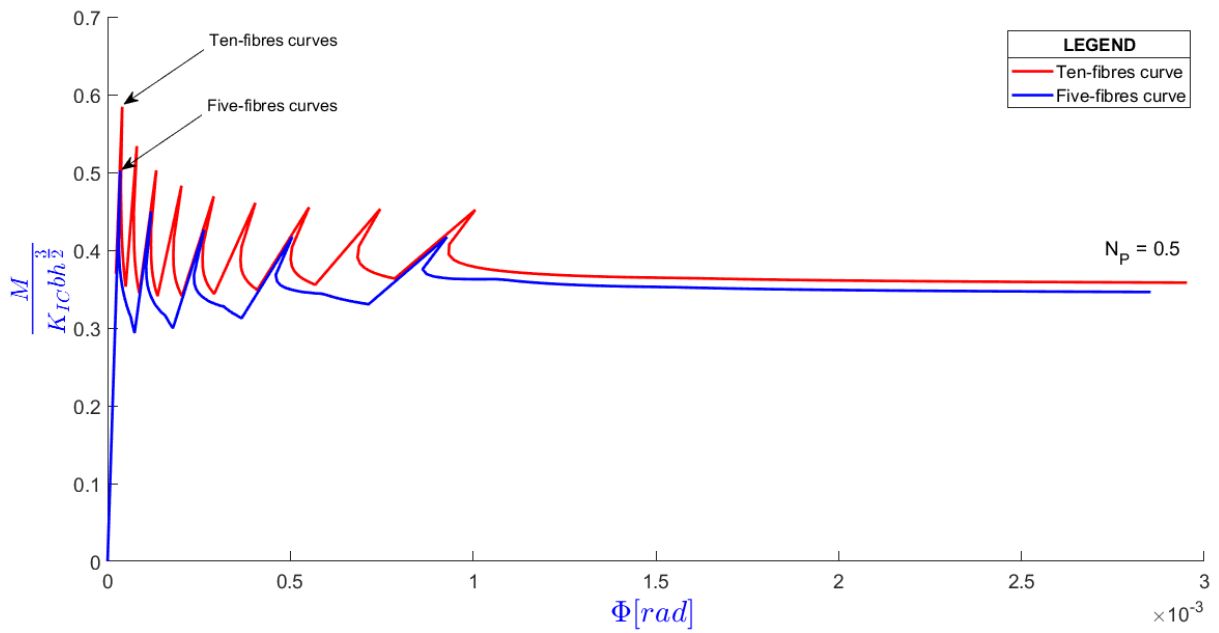


Fig 5. 13- Superposition of a ten-fibres curve and a five-fibres curve for  $N_p$  equal to 0.5.

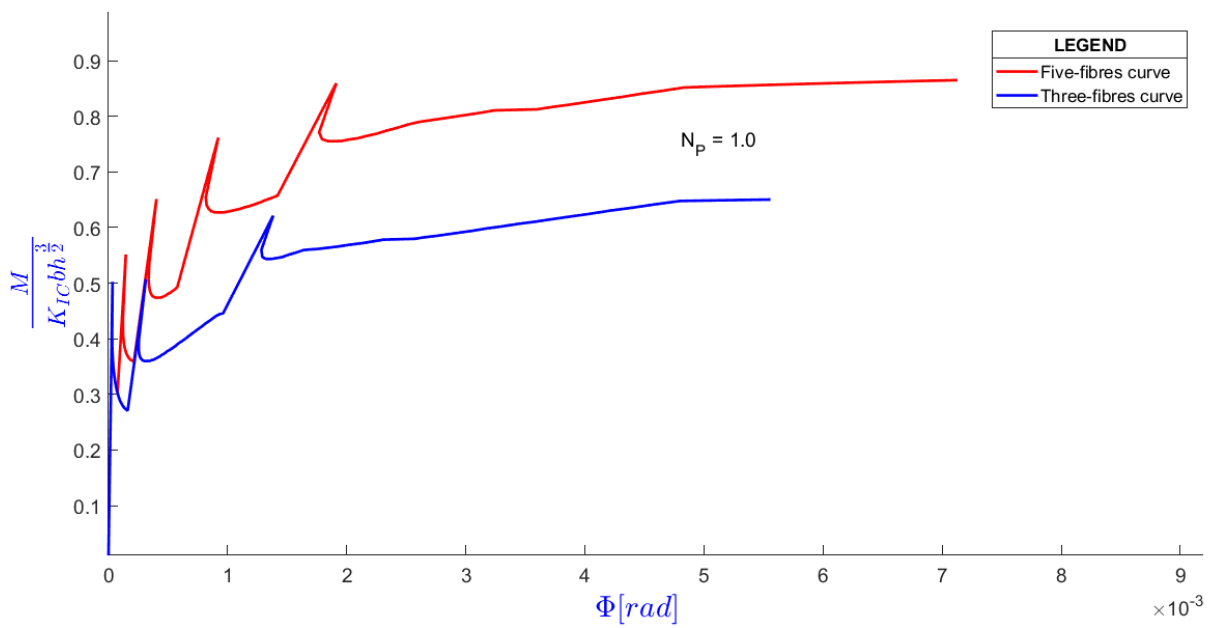


Fig 5. 14- Superposition of a five-fibres curve and a three-fibres curve for  $N_p$  equal to 1.0.

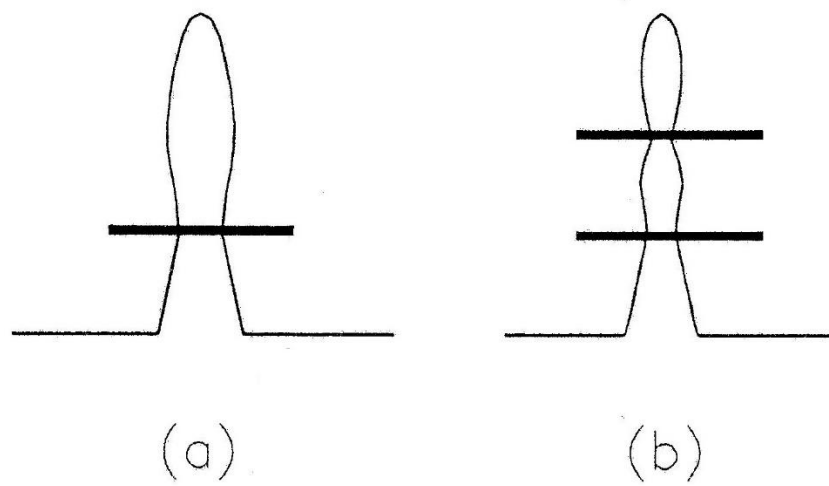


Fig 5. 15- Qualitative crack opening in presence of one or two fibres.

# Conclusion

---

From the literature review, it emerges that different approaches have been used to study the constitutive response of composite materials; the most used ones coming from numerical or Finite Element Model analysis. Although these models are useful for studying some specific problems, the Bridged Crack model described in this work has a larger field of application.

Indeed, the constitutive flexural response of a beam made by a brittle matrix and reinforced with ductile reinforcement layers, can be analysed through the theoretical model summarized in this dissertation.

The Bridged Crack model is based on Fracture Mechanics concepts, and analyses the propagation phenomena of cracks in the critical cross section of an element in bending. The fibre action, which opposes to the crack opening and the crack propagation, is represented through two concentrated closing forces that are applied directly at the crack faces. These forces are evaluated applying compatibility conditions.

The flexural response of a fibre-reinforced element is controlled by a dimensionless parameter called brittleness number  $N_P$ , which depends on the reinforcement percentage, on the fibre yield strength, on the matrix fracture toughness, and on its characteristic size. In particular, by varying the brittleness number, a transition in the structural response arises. The response is *strain-hardening* for high  $N_P$  values, coming from high reinforcement percentage, large size, and/or low values of fracture toughness. Vice versa, for low  $N_P$  values, namely for beams with small reinforcement percentage, with small size, and/or with high values of fracture toughness, the structural response results *strain-softening*. The reinforcement induces some local discontinuities in the moment-rotation diagram, caused by *snap-back* and *snap-through* instabilities.

Moreover, the application of the Bridged Crack model to beams reinforced with  $n$  fibres allows to remark how a diffuse reinforcement induces a structural response globally more ductile than the one related to a beam characterised by localized reinforcements.

One of the most useful applications remarked in this study is the possibility to define a minimum reinforcement criterion.

Varying the number of fibres, for each case study it is possible to define a specific brittleness number,  $N_P$ , which determines the transition from brittle to ductile behaviour (minimum reinforcement). It is worth noting that, in accordance to the slight increase in  $N_P$  related to the

increase in the number of fibres, the minimum reinforcement condition varies from  $N_p = 0.5$  for an element reinforced with one single fibre, to  $N_p = 1.1$  for an element reinforced with ten fibres.

# References

---

- Agraval G.L., Tullin L. G. and Gentle G. L. (1965) Response of doubly reinforced concrete beams to cyclic loading, *ACI Journal*, proceedings, 62(7), pp. 823-836.
- Anderson J.C. and Townsend W.H. (1977) *Models for r.c. frames with degrading stiffness*, *Journal of Structural Engineering*, 103(12), pp. 2361-2376.
- Azevedo N.M., Lemos J.V. and Almeida J.R. (2010) *A discrete particle model for reinforced concrete fracture analysis*, *Structural Engineering and Mechanics*, 36 (3), pp. 343-361.
- Balaguru P.N. and Shah S.P. (1992) *Fiber-reinforced cement composites*, McGraw-Hill Inc.
- Ballarini R., Shah SP. and Keer L.M. (1984) *Crack growth in cement based composites*, *Engineering Fracture Mechanics*, 20(3), pp. 433-445.
- Ballarini R., Muju S. (1991) *Stability analysis of bridged cracks in brittle matrix composites*, ASME Headquarters paper n. 91-gt-94.
- Banon H., Biggs J .M. and Irvine H.M. (1981) *Seismic damage in reinforced concrete frames*, *Journal of Structural Engineering*, 107(9), pp. 1713-1729.
- Barenblatt G.I. (1959) *The formation of equilibrium cracks during brittle fracture. General ideas and hypotheses. Axially-symmetric cracks*, *Journal of Applied Mathematics and Mechanics*, 23 (3), pp. 434-444.
- Barenblatt G.I. (1959) *Equilibrium cracks formed during brittle fracture rectilinear cracks in plane plates*, *Journal of Applied Mathematics and Mechanics*, 23 (4), pp. 706-721.
- Barenblatt G.I. (1962) *The Mathematical theory of equilibrium cracks in brittle fracture*, *Advanced in Applied Mechanics*, 7, pp. 55-129.
- Bartos P. (1980) *Analysis of pull-out test on fibres embedded in brittle matrices*, *Journal of Mater. Science*, 15, pp. 3122-3128.
- Bartos P. (1981) *Bond in fibre reinforced cements and concretes*, *International Journal of Cement composites*, 3(3), pp. 159-177.
- Bazant Z.P. and Oh B.H. (1984) *Deformation of progressively cracking reinforced concrete*, *ACI Journal*, 81(26), pp 268-278
- Bentur A. and Mindess S. (1992) *Fiber reinforced cementitious composites*, Elsevier applied science, London.
- Becker P.F. (1990) *Crack bridging processes in toughened ceramics*, proceedings of the NATO Advanced Research Workshop on Toughening mechanisms in quasi-brittle materials, Evanston, pp. 19-37.
- Becker RF. C. Hsueh, Angelini P. and Tiegs T.N. (1988) *Toughening behavior in whisker-reinforced ceramic matrix composites*, *Journal of Am. Ceram. Soc.*, 71(12), pp. 1050-1061.

- Bosco C., Carpinteri A. and Debernardi P. G. (1990) *Minimum reinforcement in high-strength concrete*, Journal of Structural Engineering, 116(2), pp. 427-437.
- Bosco C., Carpinteri A. and Debernardi P. G. (1990) *Fracture of reinforced concrete: scale effects and snap-back Instability*. Engineering Fracture Mechanics, 35(4-5), 1990, pp. 665-677.
- Bosco C. and Carpinteri A. (1991) *Fibre toughening and crack growth stability in Fibre-reinforced disordered materials*, Proceedings International Conference on Fracture in Brittle Disordered Materials, Noordwijk, The Netherlands, 1, pp. 295-305.
- Bosco C. and Carpinteri A. (1992) *Softening and snap-trough behavior of reinforced elements*, Journal of Engineering Mechanics, 118 (8), pp. 1564-1577.
- Brasiliano A., Souza W.R., Doz G.N. and Brito, J.L.V. (2008) *A study of damage identification and crack propagation in concrete beams*, SDHM Structural Durability and Health Monitoring, 4 (2), pp. 53-65.
- Broms B.B., Shah SP. and Abeles P.W. (1963) *Mechanics of crack arrest in concrete (discussion)*, Journal of Structural Engineering, 60(6), pp. 775-790.
- Brown RH. and Jirsa J.O. (1971) *Reinforced concrete beams under load reversals*, ACI Journal, 68(39), pp. 380-390.
- Budiansky B., Hutchinson J. W. and Evans A. G. (1986) *Matrix fracture in fiber-reinforced ceramics*, Journal of Mechanics Physics of Solids, 34, pp. 167-189.
- Burakiewicz A. (1987) *Testing of fibre bond strength in cement matrix*, in Testing and test methods of fiber cement composites, ed. Swamy., The Construction LTD, pp. 355-369.
- Burns NH. and Siess C. P. (1966) *Plastic hinging in reinforced concrete*, Journal of Structural Engineering, 92(5), pp. 45-64.
- Burns NH. and Siess C. P. (1966) *Repeated and reversed loading in reinforced concrete*, Journal of Structural Engineering, 92(5), pp. 65-78.
- Carpinteri A. (1981) *A fracture mechanics model for reinforced concrete*, IABSE Colloquium on Adv. Mech. of Reinforced Concrete, Delft, pp. 17-31
- Carpinteri A. (1981) *Static and energetic fracture parameters for rocks and concretes*, Mater. and Struct. RILEM, 14, pp. 151-162.
- Carpinteri A. (1984) *Stability of fracturing process in r.c. beams*, Journal of Structural Engineering, 110, pp. 544-558.
- Carpinteri A. and Carpinteri An. (1984) *Hysteretic behavior of r.c. beams*, Journal of Structural Engineering, 110, pp. 2173-2084.
- Carpinteri A. (1984) *Interpretation of Griffith instability as a bifurcation of the global equilibrium*, NATO advanced research workshop on application of fracture mechanics to cementitious composites, Northwestern Univ., Evanston, pp. 287-316.

- Carpinteri A. (1989) *Development of realistic concrete models including scaling effects*, (final report) Commission of the European Communities Nuclear science and technology, Joint research centre-Ispra Site.
- Carpinteri A. (1989) *Cusp catastrophe interpretation of fracture instability*, Journal of Mechanics Physic of Solids, 37, pp 567-582
- Carpinteri, A. and Massabó R. (1992) *Discontinuità nella risposta costitutiva di una trave fibrorinforzata inflessa*, Atti dell'XI Congresso AIMETA 92, Trento, pp. 203-208.
- Carpinteri A. (editore) (1992), *Meccanica dei materiali e della frattura*, Pitagora Editrice, Bologna.
- Carpinteri A. and Massabó R. (1993) *Cyclic behavior of reinforced concrete beams: different responses depending on mechanical and geometrical properties*, in Fracture and Damage of Concrete and Rock FDCR-2, ed. Rossmannith H.P., FN Spon, Vienna, pp. 237-246.
- Carpinteri A. and Massabó R. (1993) *Comportamento ciclico di elementi strutturali in cemento armato: un approccio basato sulla meccanica della frattura*, atti del VI Convegno Nazionale su l'Ingegneria Sismica in Italia, Perugia, 1993, pp. 867-876.
- Carpinteri A. and Massabó R. (1993) *Nonlinear fracture mechanics models for fibre reinforced materials*, Proceedings of the International Conference on Advanced Technology on Design and Fabrication of Composite Materials and Structures, eds Sih G.C., Carpinteri A. and Surace G., Torino.
- Carpinteri A. and Massabó R. (1994) *Continuous versus discontinuous bridged crack in the description of reinforced material flexural collapse*, Proceedings of the EURO-C 1994, Innsbruck.
- Carpinteri A. and Massabó R. (1996) *Bridged versus cohesive crack in the flexural behaviour of brittle-matrix composites*, International Journal of Fracture, 81 (2), pp. 125-145.
- Carpinteri A. and Massabó R. (1997) *Continuous vs discontinuous bridged crack model for fibre-reinforced materials in flexure*, International Journal of Solid Structures, 34 (18), pp. 2321-2338.
- Carpinteri A. and Massabó R. (1997) *Reversal in failure scaling transition of fibrous composites*, Journal of Engineering Mechanics, 123 (2), pp. 107-114.
- Carpinteri A. and Chiaia B. (2002) *Embrittlement and decrease of apparent strength in large-sized concrete structures*, Sadhana - Academy Proceedings in Engineering Sciences, 27 (4), pp. 425-448.
- Carpinteri A., Ferro G. and Ventura G. (2004) *Double brittle-to-ductile transition in bending of fibre reinforced concrete beams with rebars*, International Journal for Numerical and Analytical Methods in Geomechanics, 28 (7-8), pp. 737-756
- Carpinteri A., Corrado M., Paggi M. and Mancini G. (2007) *Cohesive versus overlapping crack model for a size effect analysis of RC elements in bending*, Proceedings of the 6th International Conference on Fracture Mechanics of Concrete and Concrete Structures, 2, pp. 655-663.
- Carpinteri A. and Corrado M. (2009) *An extended (fractal) Overlapping Crack Model to describe crushing size-scale effects in compression*, Engineering Failure Analysis, 16 (8), pp. 2530-2540.
- Carpinteri A., Corrado M., Mancini G. and Paggi M. (2009) *A numerical approach to modelling size effects on the flexural ductility of RC beams*, Materials and Structures, 42 (10), pp. 1353-1367.

- Carpinteri A., Corrado M., Mancini G. and Paggi M. (2009) *The overlapping crack model for uniaxial and eccentric concrete compression tests*, Magazine of Concrete Research, 61 (9), pp. 745-757.
- Carpinteri A., Corrado M., Mancini G. and Paggi M. (2009) *Size-Scale Effects on Plastic Rotational Capacity of Reinforced Concrete Beams*, ACI Structural Journal, 106 (6), pp. 887-896.
- Carpinteri A., Corrado M., Paggi M., Mancini G. (2009) *New model for the analysis of size-scale effects on the ductility of reinforced concrete elements in bending*, Journal of Engineering Mechanics, 135 (3), pp. 221-229.
- Carpinteri, A., Carmona, J.R., Ventura, G. (2011) *Failure mode transitions in reinforced concrete beams- Part 1: Theoretical model*, ACI Structural Journal, 108 (3), pp. 277-285.
- Carpinteri A., El-Khatieb M. and Cadamuro E. (2013) *Failure mode transitions in RC beams: A cohesive/overlapping crack model application*, Meccanica, 48 (10), pp. 2349-2366.
- Chen M.T. and Ho J.C.M. (2015) *Concurrent flexural strength and ductility design of RC beams via strain-gradient-dependent concrete stress-strain curve*, Structural Design of Tall and Special Buildings, 24 (9), pp. 629-652.
- Chiaia B., Fantilli A.P. and Vallini P. (2007) *Evaluation of minimum reinforcement ratio in FRC members and application to tunnel linings*, Materials and Structures/Materiaux et Constructions, 40 (6), pp. 593-604.
- Ciampi V., Eligehausen R., Bertero V. and E. Popov (1981) *Analytical model for deformed bar bond under generalized actions*, Advanced Mechanics of Reinforced Concrete, IABSE-Colloquium Final Report, Delft, The Netherlands, pp. 53-67.
- Comite Euro-International du Beton (1983) *Response of r.c. critical regions under large amplitude reversed actions*, CEB Bulletin d'Information, 161.
- Comite Euro-International du Beton (1993) *Ceb-Fip Model Code 1990*, Bulletin d'Information, pp. 213-214.
- Corrado M., Carpinteri A., Paggi M. and Mancini G. (2008) *Improvement in the plastic rotation evaluation by means of fracture mechanics concepts*, Proceedings of the International FIB Symposium - Tailor Made Concrete Structures: New Solutions for our Society
- Cotterell B., Paramasivam P. and Lam KY., (1992) *Modelling the fracture of cementitious materials*, Material and Structure, 25, pp. 14-20.
- Cox B.N. (1991) *Extrinsic factors in the mechanics of bridged cracks*, Acta Metall. Mater., 39(6), pp. 1189-1201.
- Cox B. N. and Marshall D. B. (1991) *Stable and unstable solutions for bridged cracks in various specimens*, Acta Metall. Mater., 39, pp. 579-589.
- Cox B.N. and Marshall D.B. (1992) *Concepts in the fracture and fatigue of bridged cracks*, submitted to Acta Metall. Mater. .
- Cox B.N., Bale H.A., Begley M., Blacklock M., Do B.-C., Fast T., Naderi M., Novak M., Rajan V.P., Rinaldi R.G., Ritchie R.O., Rossol M.N., Shaw J.H., Sudre O., Yang Q., Zok F.W. and Marshall, D.B.

- (2014) *Stochastic virtual tests for high-temperature ceramic matrix composites*, Annual Review of Materials Research, 44, pp. 479-529.
- Desayi P. and Ganesan N. (1986) *Fracture behavior of ferrocement beams*, Journal Structure of Engineering, 112(7), pp. 1509-1525.
- Dugdale D.S. (1960) *Yielding of steel sheets containing slits*, Journal of Mechanics and Physics of Solids, 8, pp. 100-104.
- Emori K. and Schnobrich W.C. (1981) *Inelastic behavior of concrete frame wall structures*, Journal of Structural Engineering, 107(1), pp. 145-164.
- El-Din S. and Nassef E.A. (1975) *A modified approach for estimating the crackm; moment of reinforced concrete beams*, ACI Journal, 72(27), pp. 356-360.
- Erdogan F. and Joseph P.F. (1987) *Toughening of ceramics through crack bridging by ductile particles*, Journal of Mechanics Physics of Solids, 35, pp. 262-270.
- Fantilli A.P., Ferretti D., Iori I. and Vallini, P. (1999) *Behaviour of R/C elements in bending and tension: The problem of minimum reinforcement ratio*, European Structural Integrity Society, 24(C), pp. 99-125.
- Fantilli A.P., Mihashi H. and Vallini, P. (2007) *Crack profile in RC, R/FRCC and R/HPFRCC members in tension*, Materials and Structures/Materiaux et Constructions, 40 (10), pp. 1099-1114.
- Fantilli A.P., Chiaia B. and Gorino A. (2016) *Minimum reinforcement and ductility index of lightly reinforced concrete beams*, Computers and Concrete, 18 (6), pp. 1175-1194.
- Fantilli A.P., Chiaia B. and Gorino A. (2016) *Unified approach for minimum reinforcement of concrete beams*, ACI Structural Journal, 113 (5), pp. 1107-1116.
- Fantilli A.P., Chiaia B. and Gorino A. (2016) *Fiber volume fraction and ductility index of concrete beams*, Cement and Concrete Composites Volume, 65, pp. 139-149.
- Fayyad T.M. and Lees J.M. (2015) *Evaluation of a minimum flexural reinforcement ratio using fracture-based modelling*, IABSE Conference, Geneva 2015: Structural Engineering: Providing Solutions to Global.
- Ferro G. (2002) *Multilevel bridged crack model for high-performance concretes*, Theoretical and Applied Fracture Mechanics, 38 (2), pp. 177-190.
- Ferro G., Carpinteri A. and Ventura G. (2007) *Minimum reinforcement in concrete structures and material/structural instability*, International Journal of Fracture, 146 (4), pp. 213-231.
- Filippou F.C., Popov E.P. and Bertero V.V. (1983) *Modeling of r.c. joints under cyclic excitations*, Journal of Structural Engineering, 109(11), pp. 2666-2684.
- Filippou F.C., Popov E.P. and Bertero V.V. (1986) *Analytical studies of hysteretic behavior of r.c. joints*, Journal of Structural Engineering, 112(7), pp. 1605-1622.
- Filippou F.C. and Zulfiqar N. (1993) *Models of critical regions and their effect on the seismic response of reinforced concrete frames*, Modelling and analysis of reinforced concrete structures for dynamic loading, CISM Course, Udine.

- Foote R.M.L., Mai Y.W. and Cotterell B. (1986) *Crack growth resistance curves in strain-softening materials*, Journal of Mechanics Physics of Solids, 6, pp. 593-607,
- Frantz G.C. and Broen J.E. (1980) *Cracking on the side faces of large reinforced concrete beams*, ACI Journal., 77(32), pp. 307-313.
- Georgiadi-Stefanidi K., Mistakidis E., Perdikaris P. and Papatheochari T. (2011) *Numerical simulation of the nonlinear bending response of fibre-reinforced cementitious matrix beams and comparison with experimental results*, Engineering Structures, 33 (12), pp. 3579-3589.
- Gergely P. (1993) *Dynamic response of frames members and frames*, Modelling and analysis of reinforced concrete structures for dynamic loading, CISM Course, Udine.
- Giuffr  A. e Pinto P. (1970) *Il comportamento del cemento armato per sollecitazioni cicliche di forte intensit *, Genio Civile, 5, pp. 391-408.
- Giuriani E. (1981) *Experimental investigation on the bond slip law of deformed bars in concrete, Analytical model for deformed bar bond under generalized actions*, Advanced Mechanics of Reinforced Concrete, IABSE-Colloquium Final Report, Delft, The Netherlands, pp. 121-142.
- Griffith A.A. (1921) *The phenomena of rupture and flow in solids*, Philosophical Transactions of the Royal Society, London, A-221, pp. 163-198.
- Griffith A.A. (1924) *The theory of rupture*, Proceedings of First International Congress Applied Mechanics, Delft, pp. 55-63.
- Goldstein R. and Perelmuter M. (1999) *Modelling of bonding at an interface crack*, International Journal of Fracture, 99 (1-2), pp. 53-79.
- Hillerborg A., Mooder M. and Petersson P. E. (1976) *Analysis of crack formation and crack growth in concrete by means of fracture mechanics and finite elements*, Cem. Conc. Research, 6, pp. 773-782.
- Hillerborg A. (1980) *Analysis of fracture by means of the fictitious crack model, particularly for fibre reinforced concrete*, International Journal of Cement Composites, 2(4), pp. 177-184.
- Hilsdorf H.K. and Brameshuber W. (1991) *Code-type formulation of fracture mechanics concepts for concrete*, International Journal of Fracture, 51, pp. 61-72.
- Irwin G.R. (1957) *Analysis of stresses and strain near the end of a crack traversing a plate*, Journal of Applied Mechanics, 24, pp. 361-364
- Irwin G.R. (1958) *Fracture*, in Handbuch der Physik, VI, ed. Flugge S., pp. 551-590.
- Jenkins M.G., Kobayashi A.S., White K.W. and Bradt R. C. (1987) *Crack initiation and arrest in a SiC whisker/Al<sub>2</sub>O<sub>3</sub> matrix composite*, Journal of Am. Ceram. Soc., 70(6), pp. 393-395.
- Jenq Y. S. and Shah S.P. (1985) *Crack propagation in fiber-reinforced concrete*, Journal of Engineering Mechanics, 112, pp. 19-34
- Jenq Y.S. and Shah S.P. (1985) *Two parameter fracture model for concrete*, Journal of engineering mechanics, 111(10), pp. 1227-1241.

- Khanna S.H. and Shukla A. (1993) *Energy absorption mechanisms during dynamic fracturing of fibre reinforced composites*, Journal of Material Science, 28, pp. 3722-3730.
- Levi F., Bosco C. and Debernardi P G (1988) *Two aspects of the behavior of slightly reinforced structures*, CEB Bulletin d'information, 185, pp. 39-50.
- Li V.C. and Liang E. (1986) *Fracture processes in concrete and fiber reinforced cementitious composites*, Journal of Engineering Mechanics, 112(6), pp. 566-586.
- Li V.C., Wang Y. and Backers S. (1991) *A micromechanical model of tension softening and bridging toughening of short random fiber reinforced brittle matrix composites*, Journal of Mechanics Physics of Solids, 39(5), pp. 607-625.
- Li Z., Mobasher B. and Shah S.P. (1991) *Characterization of interfacial properties in fiber reinforced cementitious composites*, Journal of Am. Ceram. Soc., 74(9), pp. 2156-2164.
- Lu Y. and Henry R.S. (2017) *Numerical modelling of reinforced concrete walls with minimum vertical reinforcement*, Engineering Structures, 143, pp. 330-345.
- Mai Y.W. (1985) *Fracture measurements for cementitious composites*, in *Application of fracture mechanics to cementitious composites*, ed. Shah S. P., Martinus Nijhoff Dordrecht, pp. 399-429.
- Mai Y.W. and Lawn B.R. (1986) *Crack stability and toughness characteristics in brittle materials*, Annual Review Mater. Sci., 16, pp. 415-439.
- Mai Y.W. (1991) *Fracture and fatigue of non-transformable ceramics, the role of crack-interface bridging*, in *Fracture Processes in concrete, rock and ceramics*, ed. Van Mier, E.&F.N. Spon, London, pp. 3-26.
- Mantegazza G. (1993) *Carbon fiber cementitious properties and applications, proc. of the Int. Seminar on The application of FRP in civil structural engineering*, Bologna.
- Marchese B. and Marchese G. (1993) *Il pull-out di fibre d'acciaio da matrici cementizie*, L'industria italiana del cemento, 683, pp. 811-822.
- Marfia S. and Sacco E. (2003) *Numerical techniques for the analysis of crack propagation in cohesive materials*, International Journal for Numerical Methods in Engineering, 57 (11), pp. 1577-1602.
- Marshall D. B. and Cox B. N. and Evans A. G. (1985) *The mechanics of matrix cracking in brittle-matrix fiber composites*, Acta Metall. Mater., 33, pp. 2013-2021.
- Marshall D. B. and Cox B. N. (1987) *Tensile fracture of brittle matrix composites: influence of fiber strength*, Acta Metall. Mater., 35(11), pp. 2607-2619.
- Mazdiyasn K.S. (editor) (1992) *Fiber reinforced ceramic composites Materials, processing and technology*, Noyes publications, Park Ridge, USA.
- Mi Z., Li Q., Hu Y., Xu Q. and Shi J. (2016) *An analytical solution for evaluating the effect of steel bars in cracked concrete*, Engineering Fracture Mechanics, 163, pp. 381-395.
- Mobasher B., Yao Y. and Soranakom C. (2015) *Analytical solutions for flexural design of hybrid steel fiber reinforced concrete beams*, Engineering Structures, 100, pp. 164-177.

- Mortom J. and Grooves G.W. (1974) *The cracking of composites consisting of discontinuous ductile fibres in a brittle matrix. Effect of fiber orientation*, Journal of Mater. Science, 9, pp. 1439-1445.
- Naaman A.E. and Shah S.P. (1976) *Pull-out mechanism in steel fibre reinforced concrete*, Journal of Structural Engineering, 102(8), pp. 1537-1541.
- Nazmul I.M. and Matsumoto T. (2008) *Regularization of inverse problems in reinforced concrete fracture*, Journal of Engineering Mechanics, 134 (10), pp. 811-819.
- Nervi P.L. (1951) *Il ferro-cemento: sue caratteristiche e possibilità*, L'ingegnere, 1, pp. 17-25.
- Okamura H., Watanabe K. and Takano T. (1973) *Application of the Compliance Concept in Fracture Mechanics*, ASTM STP, 536, pp. 423-433.
- Okamura H., Watanabe K. and Takano T. (1975) *Deformation and strength of cracked member under bending moment and anal force*, Engineering Fracture Mechanics, 7, pp. 531-539.
- Osmiani C., Mohamed G., Treiber J.W.G., Allegri G. and Partridge, I.K. (2016) *Exploring the influence of micro-structure on the mechanical properties and crack bridging mechanisms of fibrous tufts*, Composites Part A: Applied Science and Manufacturing, 91, pp. 409-419.
- Otani S. (1974) *Inelastic analysis of r.c. frame structures*, Journal of Structural Engineering, 100(7), pp. 1433-1449.
- Perelmuter M. (2014) *Nonlocal criterion of bridged cracks growth: analytical analysis*, Acta Mechanica, 226 (2), pp. 397-418.
- Petersson P.E. (1981) *Crack growth and development of fracture zones in plain concrete and similar materials*, Ph. D. theme, Lund.
- Popov E.P. (1980) *Seismic behavior of structural sub-assemblages*, Journal of Structural Engineering, 106(7), pp. 1451-1474.
- RILEM Technical Committee TC-50 on Fracture Mechanics of concrete (1985) *Determination of the fracture energy of mortar and concrete by means of three-point bend test on notched beams*, Draft Recommendation, Materials and Structures, 18.
- Rizk E. and Marzouk H. (2009) *New formula to calculate minimum flexure reinforcement for thick high-strength concrete plates*, ACI Structural Journal, 106 (5), pp. 656-666.
- Romualdi J.P. and Batson G.B. (1963) *Behavior of reinforced concrete beams with closely spaced reinforcement*, Journal of the ACI, 40, pp. 775-789.
- Romualdi J.P. and Batson G.B. (1963) *Mechanics of crack arrest in concrete*, Journal of Engineering mechanics, 89(3), pp. 147-167.
- Rooke D.P. and Cartwright D.J. (1976) *Compendium of Stress Intensity Factors*, The Hillingdon Press, Uxbridge, Middx, England.
- Rose L.R. (1987) *Crack reinforced by distributed springs*, Journal of Mechanics Physics of Solids, 35(4), pp. 383-405.

- Ruiz G., Elices M. and Planas J. (1999) *Size effect and bond-slip dependence of lightly reinforced concrete beams*, European Structural Integrity Society, 24 (C), pp. 67-97.
- Ruiz WM. and Winter G. (1969) *Reinforced concrete beams under repeated loads*, Journal of Structural Engineering, 6, pp. 1189-1211.
- Saiidi M. (1982) *Hysteresis models for reinforced concrete*, Journal of Structural Engineering, 108(5), pp. 1077-4087.
- Sanborn S.E. and Prévost J.H. (2008) *Discrete modeling of crack bridging by a discontinuous platelet with a controlled interface*, International Journal of Solids and Structures, 45 (18-19), pp. 5059-5073.
- Shah S.P. Wang ML. and Chung L. (1987) *Model concrete beam column joints subjected to cyclic loading at two rates*, Material and Structures, 20, pp. 85-95.
- Shah S.P. (1988) *Fracture toughness of cement-based materials*, Materials and Structures, 21, pp. 145-150.
- Shah S.P. and Ouyang C. (1991) *Mechanical behavior of reinforced cement based composites*, Journal of Am. Ceram. Soc., 74(11), pp. 27-38.
- Shehata I.A.E.M., Shehata L.C.D. and Garcia, S.L.G. (2003) *Minimum steel ratios in reinforced concrete beams made of concrete with different strengths - Theoretical approach*, Materials and Structures/Materiaux et Constructions, 36 (255), pp. 3-11.
- Sih G.C. (1973) *Handbook of stress-intensity factors for researchers and engineers*, Lehigh Univ., Bethlehem, Pennsylvania.
- Sinha B.P., Gerstle K H and Tullin L. G. (1964) *Response of singly reinforced beams to cyclic loading*, ACI Journal, proceedings, 61(8),pp. 1021-1037.
- Spacone E. and Filippou F.C. (1993) *Beam and beam-column models for the nonlinear analysis of r.c. structures. A state of the art report*, Modelling and analysis of reinforced concrete structures for dynamic loading, CISM Course, Udine.
- Spacone E., Taucer FF. and Filippou F.C. (1993) *A beam column element for nonlinear dynamic analysis of reinforced concrete structures*, atti del VI Convegno Nazionale su l'Ingegneria Sismica in Italia, Perugia, pp. 837-846.
- Swanson P.L., Fairbanks C.J., Lawn B.R., Mai Y.W. and Hockey B.J. (1987) *Crack interface grain bridging as a fracture resistance mechanism in ceramics: I, experimental study on alumina*, Journal of Am. Ceram. Soc., 70(4), pp. 279-89.
- Swanson P.L., Fairbanks CJ. , Lawn B R, Mai Y W and Hockey B.J. (1987) *Crack interface grain bridging as a fracture resistance mechanism in ceramics: II, theoretical fracture mechanics model*, Journal Am. Ceram. Soc., 70(4), pp. 289-294.
- Tada H., Paris P. and Irwin G. (1985) *The Stress Analysis of Cracks Handbook (Second Edition)*, Paris Productions Incorporated (and Del Research Corporation 1963), St. Louis Missouri.
- Takeda T., Sozen M.A. and Nielsen N.N. (1970) *Reinforced concrete response to simulate earthquakes*, Journal of Structural Engineering, 96, pp. 2557-2573.

- Taliercio A. and Coruzzi R. (1999) *Mechanical behaviour of brittle matrix composites: A homogenization approach*, International Journal of Solids and Structures, 36 (24), pp. 3591-3615.
- Task Committee on FEA of r.c. structures (1982) *Finite element analysis of reinforced concrete*, Americana Society of Civil Engineers, New York, U.S.
- Ungsuwarungsri T. and Knauss W.G. (1988) *Nonlinear analysis of an equilibrium craze: part I- problem formulation and solution*, Journal of Applied Mechanics, 55, pp. 44-51.
- Visalvanich K. and Naaman A.E. (1983) *Fracture model for fiber reinforced concrete*, ACI Journal, 80(14), pp. 128-138.
- Wang ML. and Shah S.P. (1987) *Reinforced concrete hysteresis model based on the damage concept*, Earthquake Eng. Struct. Dynamics, 15, pp. 993-1003.
- Wang N. and Xia S. (2017) *Cohesive fracture of elastically heterogeneous materials: An integrative modeling and experimental study*, Journal of the Mechanics and Physics of Solids, 98, pp. 87-105.
- Wecharatana M. and Shah S.P. (1983) *A model predicting fracture resistance of fiber reinforced concrete*, Cement and Concrete research, 13, pp. 819-829.
- Westergaard H.M. (1993) *Stresses at a crack, size of the crack, and the bending of reinforced concrete*, Journal of the ACI, proceedings, pp. 93-102.
- Willis J.R. (1967), *A comparison of the fracture criteria of Griffith and Barenblatt*, Journal of Mechanic Physics of Solids, 15, pp. 151-162.
- Wu Z., Rong H., Zheng J. and Dong W. (2013) *Numerical method for mixed-mode I-II crack propagation in concrete*, Journal of Engineering Mechanics, 139 (11), pp. 1530-1538.
- Wu Z.-M., Wu Y.-F., Dong W., Wu X. and Zheng J.-J. (2014) *An analytical method for determining the crack extension resistance curve of concrete*, Magazine of Concrete Research, 66 (14), pp. 719-728.
- Yang B., Ravi-Chandar K. (1998) *Antiplane shear crack growth under quasistatic loading in a damaging material*, International Journal of Solids and Structures, 35 (28-29), pp. 3695-3715.
- Zhang J., Leung C. K.Y. and Gao Y. (2010) *Simulation of tensile performance of fiber reinforced cementitious composite with fracture mechanics model*, Fracture Mechanics of Concrete and Concrete Structures.
- Zesers A. and Tamužs V. (2014) *Cracking resistance of short-fiber-reinforced composites*, Mechanics of Composite Materials, 50 (2), pp. 165-176.